NMR and NQR Studies on New Type of Heavy Fermion Superconductors

與儀
Mamoru YOGI

OSAKA UNIVERSITY

GRADUATE SCHOOL OF ENGINEERING SCIENCE
DEPARTMENT OF PHYSICAL SCIENCE
DIVISION OF MATERIALS PHYSICS

2004

NMR and NQR Studies on New Type of Heavy Fermion Superconductors

Mamoru YOGI

OSAKA UNIVERSITY

GRADUATE SCHOOL OF ENGINEERING SCIENCE
DEPARTMENT OF PHYSICAL SCIENCE
DIVISION OF MATERIALS PHYSICS

2004

Abstract

Over the past few decades, a considerable number of superconducting materials have been discovered in strongly correlated matters where order parameter symmetries are different from *s*-wave spin-singlet superconductors. It is widely believed that the bound electron pairs in these materials are mediated by magnetic fluctuations. Furthermore, in almost all previous studies on heavy fermion (HF) superconductors, the crystal has an inversion center, which makes it possible to consider the even (spin-singlet) and odd (spin-triplet) components of the superconducting (SC) order parameter (OP) separately.

In this thesis, we deal with two kinds of new type of superconductors. One is the new antiferromagnetic (AFM) HF compound $CePt_3Si$ with no inversion center that has been quite recently discovered by Bauer and co-workers. This compound shows an AFM order at $T_N \sim 2.2$ K, and undergoes superconductivity at $T_C \sim 0.75$ K. An underlying issue is whether the HF superconductivity in the case of non centro-symmetry realized $CePt_3Si$ differs in nature from the unconventional HF superconductors reported thus far, involving a possibility of such a novel type of OP realized that the spin-singlet state and spin-triplet state are mixed. The another one is the first Pr-based HF superconductor $PrOs_4Sb_{12}$. The Crystal Electric Field (CEF) ground state is inferred to be either the non-Kramers Γ_3 doublet or the Γ_1. Even though either the case is possible, the difference of low lying CEF energy between the ground state and the first excited state is very as small as $\Delta E \sim 10$ K, which makes quadrupole degree of freedom survive at low temperatures. Therefore, it may indeed argue for Cooper pairing via quadrupolar fluctuations.

In Part-II, we present NMR studies of ^{195}Pt and ^{29}Si in $CePt_3Si$ that have clarified the novel electronic and magnetic properties at the paramagnetic and AFM state and a relevant new type of HF-SC state:

1. The CEF energy separation is as small as $\Delta E \sim$ 10-16 K, consistent with the neutron result.

2. The heavy fermion state is realized at temperatures below ~ 6 K.

3. The magnetic excitations spectrum has the gap that depends on the magnetic field.

4. The HF quasi-particles remain in a gapless regime in a T region well below T_N, giving rise to a $T_1T =$ const behavior.

5. The application of magnetic field causes the reduction in size of magnetic gap and at the same time the increase in spectral weight of quasi-particles at the Fermi level, having some relevance with the presence of low-lying CEF levels.

6. The Pt-T_1 measurements have probed the anomalies due to the onset of AFM and SC orders, providing microscopic evidence for the coexistence of AFM and SC orders.

7. $CePt_3Si$ is the first HF superconductor that reveals the peak in $1/T_1T$ just below T_C and yet does not follow the T^3 law that used to be reported in most unconventional HF superconductors.

The new AFM HF compound $CePt_3Si$ loses an inversion center in its crystal symmetry. Therefore, the novel relaxation behaviors found below T_C in $CePt_3Si$ have revealed that the new class of SC state is realized in $CePt_3Si$ because of the inversion symmetry. The experimental finding presented in this work deserves future theoretical works to unravel the SC OP symmetry for the case where the inversion symmetry is absent in general. A new field in the research on HF superconductivity is now open up.

In Part-III, we report Sb-NQR study of various filled-skutterudite compounds. First, we deal with the Sb-NQR study of $PrRu_4Sb_{12}$, which shows SC transition at $T_C \sim 1.3$ K. $PrRu_4Sb_{12}$ is characterized by the nonmagnetic CEF ground state Γ_1, and the energy separation between the ground state and the first excited state is estimated as about $\Delta E \sim 70$ K, which is very larger that $\Delta E \sim 10$ K in $PrOs_4Sb_{12}$. The $1/T_1$ measurement result indicates the Korringa law ($1/T_1T = \text{const}$) above T_C. In the SC state for $PrRu_4Sb_{12}$, $1/T_1T$ shows a distinct coherence peak, followed by an exponential decrease below T_C with an isotropic gap $2\Delta/k_BT_C = 3.1$. These results demonstrate that $PrRu_4Sb_{12}$ is the typical weak-coupling s-wave superconductors, in strong contrast with the HF superconductor $PrOs_4Sb_{12}$ that is in a unconventional strong coupling regime.

In Part-III-3, we report the Sb-NQR study of $PrOs_4Sb_{12}$ under various magnetic fields. $1/T_1T$ shows a clear anomaly below T_C. The first anomaly occurs at the phase boundary between the A-phase and B-phase revealed by the thermal conductivity, revealing that $1/T_1T$ shows a marked reduction below T_C. Furthermore, the further reduction in $1/T_1T$ appears at the deep inside of the B-phase. The $1/T_1 = \text{const}$ behavior observed at $H = 0$ well below T_C is demonstrated to be intrinsic, suggesting that the ground state is not in a completely nonmagnetic regime in origin, but a slight mixing effect with the magnetic first excited CEF states. Thus, PrO_4Sb_{12} is classified as the novel type of HF superconductor that differs from the unconventional Ce-based HF superconductors mediated by magnetic fluctuations. Rather, $PrOs_4Sb_{12}$ may be mediated by Pr-$4f^2$ derived quadrupole-fluctuations, leading to a novel kind of HF superconductivity.

In Part-III-4, we report the Sb-NQR study of $CeOs_4Sb_{12}$. The $1/T_1$ measurement has revealed the behavior $1/T_1 \propto T/\sqrt{T-0.06}$ expected for the case where AFM spin fluctuations are critically dominant and hence $CeOs_4Sb_{12}$ is closely located to the AFM quantum critical point. Even in such a situation, a remarkable finding is that the spin-density wave type of magnetic phase transition, that is of the first order type, occurs at $T = 0.9$ K, possibly triggered by the nesting effect of the Fermi surface. The present result, we believe, deserves theoretical study on the physics behind the AFM QCP realized in HF systems in general.

Contents

Part I

General Introduction

Chapter 1

NMR/NQR Theory

1.1 Nuclear spin Hamiltonian

In case there is a magnetic and electric interaction between electrons and a nuclear spin, nuclear spin Hamiltonian is shown as follows,

$$\mathscr{H} = \mathscr{H}_{\text{zeeman}} + \mathscr{H}_{\text{quadrupole}} + \mathscr{H}_{\text{hyperfine}} \tag{1.1}$$

The first term arises by applying an external magnetic field. It is the interaction between a nuclear spin moment $\boldsymbol{\mu}_{\text{n}} = \gamma_{\text{n}}\hbar\boldsymbol{I}$ (γ_{n} is nuclear gyromagnetic ratio) and external field $\boldsymbol{H}_0$;

$$\begin{aligned} \mathscr{H}_{\text{zeeman}} &= -\boldsymbol{\mu}\cdot\boldsymbol{H}_0 & (1.2)\\ &= -\frac{\gamma_{\text{n}}\hbar H}{2}(I_+\sin\theta e^{-i\phi} + I_-\sin\theta e^{i\phi} + 2I_z\cos\theta) & (1.3) \end{aligned}$$

where θ and ϕ are the polar and azimuth angles, respectively, and I_+ (I_-) are raising (lowering) operators. A nucleus has electric quadrupole moment eQ, when $I \geq 1$. The second term shows the interaction between a nuclear quadrupole moment eQ and a surrounding electric field gradient eq as follows,

$$\begin{aligned} \mathscr{H}_{\text{quadrupole}} &= \frac{e^2qQ}{4I(2I-1)}\left\{3I_z^2 - I^2 + \frac{\eta}{2}\left(I_+^2 + I_-^2\right)\right\} & (1.4)\\ \eta &= \frac{V_{xx}-V_{yy}}{V_{zz}} \quad : \quad (0 \leq \eta \leq 1) & (1.5) \end{aligned}$$

Here, η is defined as asymmetric parameter indicating the deviance from axial symmetry. The last term is the magnetic interaction through the hyperfine coupling;

$$\mathscr{H}_{\text{hyperfine}} = \gamma_{\text{e}}\gamma_{\text{n}}\hbar^2\left[\frac{8\pi}{3}\delta(r)\boldsymbol{I}\cdot\boldsymbol{S} - \left(\frac{\boldsymbol{I}\cdot\boldsymbol{S}}{r^3} - \frac{3(\boldsymbol{I}\cdot\boldsymbol{r})(\boldsymbol{S}\cdot\boldsymbol{r})}{r^5}\right) + \frac{\boldsymbol{I}\cdot\boldsymbol{l}}{r^3}\right] \tag{1.6}$$

The first term of this expression is called Fermi contact interaction, which is caused by the finite probability of polarized s-electrons in a nucleus position. The second term is the classic dipole-dipole interaction caused by existence of non s-electrons. The last term expresses the interaction of a nuclear spin and angular momentum.

The local magnetic field ($\boldsymbol{H}_{\mathrm{loc}}$) produced in a nuclear position by the hyperfine interaction can be shown as follows,

$$\mathscr{H}_{\mathrm{hyperfine}} = -\gamma_{\mathrm{n}}\hbar \boldsymbol{I} \cdot \boldsymbol{H}_{\mathrm{loc}} \tag{1.7}$$

Here, $\boldsymbol{H}_{\mathrm{loc}}$ is

$$\boldsymbol{H}_{\mathrm{loc}} = -\gamma_{\mathrm{e}}\hbar \left[\frac{8\pi}{3}\delta(r)\boldsymbol{S} - \left(\frac{\boldsymbol{S}}{r^3} - \frac{3\boldsymbol{r}(\boldsymbol{S}\cdot\boldsymbol{r})}{r^5} \right) + \frac{\boldsymbol{l}}{r^3} \right] \tag{1.8}$$

This local magnetic field $\boldsymbol{H}_{\mathrm{loc}}$ can be divided into two ingredients shown below,

$$\boldsymbol{H}_{\mathrm{loc}}(t) = \langle \boldsymbol{H}_{\mathrm{loc}} \rangle + \delta \boldsymbol{H}(t) \tag{1.9}$$

The average value $\langle \boldsymbol{H}_{\mathrm{loc}} \rangle$ produces an extra magnetic field in a nuclear position. And fluctuation component $\delta \boldsymbol{H}(t)$ causes relaxation of a nuclear spin.

1.2 Knight shift

The extra magnetic field $\langle \boldsymbol{H}_{\mathrm{loc}} \rangle$ changes a resonance magnetic field against fixed resonance frequency. The Knight shift is named after Prof. Walter Knight, who first observed the phenomenon.[1] The Knight shift is defined on fixed frequency by the following formula,

$$K = \frac{H_0 - H_{\mathrm{res}}}{H_0} \tag{1.10}$$

where H_0 expresses the resonance magnetic field in nonmagnetic, and nonmetallic environment. H_{res} is the resonance magnetic field. The Knight shift consists of the sum of the spin part K_{s} and the orbital (Van Vleck) part K_{orb},[2] which are connected with the spin susceptibility χ_{s} and the Van Vleck orbital susceptibility χ_{orb} as follows,

$$K = K_{\mathrm{s}}(T) + K_{\mathrm{orb}} \tag{1.11}$$

$$K_{\mathrm{s}} = \frac{H_{\mathrm{hf}}^{\mathrm{s}}}{N_{\mathrm{A}}\mu_{\mathrm{B}}}\chi_{\mathrm{s}} \tag{1.12}$$

$$K_{\mathrm{orb}} = \frac{H_{\mathrm{hf}}^{\mathrm{orb}}}{N_{\mathrm{A}}\mu_{\mathrm{B}}}\chi_{\mathrm{orb}} \tag{1.13}$$

where N_{A} and μ_{B} are Avogadro's number and Bohr magneton, respectively. H_{hf} is the hyperfine coupling constant. The hyperfine coupling constant can be obtained by plotting K vs χ with temperature as an implicit parameter.[3,4] In HF system, since the spin-orbit interaction is so strong, the electronic state of an ion is characterized with the total angular momentum $\boldsymbol{J}$ ($\boldsymbol{J} = \boldsymbol{S} + \boldsymbol{L}$). The lowest $\boldsymbol{J}$ manifold is split into several sublevels by Crystal Electric Field. In the case of CEF energy splitting is small, the H_{hf} shows temperature dependence.

1.3 Nuclear spin-lattice relaxation rate : $1/T_1$

A nuclear spin relaxation is caused by the fluctuating component of hyperfine field, $\delta \boldsymbol{H}(t)$. The general formula of $1/T_1$ is shown as follows,

$$\frac{1}{T_1} = \frac{2\gamma_n^2 k_B T}{(\gamma_e \hbar)^2} \sum_q A_q A_{-q} \frac{\chi_\perp''(q, \omega_0)}{\omega_0} \tag{1.14}$$

where A_q is the hyperfine coupling constant between the nuclear spin and the q component of the electron spin density. As shown above, $1/T_1$ is probing q-averaged imaginary part of the dynamical susceptibility.[5]

Itinerant electron system

In the itinerant electron system, the nuclear relaxation rate $1/T_1$ described in eq.(1.14) is represented as follows,

$$\frac{1}{T_1} = \pi \gamma_n^2 \hbar \langle A_q A_{-q} \rangle N^2(E_F) k_B T \tag{1.15}$$

where $N(E_F)$ is the renormalized density of states at Fermi energy. The constant behavior of $1/T_1 T$ is often called Korringa law.[6]

Localized electron system

If we consider that each localized f electrons are fluctuating independently, eq.(1.14) can be replaced by

$$\frac{1}{T_1} \propto T\chi_0 \propto T\frac{C}{T+\theta} \tag{1.16}$$

Here, we consider that χ_0 obeys Currie-Weiss law. If θ is small, $1/T_1$ hardly shows temperature dependence.[7]

In NMR measurement, we can observe the crossover from the localized to itinerant f electrons in HF systems as shown in Fig.1.1.

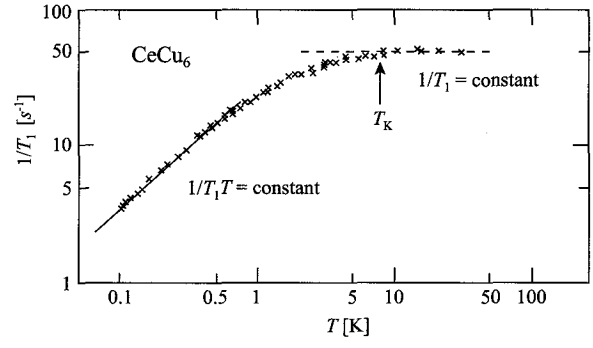

Figure 1.1: Temperature dependence of $1/T_1$ in $CeCu_6$.[8] Dashed (Solid) line represents the relation $1/T_1 =$ constant ($1/T_1T =$ constant).

1.4 Nuclear spin-lattice relaxation in the superconducting state

In the SC state, nuclear spin-lattice relaxation is caused by thermally excited quasi-particles above SC gap. Therefore, temperature dependence of $1/T_1$ is affected by SC gap structure. The gap structures in s-wave (BCS[9]) and p-wave (BW,[10] ABM,[11,12] polar) superconducting state are shown below.

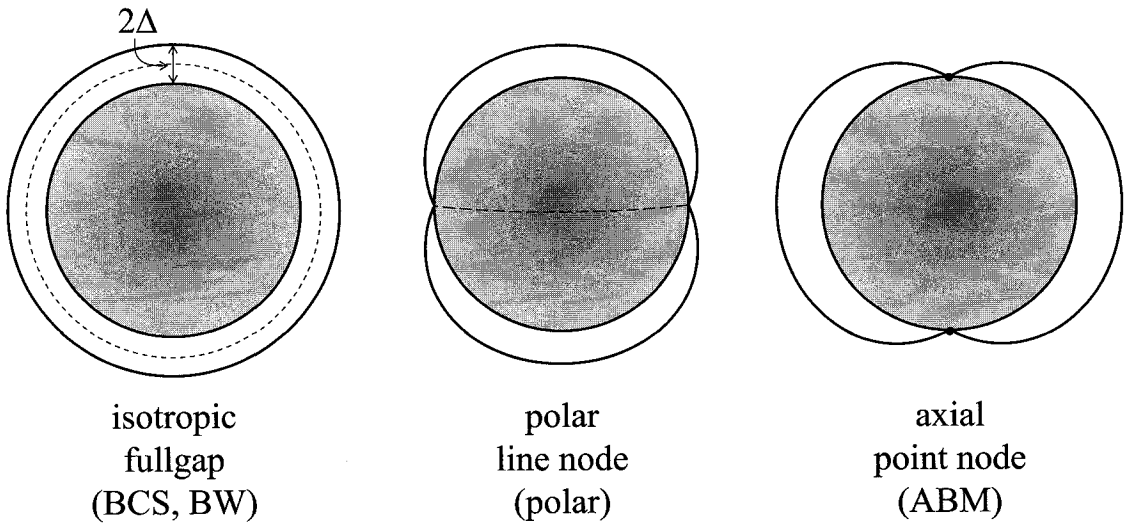

Figure 1.2: SC energy gap for BCS and BW (isotropic), ABM (axial), polar state.

The BCS and BW state have isotropic energy gap with no node. The ABM and polar state have gap zero nodes at point (line). In BCS and BW state, using the energy gap $\Delta(\theta,\phi)=\Delta$, the density of state is given by,

$$N_{\rm isotropic}(E)=\begin{cases}\frac{N(0)E}{\sqrt{E^2-\Delta^2}} & (|E|\geq\Delta)\\ \\ 0 & (|E|<\Delta)\end{cases} \tag{1.17}$$

In polar state, using the energy gap $\Delta(\theta,\phi)=\Delta\cos\theta e^{i\phi}$, the density of state is given by,

$$N_{\rm polar}(E)=\begin{cases}\frac{\pi}{2}\frac{N(0)E}{\Delta} & (|E|<\Delta)\\ \\ \frac{N(0)E}{\Delta}\sin^{-1}\frac{\Delta}{E} & (|E|\geq\Delta)\end{cases} \quad \cdots \text{ Line nodes} \tag{1.18}$$

In ABM state, using the energy gap $\Delta(\theta,\phi)=\Delta\sin\theta e^{i\phi}$, the density of state is given by,

$$N_{\rm ABM}(E)=\frac{N(0)E}{2\Delta}\ln\left|\frac{E+\Delta}{E-\Delta}\right| \quad \cdots \text{ Point nodes} \tag{1.19}$$

The density of states of quasi-particles with isotropic gap, line and point nodes are shown in Fig.1.3.

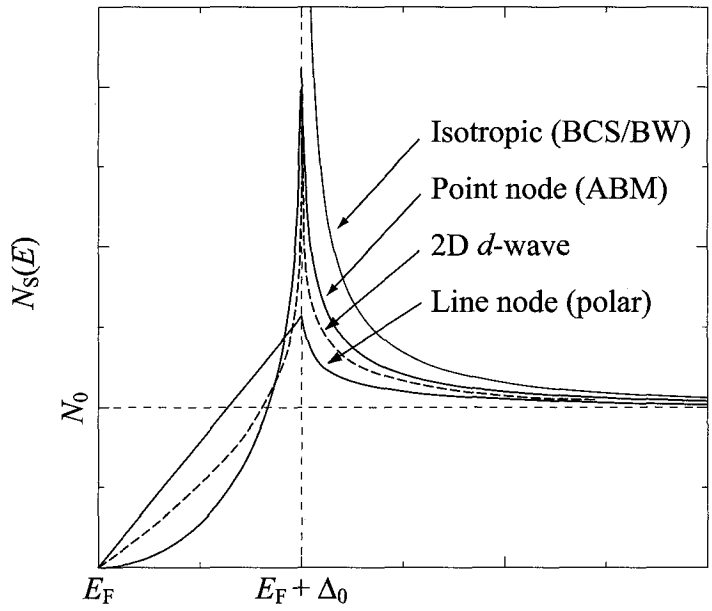

Figure 1.3: The density of state in the SC state for isotropic s-wave, anisotropic p-wave, and 2D d-wave, respectively.

The nuclear spin-lattice relaxation rate $1/T_1$ in the SC state is represented as follows,

$$\frac{1}{T_1} = \frac{\pi A^2}{\hbar}\int_0^\infty\int_0^\infty\left(1+\frac{\Delta^2}{EE'}\right)N_s(E)N_s(E')f(E)(1-f(E'))\delta(E-E')dEdE' \quad (1.20)$$

$$= \frac{2\pi A^2}{\hbar}\int_0^\infty\left[N_s^2(E)+M_s^2(E)\right]f(E)(1-f(E))dE \quad (1.21)$$

$$M_s(E) = \frac{N(0)}{4\pi}\int_0^{2\pi}\int_0^{\pi}\frac{\Delta(\theta,\phi)}{\sqrt{E^2-\Delta^2(\theta,\phi)}}\sin\theta d\theta d\phi \quad (1.22)$$

Here, $N_s(E)$ is shown in eq.(1.17), (1.18) and (1.19). $M_s(E)$ is called anomalous density of state and originated in the coherence effect. In the BCS superconductor, since $N_s(E)$ and $M_s(E)$ diverge at $E\sim\Delta$, $1/T_1$ indicates large enhancement just below T_C as shown in Fig.1.4. It is called coherence peak or Hebel-Slichter peak.[13] For the anisotropic superconducting state include BW state, the term Δ^2/E^2 in the coherence factor disappears. Therefore, $1/T_1$ is affected only $N_s(E)$. Since the coherence factor is 1 and the divergence of DOS at $E\sim\Delta$ is weak, the enhancement of $1/T_1$ just below T_C is much smaller than the BCS superconductivity and moreover in case of a maximum energy gap is large, the enhancement is suppressed. At low temperature where $T\ll T_C$ or $E\ll\Delta_0$, $1/T_1$ obeys the power law as follows,

$$\frac{1}{T_1} = \begin{cases} e^{-\frac{\Delta}{k_B T_C}} & : \text{fullgap} \\ T^3 & : \text{line node} \\ T^5 & : \text{point node} \\ T & : \text{gapless} \end{cases} \quad (1.23)$$

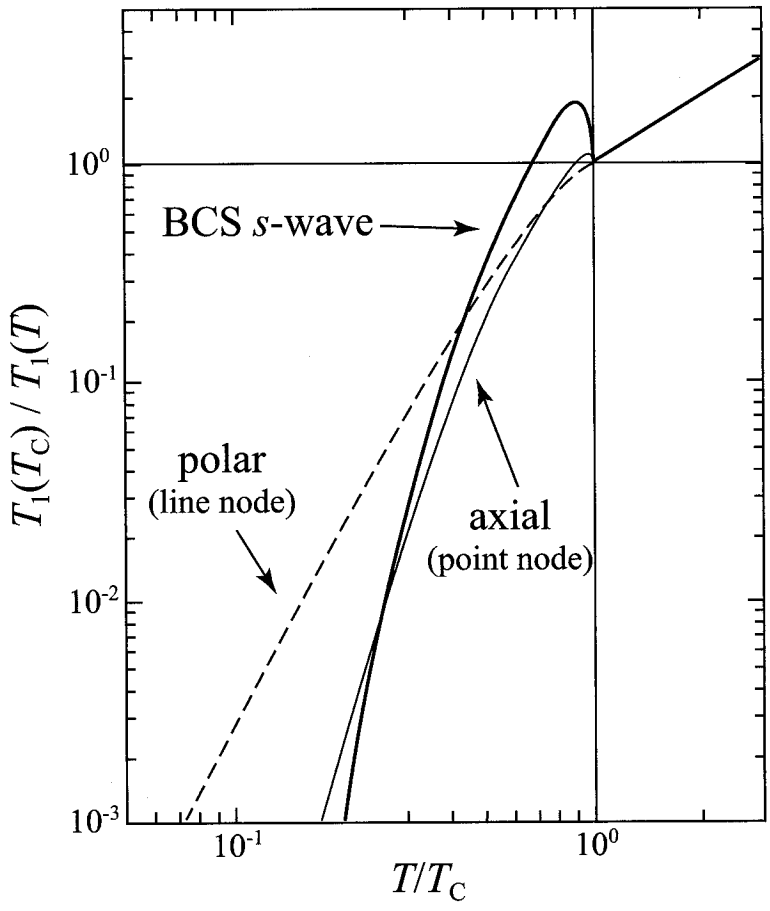

Figure 1.4: Temperature dependence of $1/T_1$ in SC state for isotropic s-wave SC and anisotropic p-wave SC.

Bibliography

[1] W. D. Knight : "Electron Paramagnetism and Nuclear Magnetic Resonance in Metals", in *Solid State Physics*, Vol. 2, ed. by F. Seitz, D. Turnbull (Academic, New York 1956) pp.93-136

[2] R. Kubo, and Y. Obata, J. Phys. Soc. Jpn. **11**, 547 (1956).

[3] J. A. Seitchik, A. G. Gossard, and V. Jaccarino, Phys. Rev. **136A**, 119 (1964).

[4] A. M. Clogston, A. C. Gossard, and Y. Yafet, Rev. Mod. Phys. **36**, 170 (1964).

[5] T. Moriya, J. Phys. Soc. Jpn. **18**, 516 (1963).

[6] J. Korringa, Physica **16**, 601 (1950).

[7] T. Moriya, Prog. Theort. Phys. (Kyoto), **16**, 23 (1956), **16**, 641 (1956).

[8] Nuclear Magnetic Resonance in Heavy Fermion systems : Theoretical and Experimental Aspects of Valence Fluctuations and Heavy Fermions, eds. L. C. Gupta and S. K. Malik (Plenum, 1987) 297, Y. Kitaoka, K. Ueda, T. Kohara, Y. Kohori, and K. Asayama.

[9] J. Bardeen, L. Cooper, and J. R. Schrieffer, Phys. Rev. **108**, 1175 (1957).

[10] R. Balian, and N. R. Werthamer, Phys. Rev. **131**, 1553 (1963).

[11] P. W. Anderson, and P. Morel, Phys. Rev. **123**, 1911 (1961).

[12] P. W. Anderson, and W. F. Brinkman, Phys. Rev. Lett. **30**, 1108 (1973).

[13] L. C. Hebel, and C. P. Slichter, Phys. Rev. **113**, 1504 (1959).

[14] Nuclear Magnetic Resonance in Itinerant Electron system : Magnetism and Superconductivity (Shokabo, 2002) K. Asayama.

Chapter 2

Equipments

2.1 NMR spectrometer

NMR and NQR measurement were carried out by the spin-echo method using a conventional type spectrometer. We used home-made type spectrometer with super-heterodyne system and commercial double super-heterodyne system spectrometer.[1] The block diagram of a super-heterodyne system is shown in Fig.2.1. The resonance circuit used for NMR/NQR measurement is also shown in Fig.2.2. The series resonance circuit was used below 40MHz and the parallel resonance circuit was used above 40MHz. In order to take impedance matching from power amplifier to NMR circuit and NMR circuit to receiver, duplexer is used in the parallel circuit. In the series circuit, we use home-made type narrow band pre-amplifier and take matching using both NMR/NQR probe and pre-amplifier.

The NMR spectrum was obtained by integrating the spin-echo intensity using box-car integrator as a function of external field at fixed frequency. The NQR spectrum was obtained by measuring the spin-echo intensity as a function of frequency in the zero field. Nuclear spin-lattice relaxation time T_1 was measured by the saturation recovery method.

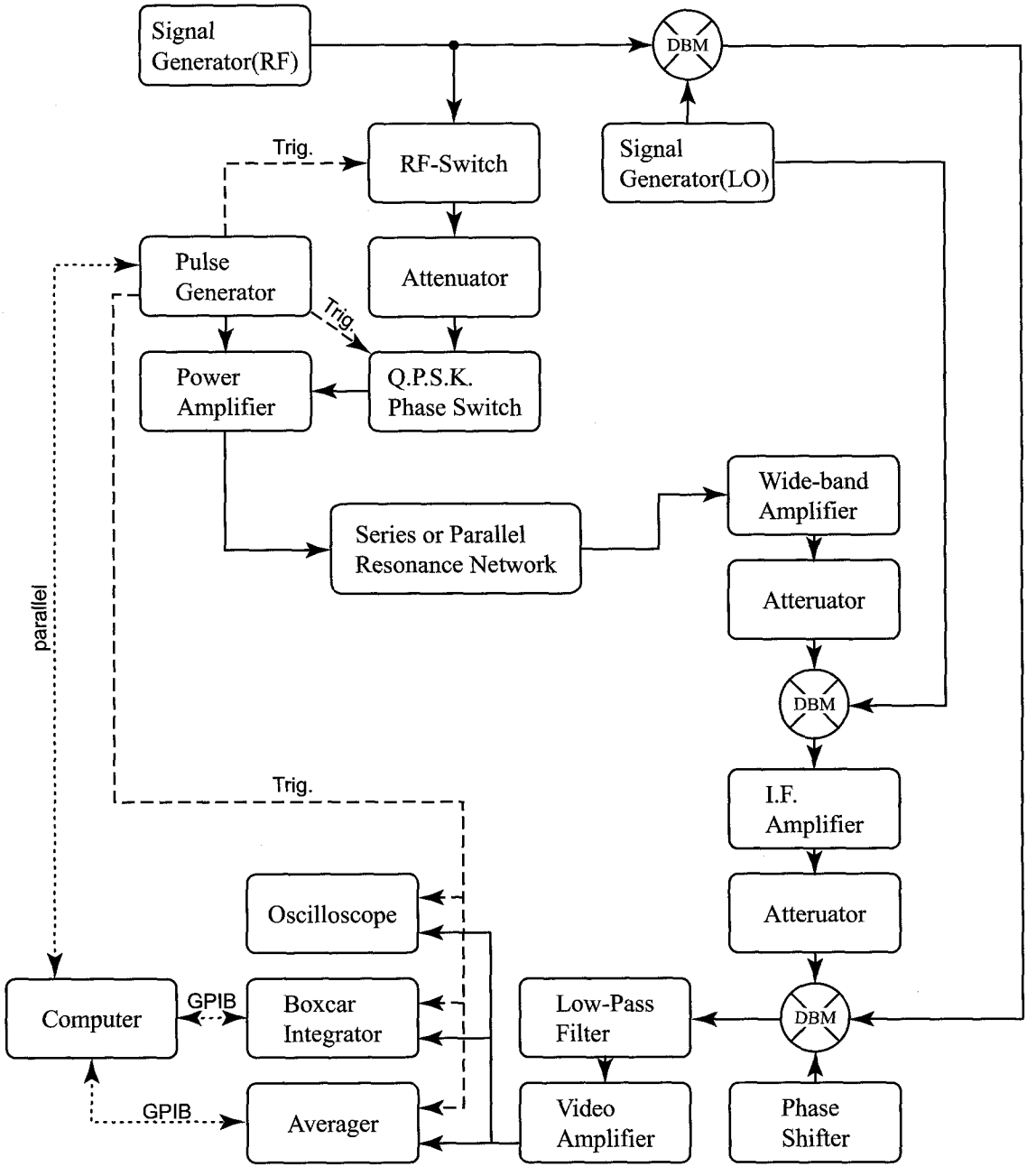

Figure 2.1: NMR/NQR block diagram.

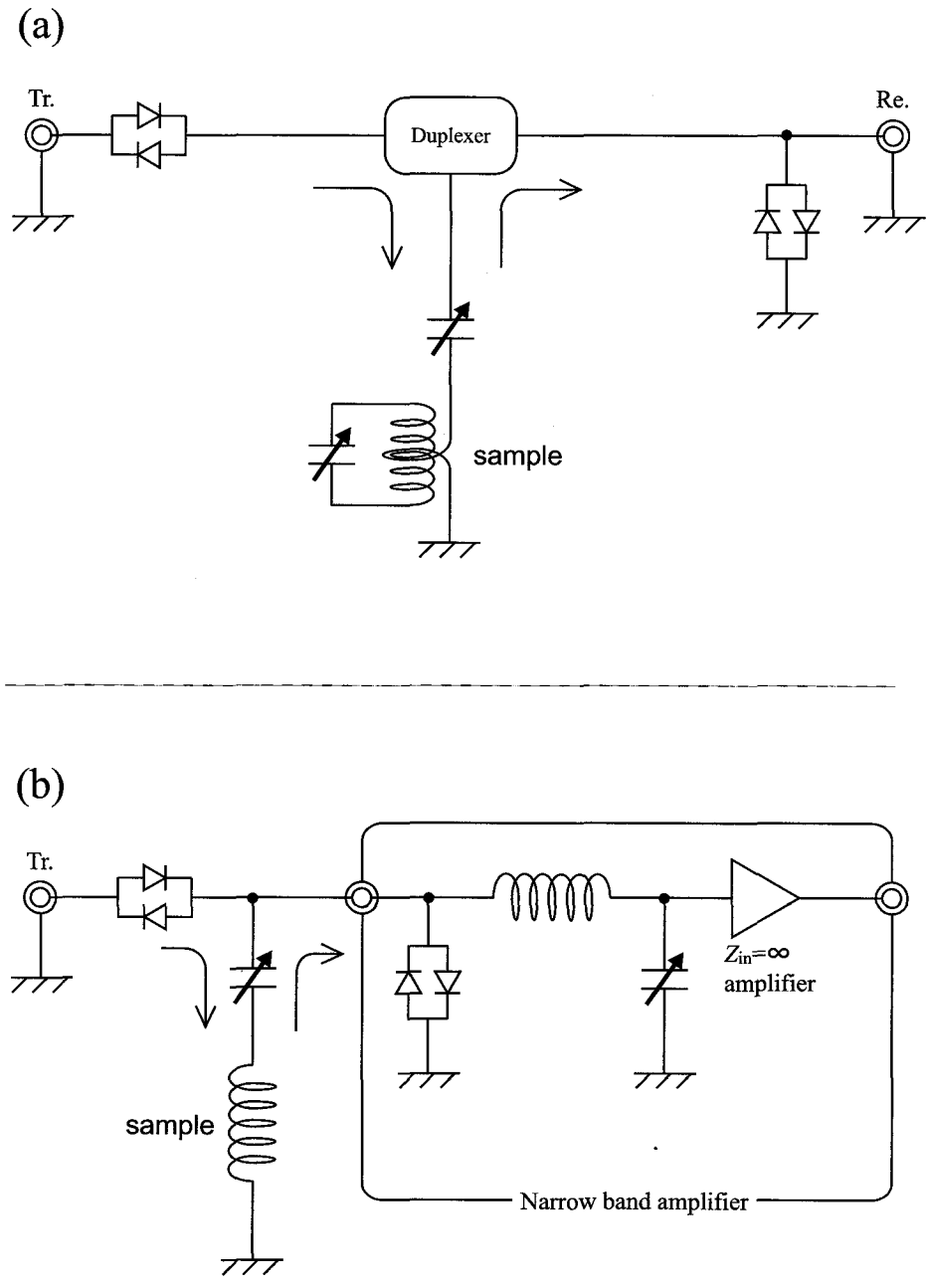

Figure 2.2: Resonance circuit for NMR/NQR. (a) Parallel circuit. (b) Series circuit.

2.2 Magnetic field and low temperature

In order to measure at a high magnetic field and low temperature for a long time, Cryostat made from stainless steel is used. The solenoid coil type superconducting magnet made by Oxford Instruments is shown in Fig.2.3.[2] Inhomogeneity of the magnetic field at the center of superconducting magnet is less than 10^{-5}, which guarantees the precise Knight shift measurement. We can measure nuclear spin-lattice relaxation time T_1 and Knight shift in the wide temperature range of $T = 0.1 - 300$ using this superconducting magnet and ^{3}He-^{4}He dilution refrigerator.[3]

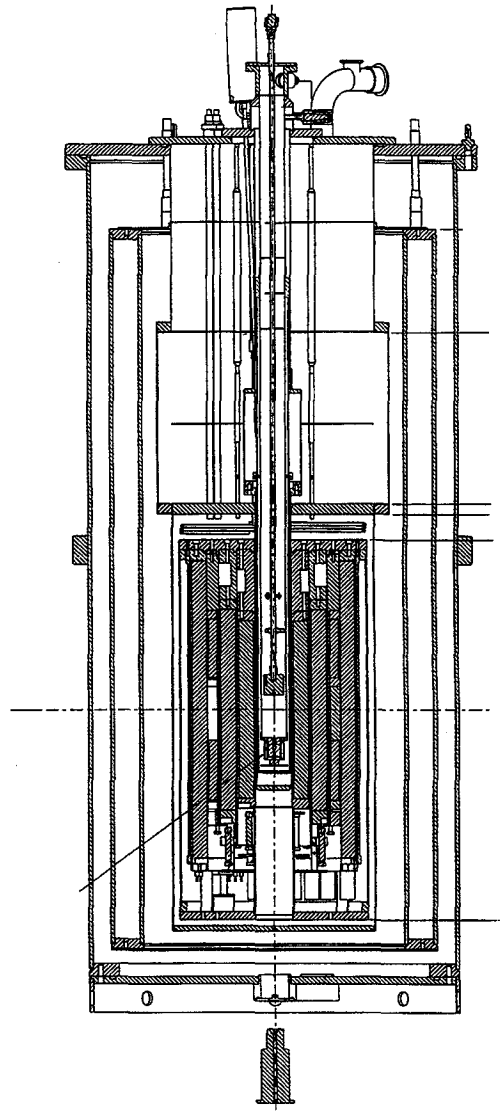

Figure 2.3: Cryostat for NMR measurement.

Bibliography

[1] Thamway Co.,Ltd.
http://www.thamway.co.jp/

[2] Oxford Instruments plc
http://www.oxford-instruments.jp/

[3] Taiyo Toyo Sanso Co.,Ltd.
http://www.saan.co.jp/

Part II

Pt and Si NMR Studies of $CePt_3Si$

Chapter 1

Introduction

1.1 Discovery of Unconventional Superconductors

The SC mechanism of conventional superconductors such as Al, Nb was explained by the Bardeen-Cooper-Schrieffer (BCS) theory. The BCS theory predicted that the onset of s-wave spin-singlet superconductivity is based on bound electron pairs coupled by deformation of lattice via the electron-phonon interaction.[1] Over the past few decades, a considerable number of superconducting (SC) materials have been discovered in strongly correlated matters where order parameter (OP) symmetries are different from s-wave spin-singlet superconductors. Since the discovery of the first unconventional superconductivity in a heavy-fermion (HF) compound, $CeCu_2Si_2$.[10] Besides Ce- or U-based HF superconductors (HFS), there is a lot of unconventional superconductors such as high-T_C cuprate superconductors, ruthenates (Sr_2RuO_4), ferromagnetic superconductors (UGe_2, URhGe)) and so on.[3–7] It is widely believed that the bound electron pairs in these materials are mediated by magnetic fluctuations. For example, high-T_C superconductors are believed to have a d-wave symmetry with an line-node energy-gap on the Fermi surface, mediated by antiferromagnetic (AFM) spin fluctuations.[8,9]

Two prototypical Ce-based HF superconductors are known to date, including the pressure induced ones: CeT_2M_2 series that crystallize in the tetragonal $ThCr_2Si_2$ structure (see Fig. 15) such as $CeCu_2Si_2$, $CeCu_2Ge_2$, $CePd_2Si_2$, $CeNi_2Ge_2$ and $CeRh_2Si_2$.[10–13] The isostructural compounds CeM_2X_2 with M = Ru, Ni, Pd, Cu, Ag, Au and X = Si, Ge exhibit a great variety of electronic and magnetic properties, allowing to clarify an interplay between the formation of magnetic order and HF behavior. The another one is $Ce_nM_mIn_{3n+2m}$ series. They belong to the broader family of materials $Ce_nM_mIn_{3n+2m}$ which can be considered as built from '$CeIn_3$' and 'MIn_2' layers stacked along the tetragonal c-axis displayed in Fig.1.1. The $n = \infty$ compound $CeIn_3$ crystallizes in the cubic $AuCu_3$ structure. $CeIn_3$ reveals from an AFM to SC transition as a function of pressure, and show the coexistence of AFM order and unconventional superconductivity under a critical pressure.[14,15] The structurally layered compounds $CeMIn_5$ crystallize in the tetragonal $HoCoGa_5$-structure. The compounds $CeMIn_5$ (M = Co, Ir, Rh) are a new family of HF systems which exhibit a SC transition at ambient pressure, including $CeCoIn_5$ with a highest transition temperature $T_C = 2.3$ K to date among HFS.[16–18] The discovery of this new class of HF compounds has also opened a way to systematically investigate an evolution from

the AFM to SC state as a function of pressure on $CeRhIn_5$.[19,20]

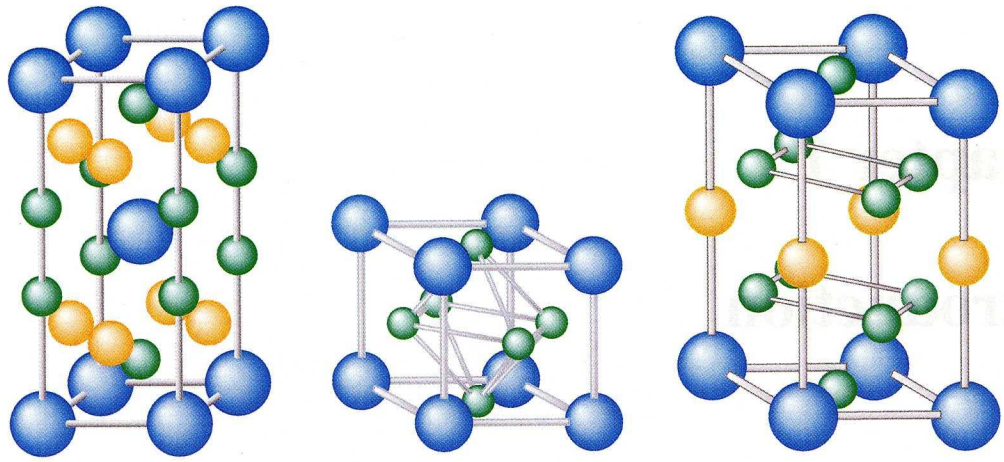

$ThCr_2Si_2$ - type $AuCu_3$ - type $HoCoGa_5$ - type

Figure 1.1: Conventional unit cell of the $ThCr_2Si_2$ structure and $Ce_nM_mIn_{3n+2m}$ structures with $n = \infty$ ($CuAu_3$ type) and 1 ($HoCoGa_5$ type).

In almost all previous studies on HFS including these new family, the crystal has an inversion center, which makes it possible to consider the even (spin-singlet) and odd (spin-triplet) components of the superconducting (SC) order parameter (OP) separately.[21,22] Although this is the case in most superconductors, there are some exceptions. In this thesis, we deal with the new class of AFM HF compound $CePt_3Si$ with no inversion center.[23] The crystal structure is shown in later. The superconductivity in strongly correlated matters is expected to emerge even under the novel electronic state that is not yet taken into account so far.

Bibliography

[1] J. Bardeen, L. Cooper, and J. R. Schrieffer, Phys. Rev. **108**, 1175 (1957).

[2] F. Steglich, J. Aarts, C. D. Bredle, W. Lieke, D. Meschede, W. Franz, and H. Schäfer, Phys. Rev. Lett. **43**, 1892 (1979)

[3] J. G. Bednorz, and K. A. Müller, Z. Phys. B, **64**, 189 (1986).

[4] S. Uchida, H. Takagi, K. Kitazawa, and S. Tanaka, Jpn J. Appl. Phys., **26**, L1 (1987).

[5] Y.Maeno, H.Hashimoto, K.Yoshida, S.Nishizaki, T.Fujita, J.G.Bednorz, and F.Lichtenberg, Nature (London) **372**, 532-534 (1994).

[6] S. S. Saxena, P. Agarwal, K. Ahilan, F. M. Grosche, R. K. W. Hasselwimmer, M. J. Steiner, E. Pugh, I. R. Walker, S. R. Julian, P. Monthoux, G. G. Lonzarich, A. Huxley, I. Sheikin, D. Braithwaite, and J. Flouquet, Nature (London) **406**, 587 (2000).

[7] D. Aoki, A. Huxley, E. Ressouche, D. Braithwaite, J. Flouquet, J. -p. Brison, E. Lhotel, and C. Paulsen, Nature (London) **413**, 613 (2001).

[8] Y. Kitaoka, K. Ishida, S. Ohsugi, K. Fujiwara, G. -q. Zheng, and K. Asayama, J. Appl. Mag. Resonance **3**, 549 (1992).

[9] K. Asayama, Y. Kitaoka, G. -q. Zheng, and K. Ishida, Prog. NMR spectroscopy **28**, 221 (1996).

[10] D. Jaccard, K. Behnia, and J. Sierro, Phys. Lett. A **163**, 475 (1992).

[11] F. M. Grosche, S. R. Julian, N. D. Mathur, and G. G. Lonzarich, Physica B 223-224, 50 (1996).
S. R. Julian, C. Pfleiderer, F. M. Grosche, N. D. Mathur, G. J. McMullan, A. J. Diver, I. R. Walker, and G. G. Lonzarich, J. Phys.: Condens. Matter **8**, 9675 (1996).
F. M. Grosche, I. R. Walker, S. R. Julian, N. D. Mathur, D. M. Freye, M. J. Steiner, and G. G. Lonzarich, J. Phys.: Condens. Matter **13**, 2845 (2001).

[12] D. Braithwaite, T. Fukuhara, A. Demuer, I. Sheikin, S. Kambe, J. -p. Brison, K. Maezawa, T. Nakak, and J. Flouquet, J. Phys.: Condens. Matter **12**, 1339 (2000).

[13] R. Movshovich, T. Graf, D. Mandrus, M. F. Hundley, J. D. Thompson, R. A. Fisher, N. E. Phillips, and J. L. Smith, Physica B **223-224**, 126 (1996).
R. Movshovich, T. Graf, D. Mandrus, J. D. Thompson, J. L. Smith, and Z. Fisk, Phys. Rev. B **53**, 8241 (1996).

[14] N. D. Mathur, F. M. Grosche, S. R. Julian, I. R. Walker, D. M. Freye, R. K. W. Haselwimmer, and G. G. Lonzarich, Nature (London) **394**, 39 (1998).

[15] S. Kawasaki, T. Mito, G. -q. Zheng, C. Thessieu, Y. Kawasaki, K. Ishida, Y. Kitaoka, T. Muramatsu, T. C. Kobayashi, D. Aoki, S. Araki, Y. Haga, R. Settai, and Y. Onuki, Phys. Rev. B 65, 020504R (2002)

[16] H. Hegger, C. Petrovic, E. G. Moshopoulou, M. F. Hundley, J. L. Sarrao, Z. Fisk, and J. D. Thompson, Phys. Rev. Lett. **84**, 4986 (2000).

[17] C. Petrovic, R. Movshovich, M. Jaime, P. G. Pagliuso, M. F. Hundley, J. L. Sarrao, Z. Fisk, and J. D. Thompson, Europhys. Lett. **84**, 354 (2001).

[18] C. Petrovic, P. G. Pagliuso, M. F. Hundley, R. Movshovich, J. L. Sarrao, J. D. Thompson, Z. Fisk, and P. Monthoux, J. Phys.: Condens. Matter **13**, L337 (2001)

[19] T. Mito, S. Kawasaki, Y. Kawasaki, G. -q. Zheng, Y. Kitaoka, D. Aoki, Y .Haga, and Y. Ōnuki, Phys. Rev. Lett. **90**, 077004 (2003).

[20] S. Kawasaki, T. Mito, Y. Kawasaki, G. -q. Zheng, Y. Kitaoka, D. Aoki, Y. Haga, and Y. Ōnuki Phys. Rev. Lett. **91**, 137001 (2003).

[21] P. W. Anderson, J. Phys. Chem. Solids **11**, 26 (1959).

[22] P. W. Anderson, Phys. Rev. B **30**, 400 (1984).

[23] E. Bauer, G. Hilscher, H. Michor, Ch. Paul, E. W. Scheidt, A. Gribanov, Yu. Seropegin, H. Noël, M. Sigrist, and P. Rogl, Phys. Rev. Lett. **92**, 027003 (2004).

Chapter 2

The Pt- and Si-NMR studies of a new class of heavy fermion antiferromagnetic superconductor $CePt_3Si$ without inversion symmetry

2.1 Introduction

In almost all previous studies on superconductors, it was assumed that the crystal has an inversion center, which makes it possible to consider the even (spin-singlet) and odd (spin-triplet) components of the superconducting (SC) order parameter (OP) separately.[1,2] Although this is the case in most superconductors, there are some exceptions. In this thesis, we deal with the new heavy fermion (HF) compound $CePt_3Si$ with no inversion center that has been quite recently discovered. The structure of $CePt_3Si$ has some relevance with a cubic $AuCu_3$ structure where Si atoms occupy an interstitial space. As a result, a tetragonal distortion takes place in the unit cell. Then the crystal structure of $CePt_3Si$ belongs to the space group $P4mm$ (No.99), exhibiting an isotropic structure with the ternary boride compound $CePt_3B$ as shown in Fig.2.1.[3,4] Interestingly, it is unexpected that $CePt_3Si$ undergoes an antiferromagnetic (AFM) order at $T_N = 2.2$ K, followed by a SC transition at $T_C = 0.75$ K that was probed by the measurements of electrical resistivity $R(T)$ and specific heat C_p. As for the AFM order, $R(T)$ does not show any clear anomaly, but C_p/T indicates a distinct peak at T_N as shown in Figure 2.2.[4] A value in an entropy release at T_N is estimated to be as small as about $\Delta S = 0.22R\log 2$. This result seems to point to the development of Kondo-like interaction between $4f$ electrons and conduction electrons below 10 K that is evidenced from a logarithmic increase in C_p/T upon cooling below 10 K as well. Concerning the SC characteristics, although a jump in C_p/T at T_C is very small, exhibiting about $\Delta C_p/\gamma T_C \sim 0.25$, but very large value of Sommerfeld coefficient $\gamma = 400$ mJ/mol K^2 suggests that HF superconductivity (HFS) is realized in this compound. Furthermore, the evidence for the HFS is corroborated from the upper critical field H_{c2} vs T plot as shown in Figure 2.3: The H_{c2} at low T exceeds the usual Pauli paramagnetic limiting field, indicative of a possibility of a spin-triplet pairing realized. But from a general argument that a lack of in-

version center does not always allow for a spin-triplet pairing to be stable, therefore, Bauer and co-workers suggest a mixing SC state of spin-singlet and spin-triplet pairing might be realized in this compound.[4]

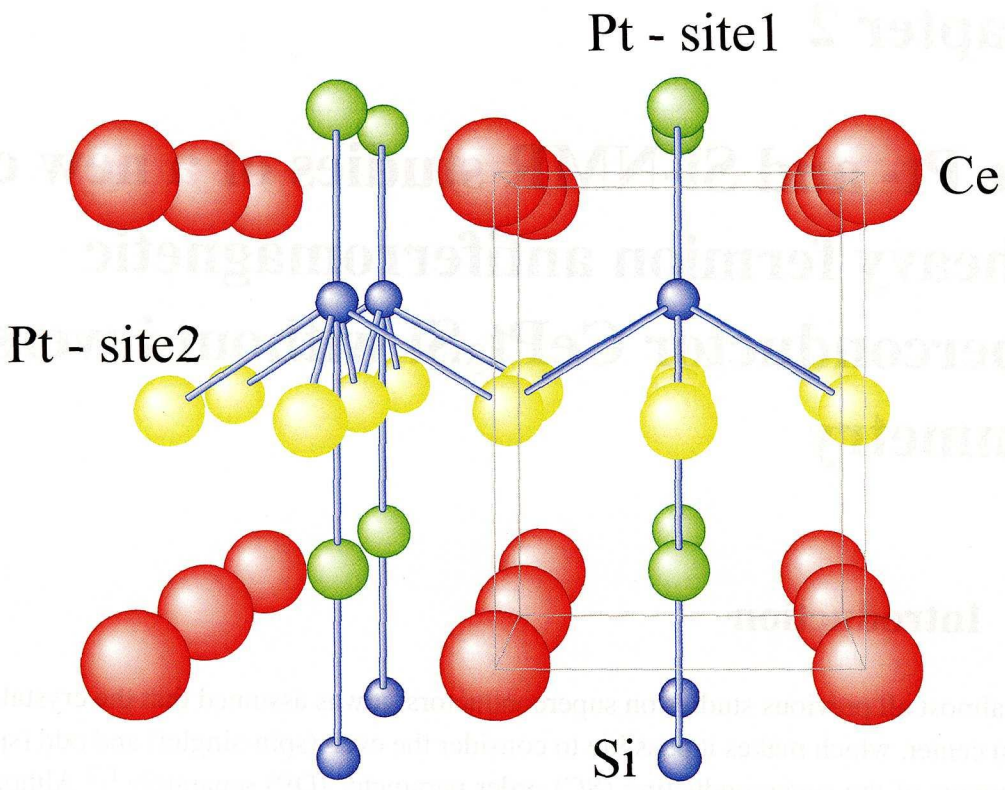

Figure 2.1: Crystal structure of $CePt_3Si$ which belongs to the space group $Pm44$(No.99).[3,4]

Very recently, neutron scattering experiment has reported magnetic properties on $CePt_3Si$.[5] The AFM Bragg reflection was observed at a wave vector $\mathbf{Q}$ =(0, 0, 1/2) and (1, 0, 1/2), indicating that Ce-4f derived magnetic moments $\sim 0.3\mu_B$/Ce at $T = 1.8$ K lies ferromagnetically in the c-plane and stacked antiferromagnetically along the c-axis as shown in Figure 2.4. Its size is very smaller than a value that is expected from a Ce^{3+} crystal electric field (CEF) ground state with either Γ_7 or Γ_6 Kramers doublet in the tetragonal point symmetry, which suggests that the Kondo-like interaction becomes effective to reduce the size of the AFM moments expected from a localized picture. This is consistent with the result of specific-heat measurement that indicates the small change in entropy release at T_N as mentioned above.[4] The neutron scattering experiment has provided information for a CEF energy scheme as displayed in Figure 2.4.[5] A remarkable finding is that the well defined CEF excitations are observed in this compound. Usually, it is believed that no well defined CEF excitations may be observed if $4f$ electrons are hybridized with conduction electrons to form heavy quasi-particles. A similar case was reported in the first Pr-$4f^2$-derived HF superconductor $PrOs_4Sb_{12}$.[6] In this case, it was revealed from the band calculations and the de Haas-van Alphen effect measurement that $4f$ electrons are almost localized.[7]

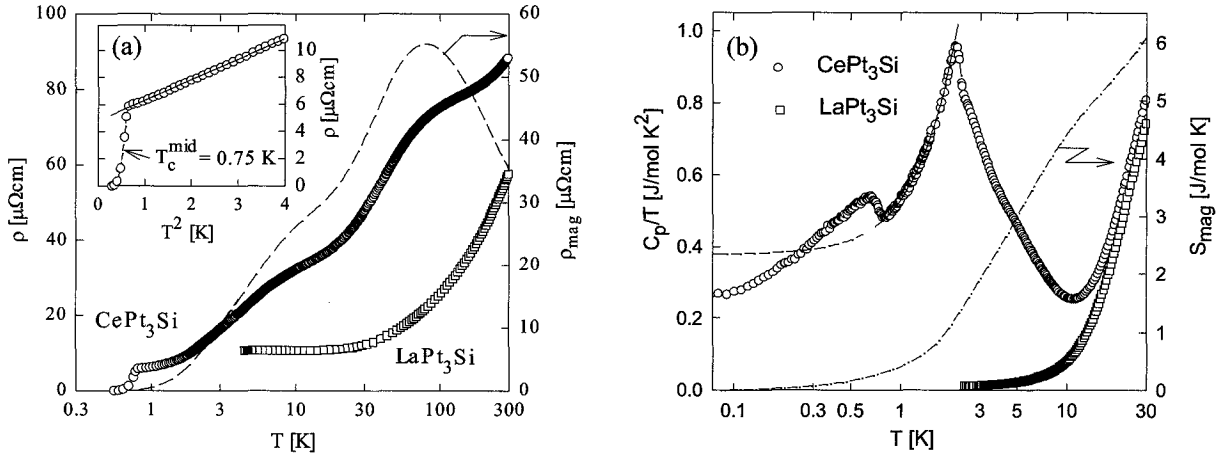

Figure 2.2: (a) The T dependence of electrical resistivity $R(T)$ of $CePt_3Si$ and $LaPt_3Si$. (b) The T dependence of specific C_p of $CePt_3Si$ and $LaPt_3Si$ where C_p/T is plotted as a function of $\ln T$.[4]

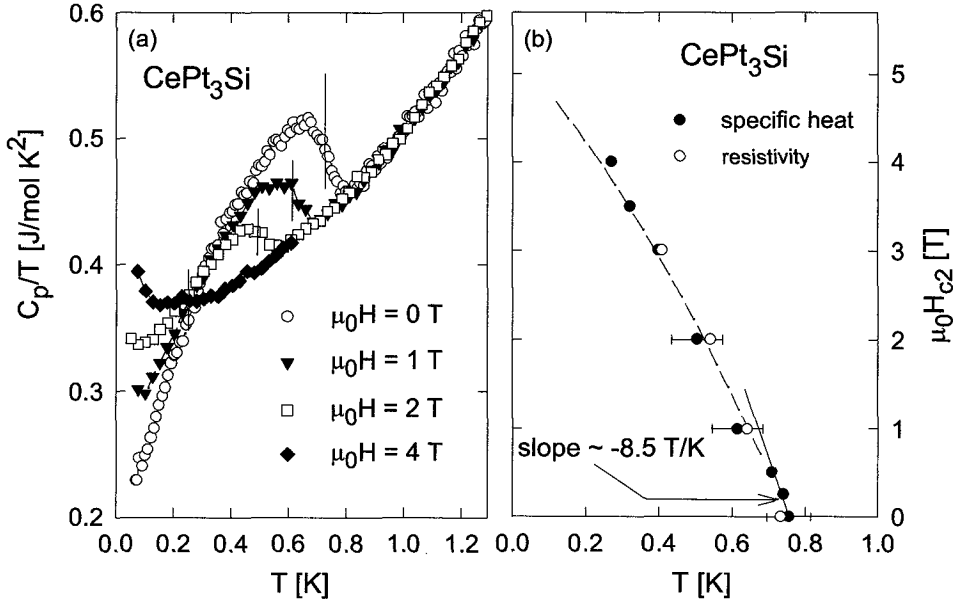

Figure 2.3: (a) The T dependence of C_p/T at low T near T_C for various external magnetic fields. (b) The T dependence of the upper critical field H_{c2} determined by the measurements of $R(T)$ and C_p/T.[4]

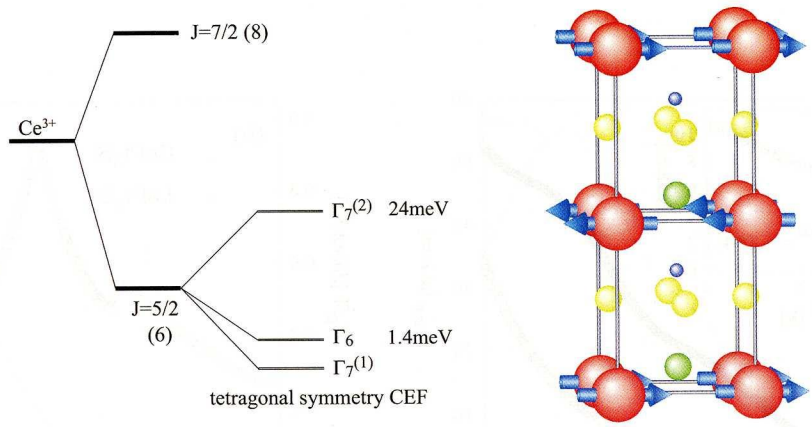

Figure 2.4: Left figure: Crystal electric field (CEF) energy scheme for $CePt_3Si$. Right figure : Magnetic structure of $CePt_3Si$. The Ce magnetic moments lie ferromagnetically in the c-plane and stacked antiferromagnetically along the c-axis.[5]

In order to gain an insight into a possible OP symmetry in $CePt_3Si$ without inversion symmetry, several theoretical works have been put forth thus far. P. Frigeri *et al.* have shown that in contrast to common believe, spin-triplet pairing is not entirely excluded in such systems.[8] Moreover, the Pauli paramagnetic limit in $H_{c2}(0)$ was analyzed for both spin-singlet and spin-triplet pairing. $CePt_3Si$ has a possibility of p-wave spin-triplet pairing state ($\boldsymbol{d}(\boldsymbol{k}) = \hat{\boldsymbol{x}}k_y - \hat{\boldsymbol{y}}k_x$), that can explain the absence of the Pauli paramagnetic limit reported by Bauer *et al.* On the other hand, noting that its superconductivity emerges under the background of AFM ordering, it seems more natural to assume a spin-singlet type of pairing, and they argue, in this case, the Pauli paramagnetic limit is rendered less effectively by the presence of spin-orbit coupling arising from broken inversion center. The study by the band calculation reveals that a possible gap structure of $CePt_3Si$ depends on the dimensionality of SC OP, and if the SC OP corresponds to a one-dimensional representation, then the gap has line nodes where the Fermi surface crosses the high-symmetry planes or the boundaries of the Brillouin zone.[9]

In this section, we report microscopic study of $CePt_3Si$ via the measurements of nuclear magnetic resonance (NMR) of ^{195}Pt and ^{29}Si. Their nuclear parameters are shown in Table 2.1. The advantage of NMR is that the magnetic and electronic properties can selectively measure at each atomic site. $CePt_3Si$ has two Pt sites and one Si site. Our aim is to clarify novel magnetic and SC characteristics inherent to the first superconductor $CePt_3Si$ without inversion symmetry and provide microscopic evidence for the co-existence of antiferromagnetism and superconductivity in $CePt_3Si$.

Table 2.1: The nuclear parameters of ^{195}Pt and ^{29}Si.

nuclei	Nuclear Spin	gyromagnetic ratio (MHz/T)	Natural Abundance (%)
^{195}Pt	1/2	9.153	33.8
^{29}Si	1/2	8.4578	4.7

2.2 Sample preparation

Two polycrystalline samples were used for the NMR measurements in this work. One of those supplied by E. Bauer *et al*. was prepared by arc melting under argon atmosphere and a subsequent heat treatment under high vacuum at 870°C for three weeks.[4] Another samples provided by Y. Ōnuki *et al*. were synthesized by arc-melting under argon atmosphere using 99.9% - pure Ce, 99.99%-Pt and 99.999%-Si in the stoichiometric proportion. Single crystals were successfully prepared by both the pulling method in a tetra-arc furnace and mineralization.[5] The X-ray diffraction measurement indicates that all the samples used here are well characterized to consist of a single phase. The AFM and SC transition temperatures are confirmed from the measurements of resistivity $R(T)$ and specific heat $C_p(T)$. For the ^{195}Pt and ^{29}Si-NMR measurements, the samples are crushed into powder to make rf-field penetrate easily.

Table 2.2: The status of the samples used for the Pt and Si-NMR measurement

			weight	NMR frequency
sample A	:	powdered polycrystalline	$\sim$ 10mm^3	46.2, 18.1, 8.9 MHz
sample B	:	powdered single crystal	$\sim$ 50mm^3	18.1, 8.9 MHz

Fig.2.5 displays Pt-NMR spectrum at 8.9 MHz for the powder oriented along the c-axis parallel to magnetic field H. $CePt_3Si$ has two Pt sites (see the inset of 2.5) that occupy inequivalent crystallographic sites. One of Pt sites (green circle) is surrounded by four Ce atoms in the ab plane, labeled as site-I and another one (yellow circle) as site-II. The respective full-width-half-maximum (FWHM) in the Pt-NMR spectral shape are as small as 25 and 8 Oe at the site-I and site-II, assuring that the samples are well characterized.

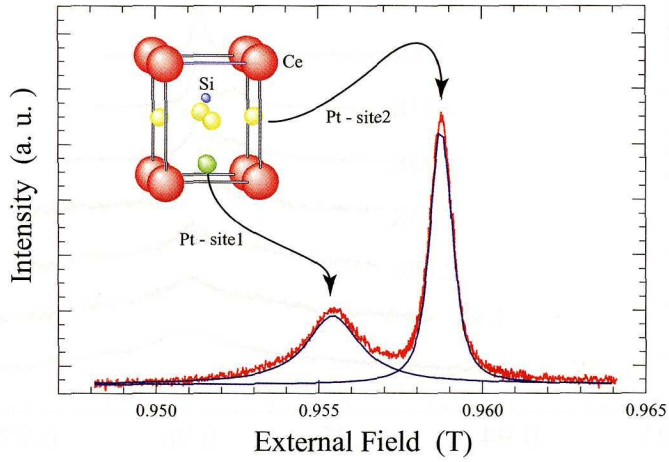

Figure 2.5: The Pt-NMR spectrum of the sample B at 4.2 K.

2.3 Results and Discussions

2.3.1 The ^{195}Pt-NMR study

NMR spectrum

Fig.2.6 indicates the T dependence of Pt-NMR spectrum at 8.9 MHz for the oriented powder $CePt_3Si$. In the paramagnetic state above $T_N \sim 2.2$ K, the Pt-NMR spectra at the site-I and -II exhibit no significant change and positive values of Knight shift. Below T_N, however, their FWHM's actually start to be increased, associated with the appearance of internal field due to the onset of AFM order. As a result, the spectra arising from the site-I and -II overlap below T_N. Note that the peak in the spectrum below T_N is mainly assigned to the site-II from the overall T dependence of the spectrum below T_N.

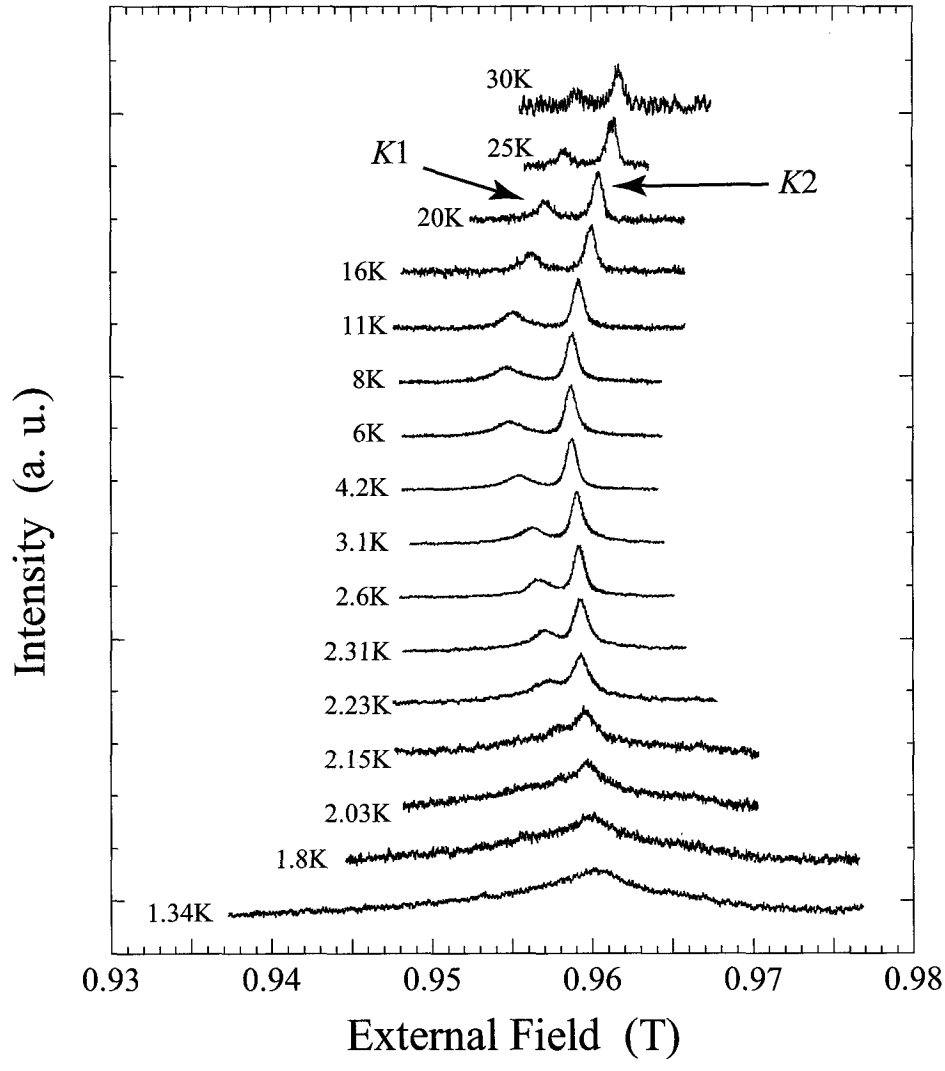

Figure 2.6: The T dependence of Pt spectrum for the oriented powder of $CePt_3Si$ with H parallel to the c-axis at 8.9 MHz.

Fig.2.7 indicates the T dependencies of Knight shifts $K1(T)$ and $K2(T)$ at the site-I and -II that were measured at 8.9 MHz ($H \sim 1$ T), 18.1 MHz ($H \sim 2$ T) and 46.2 MHz (~ 5 T). $K1$ and $K2$ increase upon cooling, exhibiting a peak around 7 K. It should be noted that $K1$ and $K2$ depend on H, and the peaks in their T dependencies shift to lower temperatures as H increases. These H and T variations of $K1$ and $K2$ would be naturally expected from the CEF energy scheme where the energy separation ΔE_1 is as small as $\Delta E_1 \sim 1.4$ meV (16 K) between the ground state doublet and the first excited doublet.

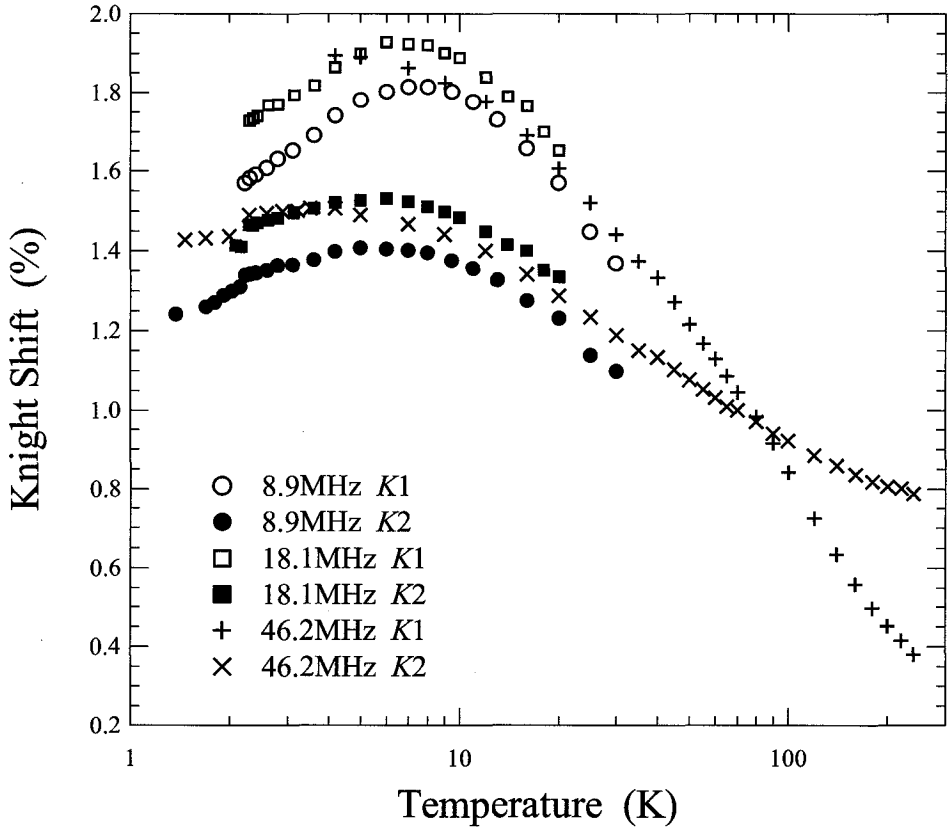

Figure 2.7: The T dependence of Knight shift $K1$ and $K2$ for the site-I and -II at 8.9 MHz ($H \sim 1$ T), 18.1 MHz (~ 2 T) and 46.2 MHz (~ 5 T).

In general, Knight shift K is related to magnetic susceptibility χ. Therefore, the Knight shift is plotted against the magnetic susceptibility with temperature as an implicit parameter.[10] Since $K1$ and $K2$ depend on H, χ does too. However, at present, the available data of χ on polycrystalline samples are measured at a small H by means of a SQUID magnetometer. Accordingly, a $K-\chi$ plot was tentatively performed using this χ data at low H. Fig.2.8 (a) presents the $K1-\chi$ and $K2-\chi$ plots at $f = 46.2$ MHz. The hyperfine-coupling constant H_{hf} obtained from the slope in $K-\chi$ plots at various frequencies is listed up in Table 2.3. The $K-\chi$ plots at low temperatures at various frequencies are shown in Fig.2.8 (b). It is anticipated that the H dependence of H_{hf} arises from that of the magnetic susceptibility associated with the presence of low-lying CEF level. In this context, the H_{hf} inherent to the HF state at low T,

where AFM and SC orders occur, should be determined by K vs χ plot at fields significantly lower than $\Delta E_1 \sim 1.4$ meV, or 1.5 T and furthermore, at temperatures lower than $\Delta E_1 \sim 1.4$ meV, i.e. 16 K. At present, there are not yet reliable data to deduce H_{hf} at the HF state realized at low T.

Table 2.3: Hyperfine-coupling constant (H_{hf}) at Pt site-I and -II at various frequencies or magnetic field in the given T range.

Frequency (MHz)	46.2	46.2	8.9	18.1
Temperature (K)	240-80	40-7	6-3.6	6-3.6
H_{hf} site-I (kOe/μ_B)	9.6	6.7	113.2	105.6
H_{hf} site-II (kOe/μ_B)	2.9	4.2	30.668	23.4

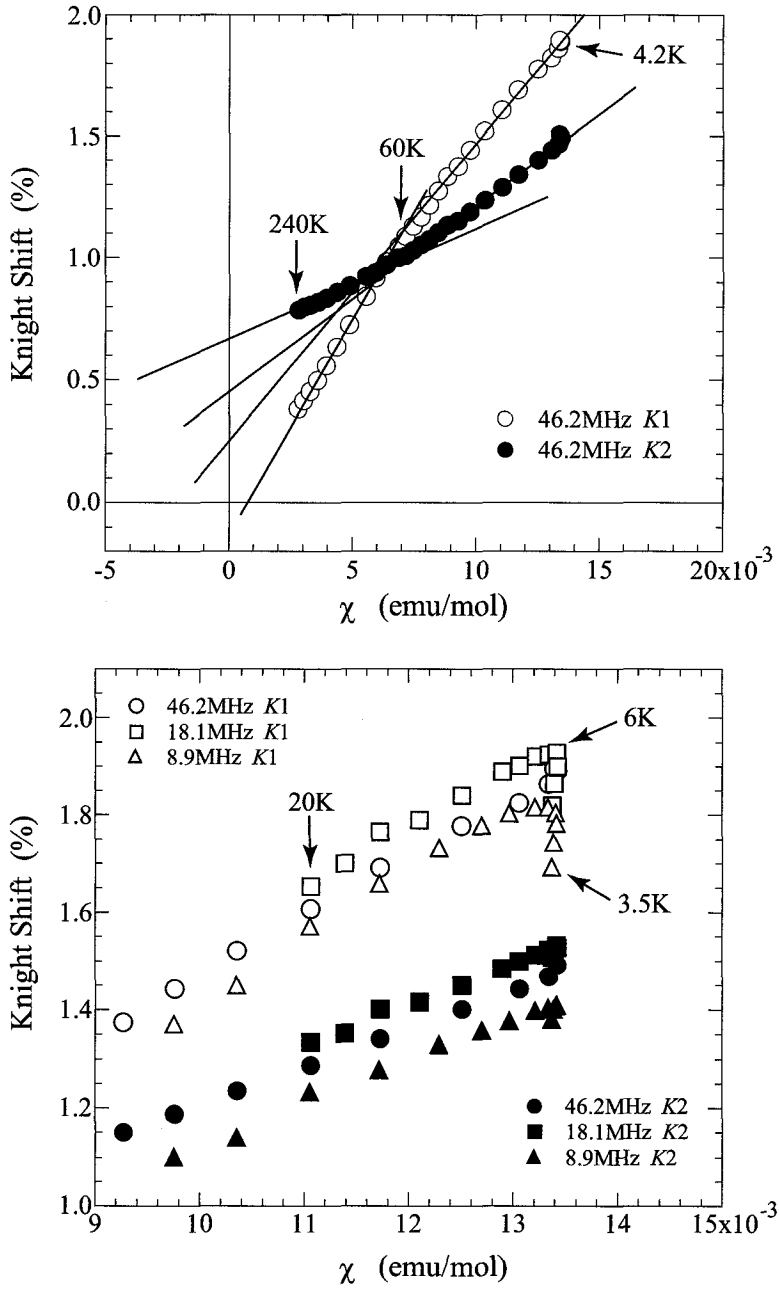

Figure 2.8: (a) $K-\chi$ plot at $f = 46.2$ MHz in the range of $T = 4.2-240$ K. (b) $K-\chi$ plots at various frequencies at low temperatures. Here note that the susceptibility data were taken at a very low field by means of a SQUID magnetometer.

Nuclear spin-lattice relaxation time T_1

Fig. 2.9 demonstrates recovery curves of nuclear magnetization of ^{195}Pt at the site-I and II. Since Pt nuclei has a nuclear spin $I = 1/2$, it follows a simple exponential form given by

$$\frac{M(\infty) - M(t)}{M(\infty)} = \exp(-t/T_1) \tag{2.1}$$

where $M(\infty)$ and $M(t)$ are the nuclear magnetization in the thermal equilibrium condition and at a time t after the saturation pulse, respectively. $1/T_1$ is uniquely determined with a single component above T_C. The solid lines in the figure are a best fit of the data to a single exponential curve. At temperatures well below T_C, however, two components in T_1 appear: a long component is attributed to an intrinsic relaxation, whereas a short one arises from the presence of vortex core induced by applying H.

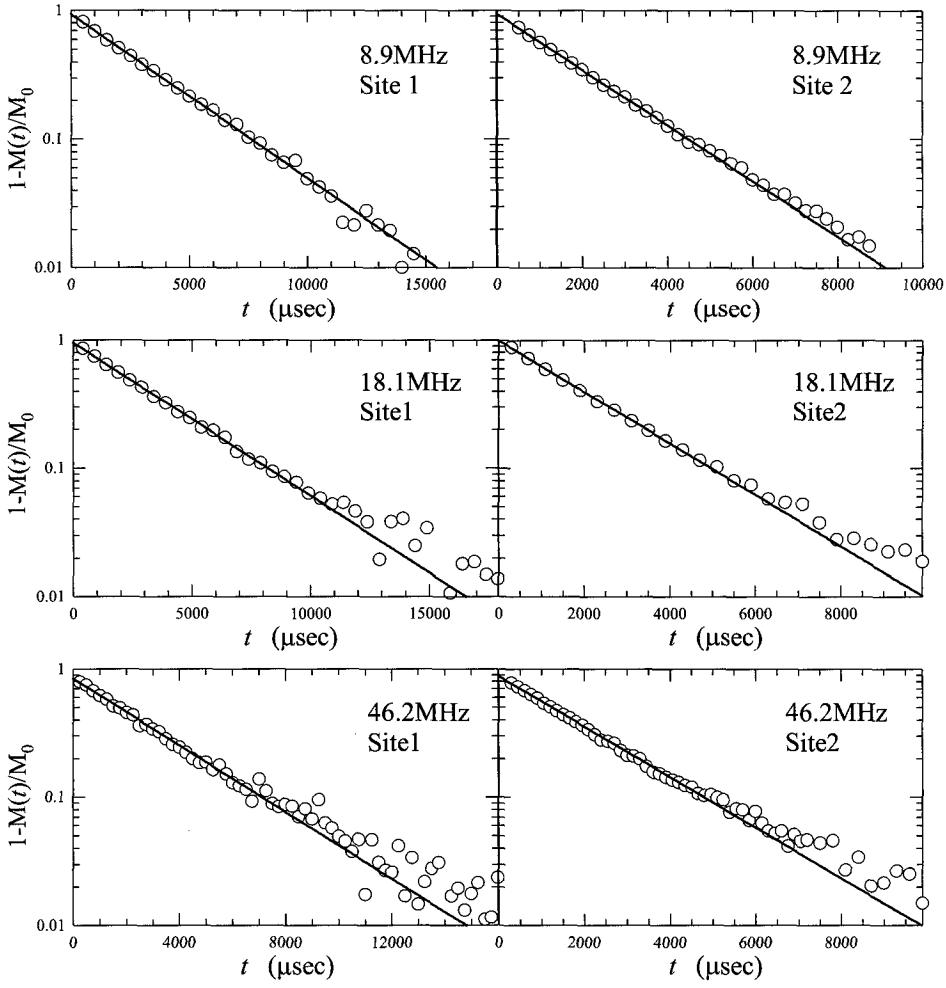

Figure 2.9: Typical recovery curves of the ^{195}Pt nuclear magnetization at 7 K for the site-I and -II at $H \sim 1$ T, 2 T, and 5 T.

Normal State

Fig.2.10 presents the T dependence of $1/T_1T$ at the site-I at $f = 8.9$ MHz, 18.1 MHz, and 46.2 MHz together with the result of $LaPt_3Si$ that is consistent with a Korringa law with $1/T_1T$ = 17.193 $sec^{-1}K^{-1}$ in the measured T range as expected. Apparently, the $1/T_1T$ in $CePt_3Si$ is enhanced upon cooling due to the development of $4f$ derived magnetic fluctuations, exhibiting almost equivalent T dependence down to 10 K regardless of the strength of H. It is noteworthy that $1/T_1T$ undergoes a significant H dependence below a characteristic temperature 10 K that coincides with the CEF energy separation $\Delta E_1 \sim 16$ K. Correspondingly to this, the $1/T_1T$ at $f = 8.9$ MHz seems to be saturated below 10 K, whereas at $f = 46.2$ MHz, it reveals a sharp cusp at $T \sim 3$ K. These results suggest that the CEF effect makes the relaxation behavior depend on H at low T. Furthermore, the fact that $1/T_1T$ starts to decrease rapidly below T_N assures the onset of AFM order, consistent with the specific-heat result. Unfortunately since the broadening in the spectrum below T_N makes it difficult to separately measure the spectrum at the site-I and II, $1/T_1$ cannot be measured below T_N at the site-I.

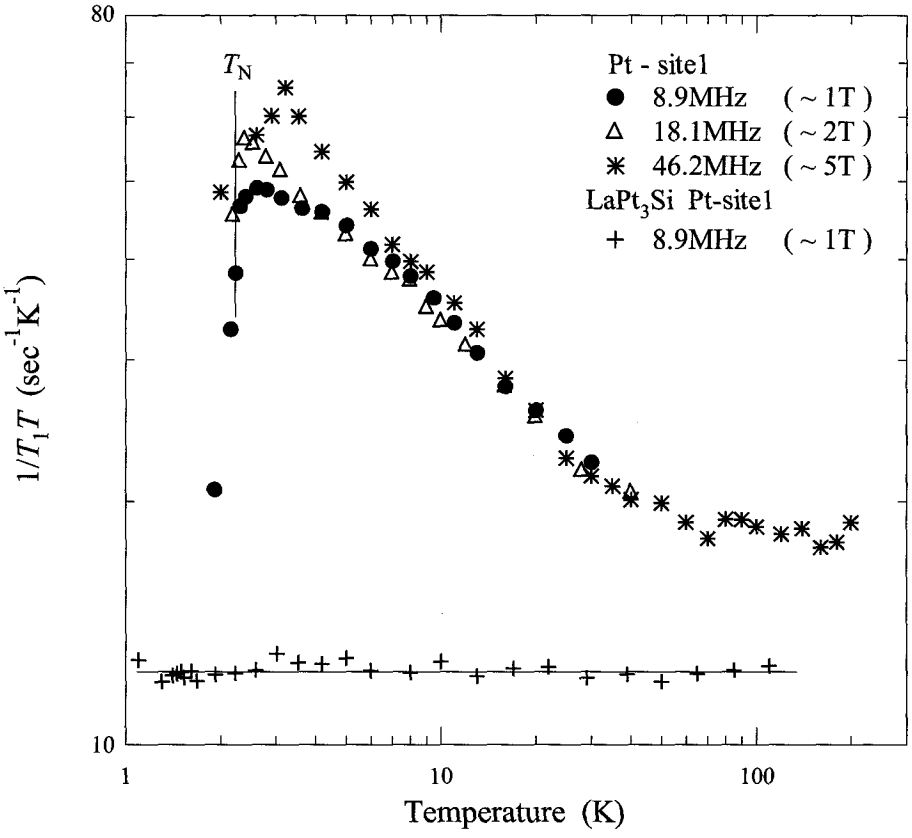

Figure 2.10: Temperature dependence of $1/T_1T$ of Pt site-I for $CePt_3Si$ and $LaPt_3Si$.

Instead, the T dependence of $1/T_1T$ at the site-II for $CePt_3Si$ and $LaPt_3Si$ is presented in a wide T range in Fig.2.11 where the Korringa law $1/T_1T$ = 12.35 $sec^{-1}K^{-1}$ is valid at the site-II as well as the site-I of $LaPt_3Si$. A difference in $1/T_1T$ is evident at the site-I and -II for $CePt_3Si$. In contrast to the result at the site-I, the $1/T_1T$ at the site-II shows a shallow peak around 6 K at $H \sim 1$ T (8.9 MHz) and stays constantly below ~ 8 K at $H \sim 5$ T (46.2 MHz). The latter result

is consistent with the $4f$ derived HF state that is evidenced by a value of $1/T_1T$ being strongly enhanced than the value in $LaPt_3Si$ as observed in either Ce or U-based HF compounds.

This H dependence of $1/T_1T$ observed at the site-II originates from the low-lying CEF effect as well as observed already at the site-I. It is expected that the reduction in $1/T_1T$ observed at low values of $H \sim 1$ and 2 T is also caused by the low-lying CEF level. This result contrasts with conventional Ce-based HF compounds where any well defined low-lying CEF effect does not survive at low T. We point out that a similar T dependence of $1/T_1T$ was reported for the Pr-based HF superconductor $PrOs_4Sb_{12}$ although the low-lying CEF level is characterized by the non-Kramers doublet, yielding a broad peak around 3.5 K.

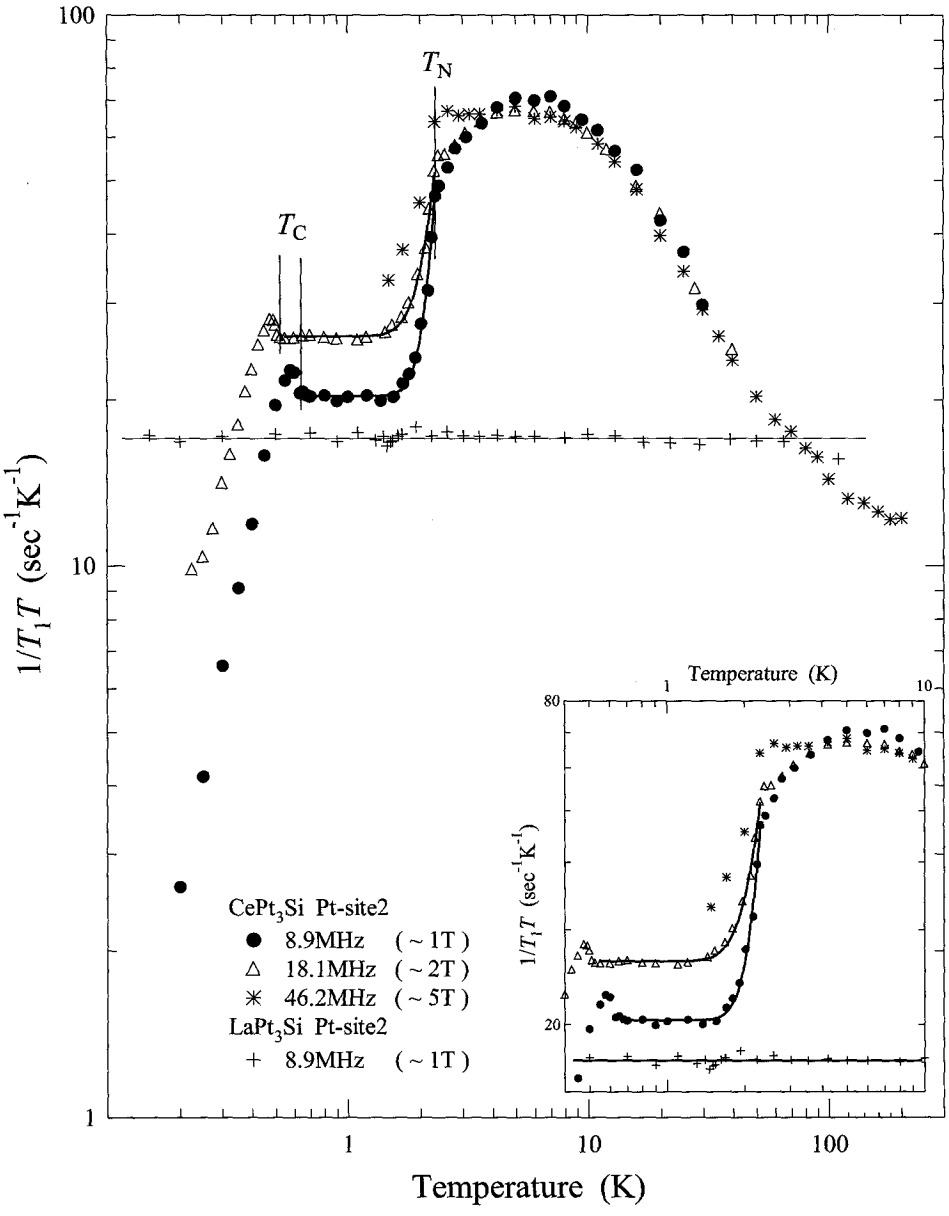

Figure 2.11: The T dependence of $1/T_1T$ at the site-II for $CePt_3Si$ and $LaPt_3Si$. The inset shows their detailed T dependencies near $T_N = 2.2$ K.

Antiferromagnetic (AFM) State

The T dependence of $1/T_1T$ undergoes a drastic decrease below $T_N = 2.2$ K without any critical divergence associated with the onset of AFM order as shown in Fig.2.11. The $1/T_1T$ below T_N is well reproduced by the following formula,

$$\frac{1}{T_1T} = A\exp\left(-\frac{\Delta}{k_BT}\right) + C \tag{2.2}$$

as indicated by the solid lines of Fig.2.11 at $f = 8.9$ and 18.1MHz. Note that a $T_1T = \text{const}$ behavior is valid in a T range lower than T_N. The exponential decrease in $1/T_1T$ may be associated with a *gap* formed partially in the low-lying magnetic excitations spectrum below T_N. The respective values of energy gap Δ/k_B are estimated to be 23.3 K and 16.8 K at $f = 8.9$ and 18.1 MHz. The size of *gap* is suppressed by applying the magnetic field. The last term C of eq.(2.2) corresponds to the quasi-particle contribution. The respective values of $1/T_1T$ are about 20.3 $\text{sec}^{-1}\text{K}^{-1}$ and 26.2 $\text{sec}^{-1}\text{K}^{-1}$ at $f = 8.9$ and 18.1 MHz, being larger than $1/T_1T \sim 17.193$ in $LaPt_3Si$. This evidences that magnetic low-lying excitations are gapped, but the low-lying quasi-particle excitations is in a rather gapless regime, giving rise to the $T_1T = \text{const}$ law even under the background of AFM order. An intimate correlation should be noted that as *gap* size is reduced with increasing H, the value of $1/T_1T$ increases, indicative of a H induced transfer of low-energy spectral weight of quasi-particles. The present experiment has clarified the vital role of $4f$ derived CEF state in forming the HF state at low T that is realized in virtue of the existence of gap in the magnetic excitations at the AFM state. Thus, the SC transition emerges behind this unique HF state which coexists with the AFM phase.

Table 2.4: The values of energy gap Δ/k_B and $1/T_1T$.

	$CePt_3Si$		$LaPt_3Si$
Applied Field (T)	~1	~2	~1
Δ/k_B (K)	23.3	16.8	-
$1/T_1T$ ($\text{sec}^{-1}\text{K}^{-1}$)	20.3	26.2	17.193

Superconducting State

The T dependence of $1/T_1T$ is shown in Fig.2.11. Its relaxation behavior is quite different from that observed in unconventional Ce-based HF superconductors reported thus far. Most Ce-based superconductors indicate a T^3 power-law behavior that is consistent with a line-node gap below T_C without a coherence peak characteristic for conventional BCS superconductors.[11–17] By contrast, it is unexpected that the $1/T_1T$ in $CePt_3Si$ indicates a small peak just below T_C, although the observed peak in $1/T_1T$ is very smaller than that observed for the conventional BCS superconductors. In order to examine the H dependence of the relaxation behavior below T_C, the normalized value of $(1/T_1T)_{SC}/(1/T_1T)_N$ is plotted as a function of T/T_C at 8.9 MHz ($H \sim 1$ T) and 18.1 MHz ($H \sim 2$ T) as shown in Fig.2.12. Here $(1/T_1T)_N$ corresponds to the values at the normal state at 8.9 MHz ($H \sim 1$ T) and 18.1 MHz ($H \sim 2$ T). Apparently, the peak in $(1/T_1T)_{SC}/(1/T_1T)_N$ is almost independent of H. The $(1/T_1T)$ at $H \sim 2$ T seems to be saturated at low T. Actually, the recovery curve of nuclear magnetization that depends on H suggests that the relaxation process is significantly dominated by the presence of vortex cores where the normal-state region is introduced. By contrast, the $1/T_1T$ at 8.9 MHz ($H \sim 1$ T) continues to decrease down to $T = 0.2$ K, a measured lowest temperature, it appears to follow neither an exponential nor T^3 behavior as far as the data are concerned down to temperatures lower than 0.2 K. It is the first HF superconductor that reveals the peak in $1/T_1T$ just below T_C and yet does not follow the T^3 law that used to be reported in most unconventional HF superconductors.

In order to inspect an overall relaxation behavior below T_C in $CePt_3Si$ without inversion symmetry, a tentative SC model was tried to fit the data, as presented by solid line in Fig. 2.12, by applying the Balian-Werthamer model (BW isotropic spin-triplet SC state) with a value of $2\Delta/k_BT_C = 3.9$.[18] Note that the peak in $1/T_1T$ originates from the presence of isotropic energy gap, even though the *coherence effect*, inherent to the isotropic spin-singlet s-wave pairing state, is absent. It is noteworthy that the experiment is not consistent with a simple power-law behavior with the line-node gap at the Fermi surface as indicated by dashed line. It is interesting that the BW model is well fitted just below T_C.

In almost all previous studies on either conventional and unconventional superconductors, it was assumed that the crystal has an inversion center, which makes it possible to consider the even (spin-singlet) and odd (spin-triplet) components of the superconducting (SC) order parameter (OP) separately. In the HF compound $CePt_3Si$, however, an inversion center is absent in its crystal symmetry. Therefore, the novel relaxation behaviors found below T_C in $CePt_3Si$ provides clue to address a possibility of new class of SC state being realized in $CePt_3Si$ in the case without the inversion symmetry.

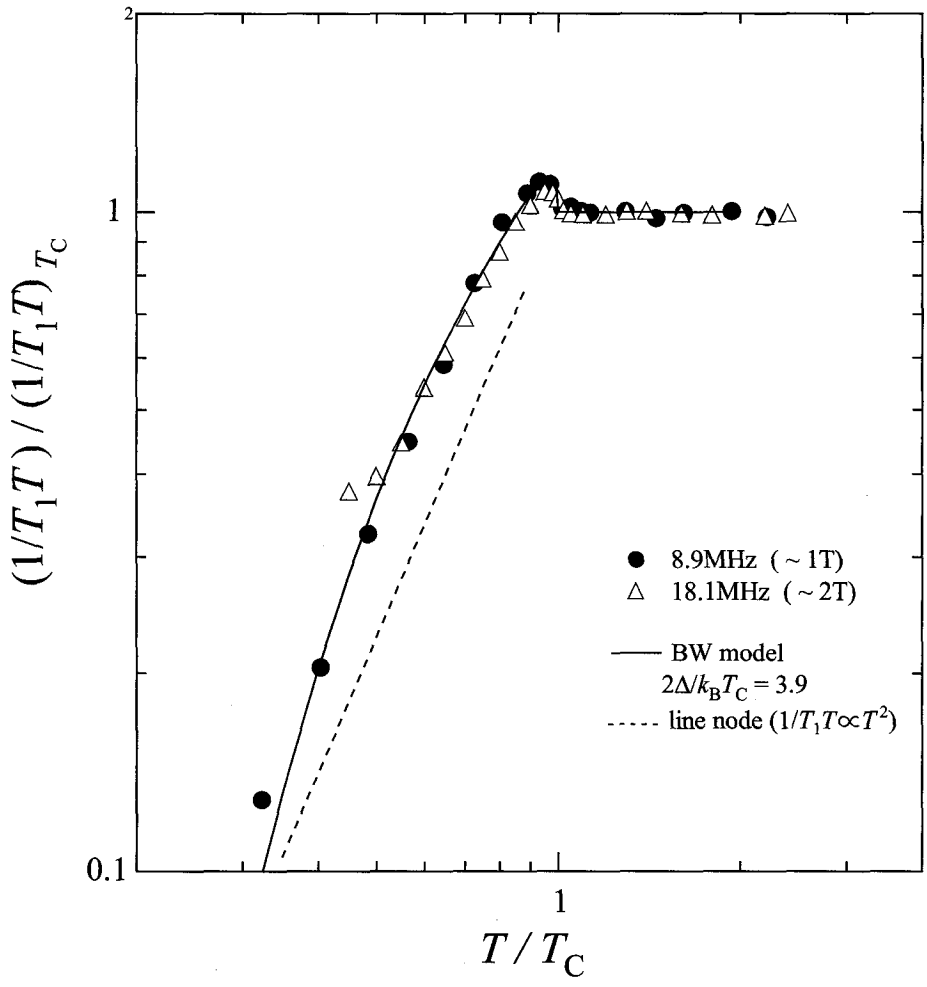

Figure 2.12: Plots of $(1/T_1T)_{SC}/(1/T_1T)_N$ vs T/T_C at 8.9 MHz ($H \sim 1$ T) and 18.1 MHz ($H \sim 2$ T). Here $(1/T_1T)_N$ corresponds to the value at the normal state at 8.9 MHz ($H \sim 1$ T) and 18.1 MHz ($H \sim 2$ T). The solid line is a fit calculated by applying the Balian-Werthamer model (BW isotropic triplet SC state) with a value of $2\Delta/k_BT_C = 3.9$.[18] Dashed line shows a line-node gap model behavior $1/T_1 \propto T^3$.

2.3.2 The ^{29}Si-NMR Study

NMR spectrum

Fig.2.13 indicates the Si-NMR spectrum for the oriented powder with the magnetic field along the c-axis. $CePt_3Si$ has only one Si site. Owing to a small natural abundance of ^{29}Si, the NMR intensity is too small to measure $^{29}K(T)$ and $1/T_1(T)$ in a wide T region. In the paramagnetic state above $T_N \sim 2.2$ K, the NMR spectral shape shows no significant change with a positive shift, but the appearance of the internal field below T_N makes it broaden to prevent from observing the Si-NMR spectrum. Thus the Si-NMR measurements are only possible in the paramagnetic state.

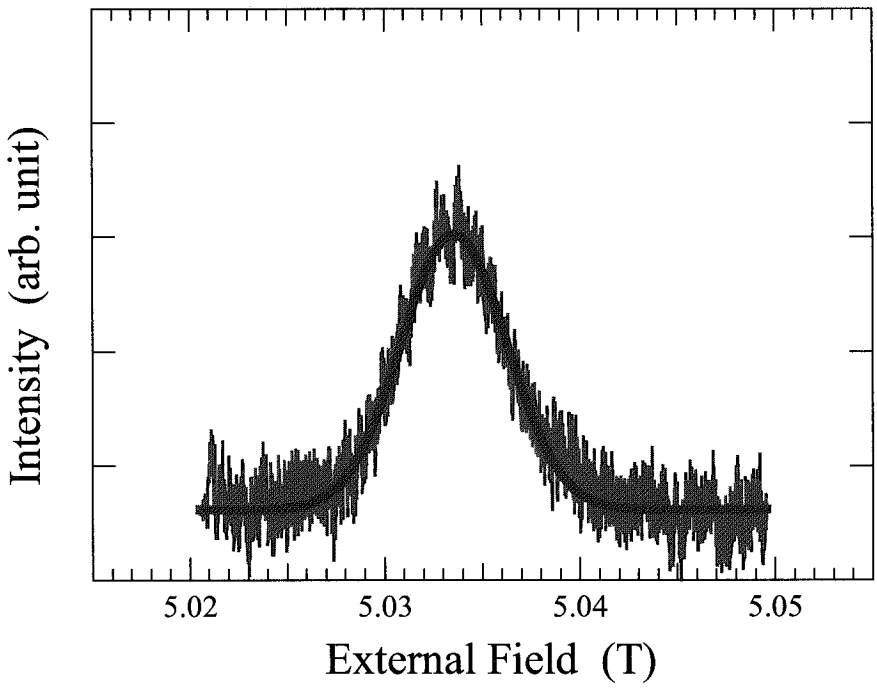

Figure 2.13: The ^{29}Si-NMR spectrum at 2.7 K and 42.77 MHz. Its full-width-half-maximum is as narrow as $\sim$ 54 Oe.

The T dependence of ^{29}K is displayed in Fig.2.14 (a), where ^{29}K decreases upon cooling with a peak at 6 K. This result resembles the T dependence of Pt-$K1$ and -$K2$. A $^{29}K - \chi$ plot reveals almost a linear relation, giving rise to $H_{hf} \sim 1.43$ kOe/μ_B.

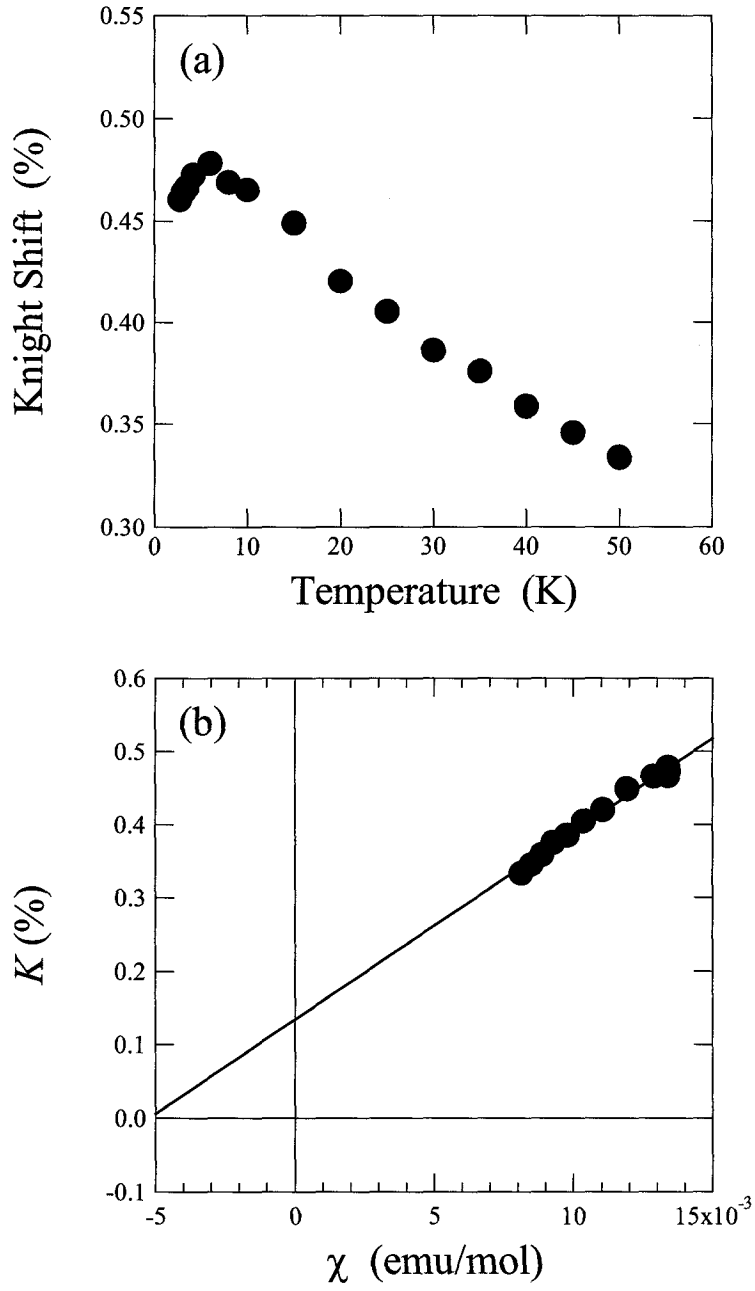

Figure 2.14: (a) The T dependence of ^{29}Si Knight Shift at 42.77 MHz ($H \sim 5$ T). (b) A $^{29}K - \chi$ plot.

Nuclear spin-lattice relaxation time T_1

As shown in Fig.2.15, likewise the case for Pt-T_1, the recovery curve of the nuclear magnetization of ^{29}Si follows a single exponential form as presented by solid line in eq.(2.1). This allows to deduce a single value of T_1. Unfortunately, the ^{29}Si NMR spectrum is significantly wiped out below T_N due to the appearance of the internal field associated with AFM order. So, the T_1 data are available only in the normal state.

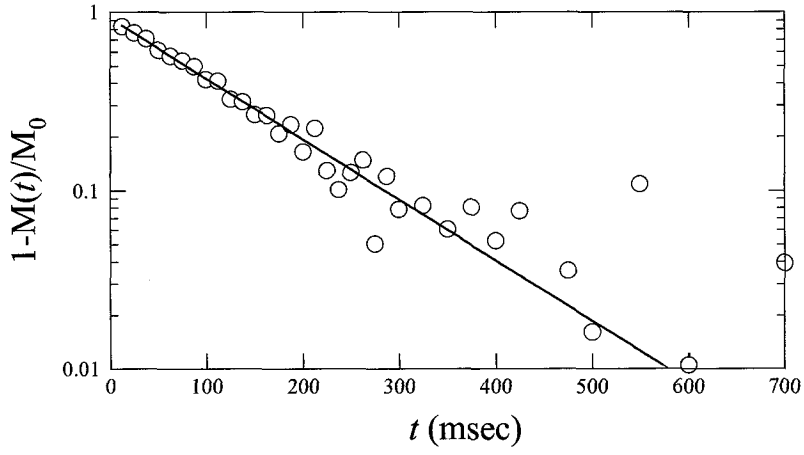

Figure 2.15: Typical recovery curve of ^{29}Si nuclei at 3.5 K and $H \sim 5$ T.

The T dependencies of $1/T_1$ and $1/T_1T$ are shown in Fig.2.16. In the T region higher than $\sim$ 10 K, $1/T_1$ stays constantly: $4f$ derived magnetic fluctuations are in a localized regime. Below 10 K, $1/T_1$ crosses over to an itinerant regime where a $1/T_1T$ stays constantly down to $T_N = 2.2$ K. Together with the Pt-T_1 result, the HF state is formed below $\sim$ 4 K. Unfortunately, since the ^{29}Si-NMR spectrum disappears below T_N, the results on the AFM and SC states are not obtained from the ^{29}Si-NMR measurement.

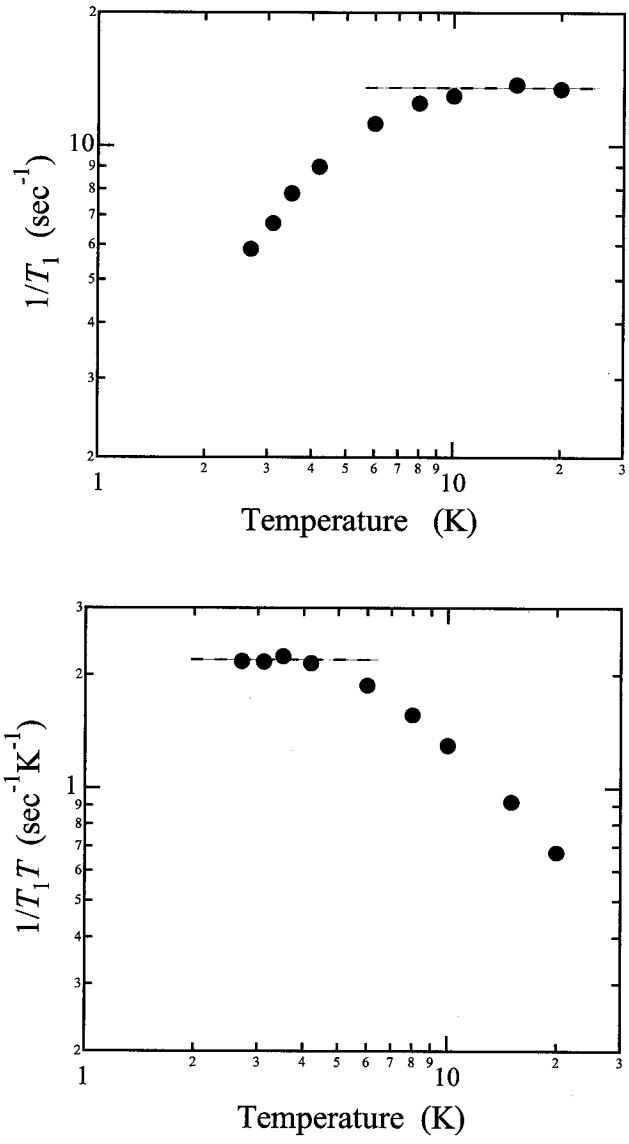

Figure 2.16: The T dependencies of (a) $1/T_1$ and (b) $1/T_1T$ of ^{29}Si in $CePt_3Si$.

2.4 Conclusion

The present NMR studies of ^{195}Pt and ^{29}Si in $CePt_3Si$ have clarified the novel electronic and magnetic properties at the paramagnetic and antiferromagnetic state and a relevant new type of heavy fermion superconducting state:

1. The CEF energy separation is as small as $\Delta E_1 \sim$ 10-16 K, consistent with the neutron result.
2. The heavy fermion state is realized at temperatures below $\sim$ 6 K.
3. The magnetic excitations spectrum has the gap that depends on the magnetic field.
4. The HF quasi-particles remain in a gapless regime in a T region well below T_N, giving rise to a T_1T = const behavior.
5. The application of magnetic field causes the reduction in size of magnetic gap and at the same time the increase in spectral weight of quasi-particles at the Fermi level, having some relevance with the presence of low-lying CEF levels.
6. The Pt-T_1 measurements have probed the anomalies due to the onset of AFM and SC orders, providing microscopic evidence for the coexistence of AFM and SC orders.
7. $CePt_3Si$ is the first HF superconductor that reveals the peak in $1/T_1T$ just below T_C and yet does not follow the T^3 law that used to be reported in most unconventional HF superconductors.

In almost all previous studies on either conventional and unconventional superconductors, it was assumed that the crystal has an inversion center, which makes it possible to consider the even (spin-singlet) and odd (spin-triplet) components of the superconducting (SC) order parameter (OP) separately. In the new AFM HF compound $CePt_3Si$, however, an inversion center is absent in its crystal symmetry. Therefore, the novel relaxation behaviors found below T_C in $CePt_3Si$ have revealed that the new class of SC state is realized in $CePt_3Si$ without the inversion symmetry. The experimental finding presented in this work deserves future theoretical works to unravel the SC OP symmetry for the case where the inversion symmetry is absent in general. A New field in the study on HFS is now open.

Bibliography

[1] P. W. Anderson, J. Phys. Chem. Solids **11**, 26 (1959).

[2] P. W. Anderson, Phys. Rev. B **30**, 400 (1984).

[3] O. L. Sologub, J. R. Hester, P. S. Salamakha, E. Leroy, and C. Godart, J. Alloys Compounds **337**, 10 (2002).

[4] E. Bauer, G. Hilscher, H. Michor, Ch. Paul, E. W. Scheidt, A. Gribanov, Yu. Seropegin, H. Noël, M. Sigrist, and P. Rogl, Phys. Rev. Lett. **92**, 027003 (2004).

[5] N. Metoki, K. Kaneko, T. D. Matsuda, A. Galatanu, T. Takeuchi, S. Hashimoto, T. Ueda, R. Settai, and Y. Ōnuki, appear in J. Phys. Soc. Jpn.

[6] M. Kohgi, K. Iwasa, M. Nakajima, N. Metoki, S. Araki, N. Bernhoeft, J. Mignot, A. Gukasov, H. Sato, Y. Aoki, and H. Sugawara, J. Phys. Soc. Jpn. **72**, 1002-1005 (2003).

[7] H. Sugawara, S. Osaki, S. R. Saha, Y. Aoki, H. Sato, Y. Inada, H. Shishido, R. Settai, Y. Ōnuki, H. Harima and K. Oikawa, Phys. Rev. B **66** (2002) 220504R.

[8] P. Frigeri, D. F. Agterberg, A. Kaga, and M. Sigrist, cond-matt/0311354 (2003).

[9] K. V. Samokhin, E. S. Zijlstra, and S. K. Bose, cond-matt/0311181 (2003).

[10] A. M. Clogston, A. C. Gossard, and Y. Yafet, Rev. Mod. Phys. **36**, 170 (1964).

[11] K. Ishida, Y. Kawasaki, K. Tabuchi, K. Kashima, Y. Kitaoka, K. Asayama, C. Geibel, and F. Steglich, Phys. Rev. Lett. **82**, 5353 (1999).

[12] Y. Kawasaki, K. Ishida, T. Mito, C. Thessieu, G.-q. Zheng, Y. Kitaoka, C. Geibel, and F. Steglich, Phys. Rev. B **63**, 140501R (2001).

[13] Y. Kohori, Y. Yamato, Y. Iwamoto, and T. Kohara, Eur. Phys. J. B **18**, 601-604 (2000)

[14] T. Mito, S. Kawasaki, G.-q. Zheng, Y. Kawasaki, K. Ishida, Y. Kitaoka, D. Aoki, Y. Haga, and Y. Ōnuki, Phys. Rev. B **63**, 220507R (2001).

[15] Y. Kohori, Y. Yamato, Y. Iwamoto, T. Kohara, E. D. Bauer, M. B. Maple, and J. L. Sarrao, Phys. Rev. B **64**, 134526 (2001).

[16] G.-q. Zheng, K. Tanabe, T. Mito, S. Kawasaki, Y. Kitaoka, D. Aoki, Y. Haga, and Y. Ōnuki, Phys. Rev. Lett. **86**, 4664 (2001).

[17] Y. Kawasaki, S. Kawasaki, M. Yashima, T. Mito, G. -q. Zheng, Y. Kitaoka, H. Shishido, R. Settai, Y. Haga, and Y. Ōnuki, J. Phys. Soc. Jpn. **72**, 2308 (2003).

[18] R. Balian, and N. R. Werthamer, Phys. Rev. **131**, 1553 (1963).

Part III

Sb-NQR Study of The Filled-Skutterudite Compounds

Chapter 1

Introduction

1.1 Crystal structure

The filled skutterudite compounds with chemical formula $RETx_4Pn_{12}$ (RE=Rare earth, Tx=Fe, Ru or Os, Pn=P, As and Sb) crystallize in a unique body-centered-cubic structure of a space group $Im\bar{3}$ (T_h^5, ♯204) of which $\langle 100 \rangle$ axes are not four-fold but two-fold.[1,2]

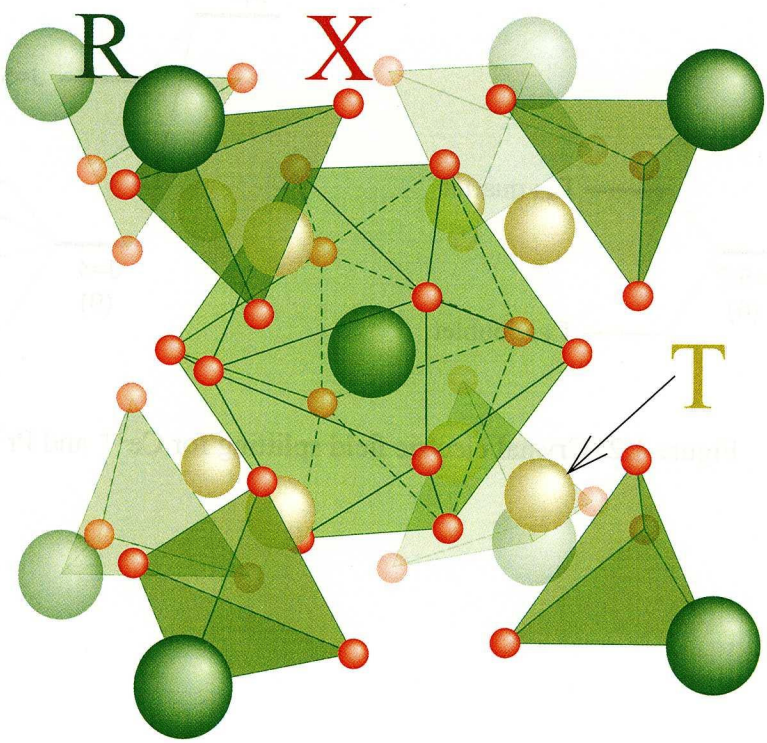

Figure 1.1: Crystal structure of the filled-skutterudite compound. It belongs to the space group $Im\bar{3}$ (T_h^5, ♯204)[2,3]

1.2 Characteristics of filled-skutterudite compounds

Since rare earth atoms are surrounded by twelve pnictogen atoms in the crystal structure, $4f$ electrons hybridize significantly with conduction electrons,[3]which causes various novel physical phenomena such as magnetic order,[4–6] quadrupole order,[7–10] metal-insulator transition (MIT),[11–13] Kondo insulating behavior,[14–16] non-Fermi liquid behavior,[4,17,18] superconductivity[4,14,19–24] and so on.[25]

A crystal-electric-field (CEF) energy schemes are shown for Ce^{3+} and Pr^{3+} ions in the case of a cubic symmetry in Fig.1.2. Pr^{3+} ion is split into four energy levels such as Γ_1, Γ_3, Γ_4, and Γ_5 where Γ_3 is the non-Kramers doublet. Cox proposed theoretically that if the ground state is the non-Kramers doublet Γ_3, the quadrupole interaction plays vital role: $PrFe_4P_{12}$ has the Γ_3 ground state and undergoes a Kondo like behavior below 100 K, followed by an antiferroquadrupole ordering at 6.5 K. In magnetic fields higher than $\sim$ 4 T, $PrFe_4P_{12}$ indicates a heavy-fermion (HF) behavior with a heavy effective mass $m_e^* \sim 80m_0$. Furthermore, $PrOs_4Sb_{12}$ reveals unconventional superconductivity, which is argued to be caused by quadrupole fluctuations via the relevant non-Kramers doublet Γ_3 hybridized with conduction electrons.[24]

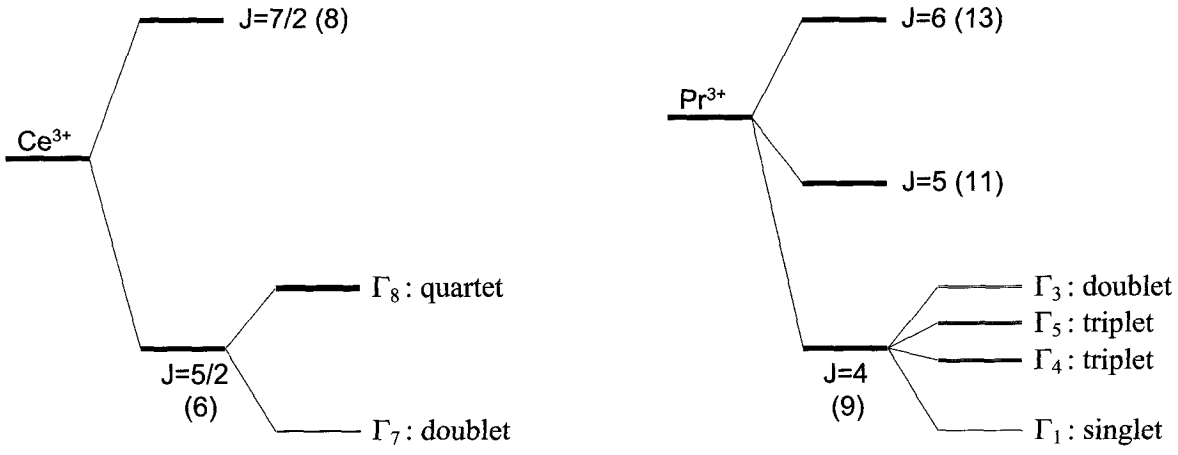

Figure 1.2: Crystal electric field splitting for Ce^{3+} and Pr^{3+}.

Table 1.1: Eigenfunction of cubic crystal electric field for Ce^{3+} and Pr^{3+}.[2,26]

Pr^{3+}	$\|\Gamma_1\rangle$	$0.4564\|-4\rangle+0.7638\|0\rangle+0.4564\|+4\rangle$
	$\|\Gamma_3^+\rangle$	$0.54(\|+4\rangle-\|-4\rangle)-0.6455\|0\rangle$
	$\|\Gamma_3^-\rangle$	$0.7071(\|+2\rangle-\|-2\rangle)$
	$\|\Gamma_4^1\rangle$	$a_1(\|+4\rangle-\|-4\rangle)+a_2(\|+2\rangle-\|-2\rangle)$
	$\|\Gamma_4^2\rangle$	$a_2(\|+4\rangle-\|-4\rangle)+a_1(\|+2\rangle-\|-2\rangle)$
Ce^{3+}	$\|\Gamma_7^\pm\rangle$	$0.4082\|\pm\frac{5}{2}\rangle-0.9129\|\mp\frac{3}{2}\rangle$
	$\|\Gamma_{8a}^\pm\rangle$	$0.9129\|\pm\frac{5}{2}\rangle+0.4082\|\mp\frac{3}{2}\rangle$
	$\|\Gamma_{8b}^\pm\rangle$	$\|\pm\frac{1}{2}\rangle$

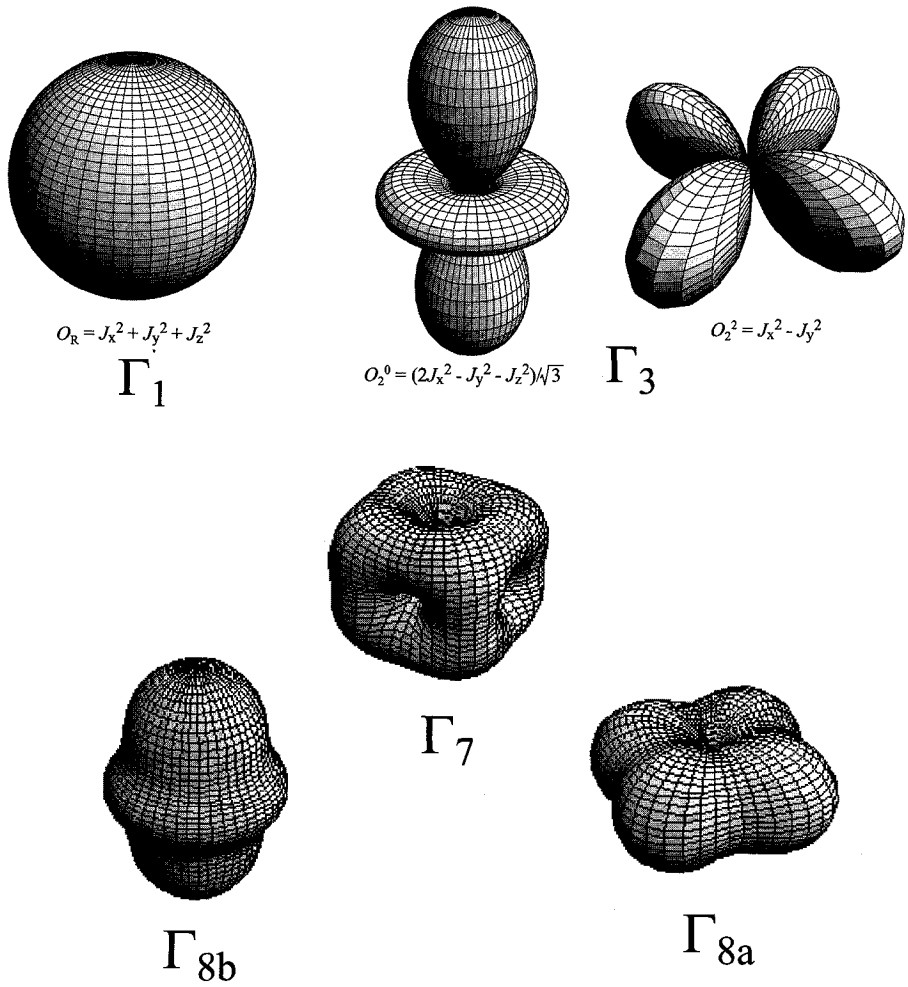

Figure 1.3: Charge distribution of $4f$ state under cubic CEF. (a) Pr^{3+} with $J = 4$. (b) Ce^{3+} with $J = 5/2$.

1.3 Outline

In this thesis we deal with $RETx_4Sb_{12}$ (RE=La, Ce, and Pr, Tx=Ru and Os) compounds.Their physical properties (with Tx=Fe compounds) are shown in Table1.2. In order to shed light on novel superconducting (SC) characteristics of the HF superconductor $PrOs_4Sb_{12}$, we have examined (1) the SC properties in $PrRu_4Sb_{12}$ and its reference $LaRu_4Sb_{12}$, (2) the quasi-particle excitations in the SC state under magnetic field on $PrOs_4Sb_{12}$, which allows us to address possibility of multi-components of SC order parameter revealed by the field dependence of thermal conductivity and the double transition in the specific-heat measurement. Furthermore, we have investigated the Kondo insulator $CeOs_4Sb_{12}$ in order to compare the physical properties between the $Ce^{3+}(J = 5/2)$ system where the CEF states compose only of the Kramers doublet and the $Pr^{3+}(J = 4)$ system where the CEF states involve the non-Kramers doublet and the non-magnetic singlet.

Table 1.2: Physical properties of Pn=Sb based filled-skutterudite compounds. SC: superconducting, Semi-C: semiconducting, Semi-M: semimetallic, FM: ferromagnetic, AFM: antiferromagnetic, HF: heavy fermion, NFL: non-Fermi liquid.[4,14,24,27,28]

	La	Ce	Pr
Fe	$LaFe_4Sb_{12}$ non-SC ($T > 4$ K)	$CeFe_4Sb_{12}$ Semi-M HF	$PrFe_4Sb_{12}$ FM or AFM $T_C = 5$ K
Ru	$LaRu_4Sb_{12}$ SC $T_C = 3.58$ K	$CeRu_4Sb_{12}$ Semi-M NFL	$PrRu_4Sb_{12}$ SC $T_C = 1.3$ K
Os	$LaOs_4Sb_{12}$ SC $T_C = 0.74$ K	$CeOs_4Sb_{12}$ Semi-C $E_g = 10$ K	$PrOs_4Sb_{12}$ HF-SC $T_C = 1.85$ K

Bibliography

[1] W. Jeitschko, and D. Braun, Acta Crystallogr. **B33**, 3401 (1977).

[2] K. Takegahara, H. Harima, and A. Yanase, J. Phys. Soc. Jpn. **70**, 1190-1193 (2001).

[3] H. Harima, and K. Takegahara, J. Phys.: Condens. Matter **15**, S2081-S2086 (2003).

[4] N. Takeda, and M. Ishikawa, J. Phys. Soc. Jpn. **57**, 868 (2000).

[5] N. Takeda, and M. Ishikawa, J. Phys.: Condens. Matter **15**, L229-L233 (2003).

[6] A lot of heavy-rare-earth atom based filled skutterudite compounds (i.e. $GdFe_4P_{12}$) indicate magnetic order.

[7] H. Sugawara, T. D. Matsuda, K. Abe, Y. Aoki, H. Sato, S. Nojiri, Y. Inada, R. Settai, and Y. Ōnuki, Phys. Rev. B **66**, 134411 (2002).

[8] T. D. Matsuda, H. Okada, H. Sugawara, Y. Aoki, H. Sato, A. V. Andreev, Y. Shiokawa, V. Sechovsky, T. Honma, E. Yamamoto, and Y. Ōnuki, Physica B **281&282**, 220-222 (2000).

[9] Y. Aoki, T. Namiki, T. D. Matsuda, K. Abe, H. Sugawara, and H. Sato, Phys. Rev. B **65**, 064446 (2002).

[10] Y. Nakanishi, T. Shimizu, M. Yoshizawa, T. D. Matsuda, H. Sugawara, and H. Sato, Phys. Rev. B **63**, 184429 (2002).

[11] C. Sekine, T. Uchiumi, and I. Shirotani, Phys. Rev. Lett. **79**, 3218 (1997).

[12] C. H. Lee, H. Matsuhata, A. Yamamoto, T. Ohta, H. Takazawa, K. Ueno, C. Sekine, I. Shirotani, and T. Hirayama, J. Phys.: Condens. Matter **13**, L45-L48 (2001).

[13] S. R. Saha, H. Sugawara, T. Namiki, Y. Aoki, H. Sato, J. Phys.: Condens. Matter **15**, S2163-S2166 (2003).

[14] E. D. Bauer, A. Ślebarski, E. J. Freeman, C. Sirvent, and M. B. Maple, J. Phys.: Condens. Matter **13**, 4495 (2001).

[15] T. Namiki, Y. Aoki, H. Sugawara, and H. Sato, Acta Phys. Pol. B, **34**, 1161 (2003).

[16] H. Sato, Y. Aoki, T. Namiki, T. D. Matsuda, K. Abe, S. Osaki, S. R. Saha, H. Sugawara, Physica B **328**, 34-38 (2003).

[17] E. D. Bauer, A. Ślebarski, R. P. Dickey, E. J. Freeman, C. Sirvent, V. S. Zapf, N. R. Dilley, and M. B. Maple, J. Phys.: Condens. Matter **13**, 5183-5193 (2001).

[18] K. Abe, H. Sato, T. D. Matsuda, T. Namiki, H. Sugawara, and Y. Aoki, J. Phys.: Condens. Matter **14**, 11757-11768 (2002).

[19] G. P. Meisner, Physica **108B**, 763 (1981).

[20] L. E. Delong and G. P. Meisner, Solid State Commun. **53**, 119 (1985).

[21] I. Shirotani, T. Uchiumi, K. Ohno, C. Sekine, Y. Nakazawa, K. Kanoda, S. Todo, and T. Yagi, Phys. Rev. B **56**, 7866 (1997).

[22] I. Shirotani, K. Ohno, C. Sekine, T. Yagi, T. Kawakami, T. Nakanishi, H. Takahashi, J. Tang, A. Matsushita, T. Matsumoto, Physica B **281&282**, 1021 (2000).

[23] H. Sugawara, S. Osaki, S. R. Saha, Y. Aoki, H. Sato, Y. Inada, H. Shishido, R. Settai, Y. Ōnuki, H. Harima, and K. Oikawa, Phys. Rev. B **66**, 220504R (2002).

[24] E. D. Bauer, N. A. Frederick, P. -C. Ho, V. S. Zapf, and M. B. Maple, Phys. Rev. B **65** (2002) 100506R.

[25] The physical property of various filled-skutterudite compounds is summarized to the following pages. http://skut.phys.metro-u.ac.jp/database/database.html

[26] K. Miyake, H. Kohno, and H. Harima, J. Phys.: Condens. Matter **15**, L275-L284 (2003).

[27] D. T. Morelli, and G. P. Meisner, J. Appl. Phys., **77** (1995) 3777

[28] M. E. Danebrock, C. B. H. Evers, and W. Jeitschko, J. Phys. Chem. Solids **57** (1996) 381.

Chapter 2

The Sb-NQR study of superconductor $PrRu_4Sb_{12}$

2.1 Introduction

In the Pr-based filled-skutterudite compounds, $PrOs_4Sb_{12}$, $PrRu_4Sb_{12}$ and $PrRu_4As_{12}$ show superconductivity.[2,3,3] Among these compounds, $PrOs_4Sb_{12}$ is the first Pr-based superconductor that shows HF behavior.[3] Its HF state was inferred from the jump in the specific heat at T_C, the slope of the upper critical field H_{c2} near T_C, and the electronic specific-heat coefficient $\gamma \sim 350 - 500$ mJ/mol K^2. Various measurements such as magnetic susceptibility, thermodynamic properties, and inelastic neutron scattering revealed the ground state of the Pr^{3+} ions in the cubic crystal electric field (CEF) to be either non-magnetic Γ_3 doublet or Γ_1 singlet.[3–7] In the Pr-based compounds with the Γ_3 ground state, electric quadrupolar interactions play an important role. In analogy with a quadrupolar Kondo model,[8] it was suggested that the HF-like behavior exhibited by $PrOs_4Sb_{12}$ may have something to do with a Pr-4f^2-derived quadrupolar Kondo-lattice. If the ground state is the Γ_3, an interesting issue to be addressed is what role of Pr-4f^2-derived quadrupolar fluctuations play in relevance with the onset of the superconductivity in this compound.

Meanwhile, we have reported the Sb-NQR results which evidence the HF behavior and the unconventional SC characteristics in $PrOs_4Sb_{12}$.[9] The T dependencies of $1/T_1$ and nuclear-quadrupole-resonance (NQR) frequency unraveled a low-lying CEF splitting below $T_0 \sim 10$ K, associated with the $Pr^{3+}(4f^2)$-derived ground state. The analysis of T_1 suggests the formation of HF state below ~ 4 K. In the SC state, $1/T_1$ shows neither a coherence peak just below $T_C = 1.85$ K nor a T^3 like power-law behavior observed for *anisotropic* HF superconductors with line-node gap. An *isotropic* energy-gap with $\Delta/k_B = 4.8$ K is suggested to open up already below $T^* \sim 2.3$ K. It is surprising that $PrOs_4Sb_{12}$ looks like an *isotropic* HF superconductor – it may indeed argue for Cooper pairing via quadrupolar fluctuations. Also, $PrRu_4Sb_{12}$ was reported to undergo the SC transition at $T_C = 1.3$ K from the measurements of the electrical resistivity and specific heat as well as $LaRu_4Sb_{12}$ with $T_C = 3.58$ K as shown in Fig.2.1 and 2.2.[2] It can be informative to compare $PrRu_4Sb_{12}$ with $PrOs_4Sb_{12}$ and the related La-based superconductors as shown in Table 2.1.[10]

Table 2.1: Comparison of the SC temperature T_C, specific heat jump ΔC divided by T_C ($\Delta C/T_C$). Sommerfeld coefficient, and effective mass m_c^* in RT_4Sb_{12} (R=La, Pr, T=Ru, Os).[10]

	$PrOs_4Sb_{12}$	$LaOs_4Sb_{12}$	$PrRu_4Sb_{12}$	$LaRu_4Sb_{12}$
T_C (K)	1.85	0.74	1.3	3.58
$\Delta C/T_C$ (mJ/mol K^2)	500	84	110	82
Sommerfeld coefficient (mJ/mol K^2)	350~750	36, 56	59	37
m_c^*/m_0 for γ-branch	7.6	2.8	1.6	1.4

The localized character of $4f$ electrons, namely the closeness of the respective Fermi surfaces with those in $LaRu_4Sb_{12}$ and $LaOs_4Sb_{12}$, has been confirmed in $PrRu_4Sb_{12}$ and $PrOs_4Sb_{12}$ from the de Haas-van Alphen (dHvA) experiment.[10,11] On the contrary, the mass enhancement in $PrRu_4Sb_{12}$ is much smaller than in $PrOs_4Sb_{12}$. For $PrOs_4Sb_{12}$, the CEF ground state was inferred to be either the non-Kramers Γ_3 doublet or the Γ_1 singlet.[3–7] Note that even though either the case is possible, the low lying CEF-energy difference between them is very as small as $\Delta E_1 \sim 10$ K, carrying quadrupole moments. By contrast, the ground state for $PrRu_4Sb_{12}$ is reported to be the Γ_1 singlet which is far separated from the first CEF levels, estimated as $\Delta E_1 \sim 70$ K.[2,12]

On the comparison in T_C with the La compounds, the two compounds have different trend; T_C for $PrOs_4Sb_{12}$ is higher than that for La compounds, which is unusual if we take into account that $PrOs_4Sb_{12}$ contains the magnetic element Pr ions. These remarkable differences in the underlying CEF level scheme and hence electronic and SC characteristics between $PrOs_4Sb_{12}$ and $PrRu_4Sb_{12}$ may be ascribed to an intimate change in the hybridization strength of Pr-4f state with conduction electrons comprising of respective Os_4Sb_{12}- and Ru_4Sb_{12}-cage. In this context, further light is indeed needed to be shed upon the SC and electronic characteristics in the Pr-based superconductors.

In this chapter, we report the normal and SC properties in the filled-skutterudite compound $PrRu_4Sb_{12}$ and $LaRu_4Sb_{12}$ via the measurements of NQR frequency ν_Q and T_1 of Sb nuclei.

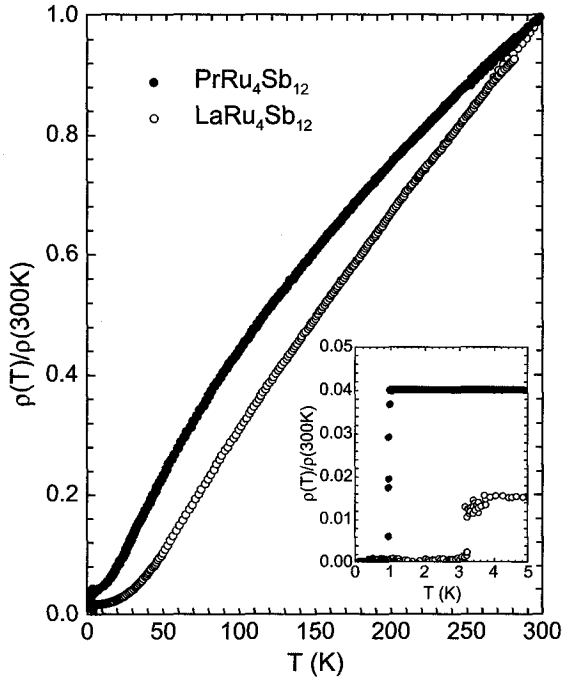

Figure 2.1: The T dependence of electrical resistivity for $RERu_4Sb_{12}$ (RE = Pr, La).[2]

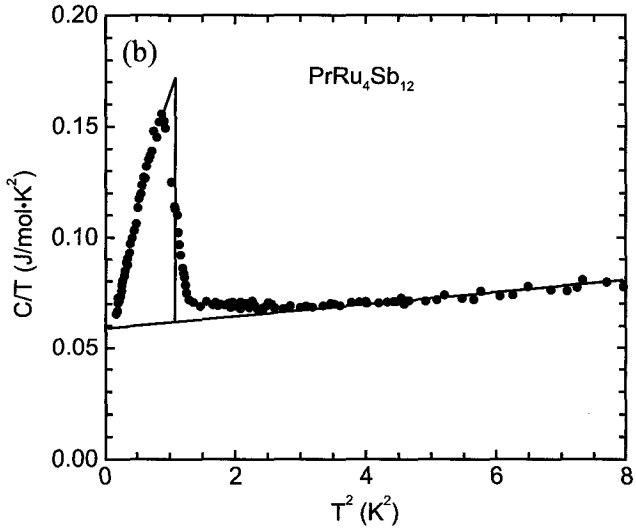

Figure 2.2: The T dependence of specific heat divided by T.[2]

2.2 Crystal Electric Field (CEF) Effect

The dHvA experiment revealed that the $4f^2$ electrons for both $PrRu_4Sb_{12}$ and $PrOs_4Sb_{12}$ have localized character, therefore, it is important to consider the CEF energy scheme and their ground state.[10,11] The CEF energy scheme for $PrRu_4Sb_{12}$ are reported by the measurements of electrical resistivity and magnetic susceptibility as shown in Fig.2.3. $PrRu_4Sb_{12}$ has the non-magnetic singlet Γ_1 ground state where the separation of the ground state Γ_1 and the first excited state Γ_5 is reported to be about 70K.[2,12] The ultrasonic measurement also indicates that the ground state of $PrRu_4Sb_{12}$ is the Γ_1 singlet.[13] Fig.2.3 also displays the CEF energy scheme for $PrOs_4Sb_{12}$. There are two models on the CEF energy scheme for $PrOs_4Sb_{12}$. In either case, a remarkable character in the CEF level scheme is that the energy separation between the ground state and the first excited state is as small as $\Delta E_1 \sim 10$ K, suggesting that both the states are mixed one another via the hybridization with conduction electrons. Such the difference in their CEF energy scheme might lead to the contrasted SC characteristics in $PrOs_4Sb_{12}$ and $PrRu_4Sb_{12}$.

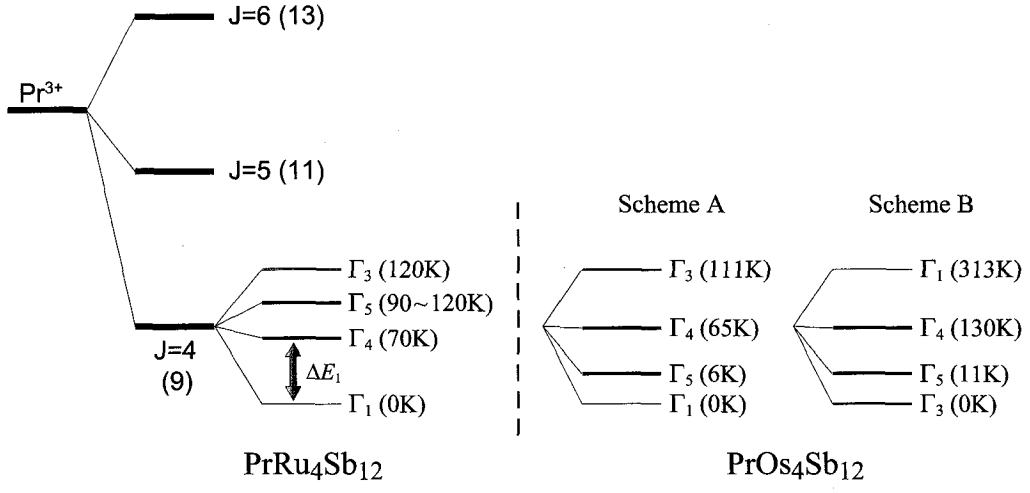

Figure 2.3: The CEF energy scheme for $PrRu_4Sb_{12}$ and $PrOs_4Sb_{12}$.[2,3,12]

2.3 Sample preparation

Single crystals of $PrRu_4Sb_{12}$ and $LaRu_4Sb_{12}$ were grown by the Sb-flux method.[2] The observation of the dHvA oscillations in both the compounds confirm the high quality of the samples.[11] Measurement of ac-susceptibility confirmed the respective SC transitions at T_C = 1.3 K and 3.5 K for $PrRu_4Sb_{12}$ and $LaRu_4Sb_{12}$. The single crystal was crushed into powder for the Sb-NQR measurement. The full-width-half-maximum (FWHM) in the NQR spectrum at ^{123}Sb $2\nu_Q$ transition is as small as $\sim$ 76 kHz at 4.2 K, proving the high quality of the sample. The ^{121,123}Sb-NQR measurements were performed using the conventional saturation-recovery method at zero field ($H = 0$).

2.4 Results and Discussion

2.4.1 NQR spectrum

Fig.2.4 displays the ^{121,123}Sb-NQR spectra at 4.2 K. Sb nuclei has two isotopes ^{121}Sb and ^{123}Sb. The respective nuclear spin $I = 5/2$ (^{121}Sb) and $7/2$ (^{123}Sb) have natural abundance 57.3 and 42.7%, and nuclear gyromagnetic ratio $\gamma_N = 10.189$ and 5.5175 [MHz/T], giving rise to two and three NQR transitions.

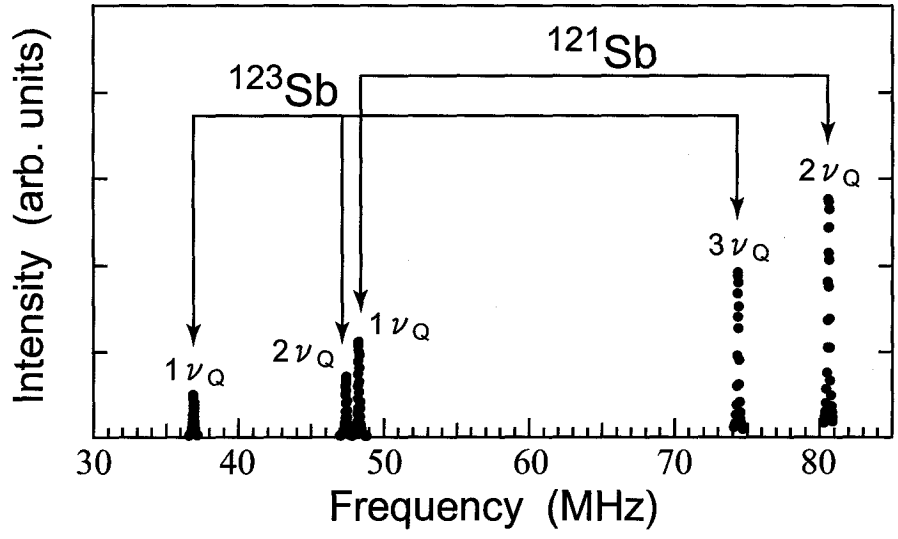

Figure 2.4: ^{121}Sb- and ^{123}Sb-NQR spectra in $PrRu_4Sb_{12}$.

Table 2.2: Comparison of the ν_Q for ^{121}Sb and ^{123}Sb, and asymmetric parameter η in RT_4Sb_{12} (R=La, Pr, T=Ru, Os).

	$PrOs_4Sb_{12}$	$LaOs_4Sb_{12}$	$PrRu_4Sb_{12}$	$LaRu_4Sb_{12}$
ν_Q for ^{121}Sb (MHz)	44.167	43.776	41.516	41.171
ν_Q for ^{123}Sb (MHz)	26.81	26.577	25.204	24.994
Asymmetric parameter η	0.459	0.450	0.402	0.406

Fig.2.5 (a) indicates the T dependencies of $\nu_Q(T)$ derived from the ^{123}Sb-$2\nu_Q$ transition in $PrRu_4Sb_{12}$ and $LaRu_4Sb_{12}$. The inset indicates $\delta\nu_Q(T) = \nu_Q(T)_{Pr} - \nu_Q(T)_{La}$, which subtracts the common effect due to lattice expansion in both the compounds. $\nu_Q(T)$ reveals a progressive increase upon cooling below $T \sim 70$ K, which corresponds to the ΔE_1. Note, as shown in Fig.2.5 (b), that the $\delta\nu_Q(T) = \nu_Q(T)_{Pr} - \nu_Q(T)_{La}$ in $PrOs_4Sb_{12}$ was observed to be increased below a temperature comparable to $\Delta E_1 \sim 10$ K. From this comparison, $\Delta E_1 \sim 70$ K is expected in $PrRu_4Sb_{12}$. This is almost consistent with the value evaluated from the analysis of susceptibility and resistivity.[2,12]

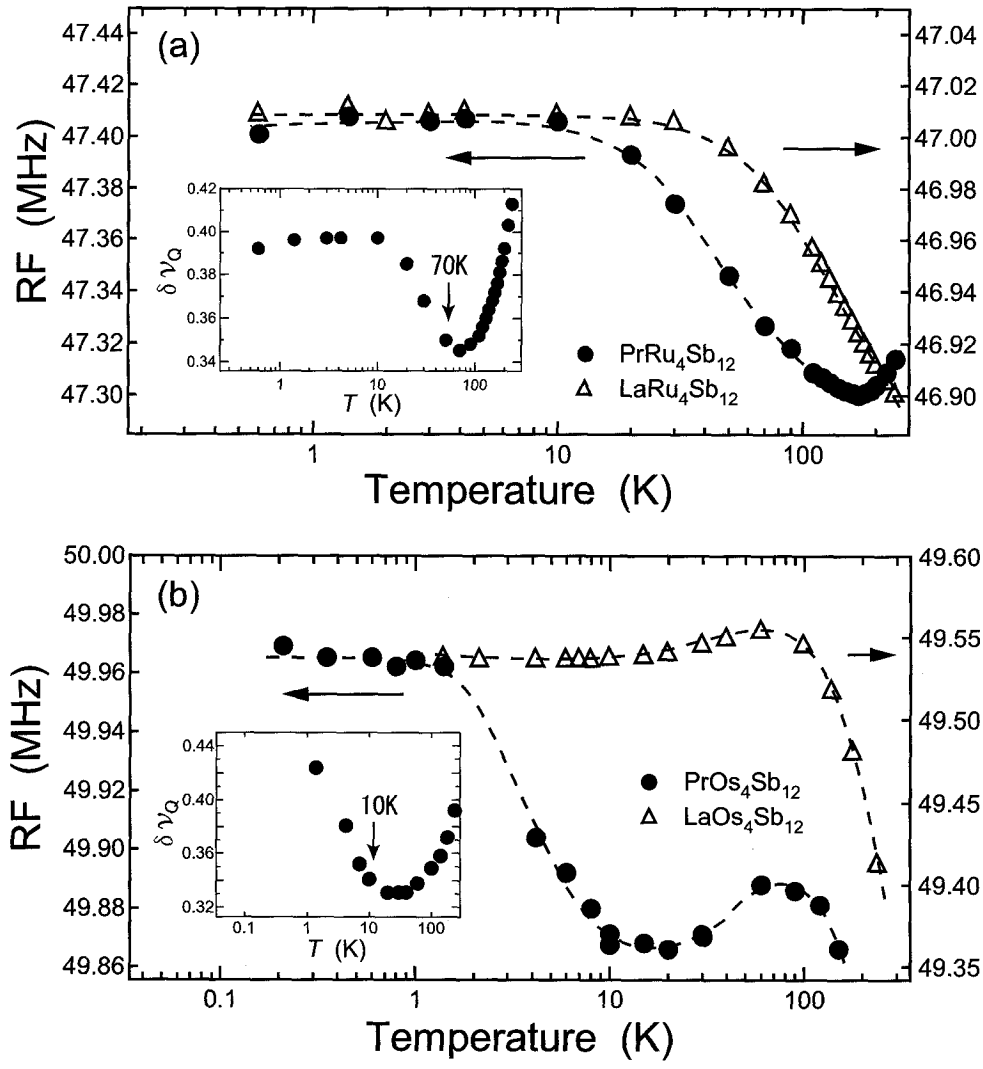

Figure 2.5: (a) The T dependence of NQR frequency ν_Q for $PrRu_4Sb_{12}$ and $LaRu_4Sb_{12}$ at the ^{123}Sb-2ν_Q transition. The inset indicates the Pr-derived contribution in ν_Q, $\delta\nu_Q = (\nu_Q)_{Pr} - (\nu_Q)_{La}$. (b) The T dependence of NQR frequency for $PrOs_4Sb_{12}$ and $LaOs_4Sb_{12}$ at ^{123}Sb-2ν_Q transition.[9] The Inset indicates $\delta\nu_Q = (\nu_Q)_{Pr} - (\nu_Q)_{La}$.

2.4.2 Nuclear spin-lattice relaxation time T_1

The recovery curve for nuclear magnetization at the $\pm 3/2 \leftrightarrow \pm 5/2$ NQR transition of ^{123}Sb nuclei ($I = 7/2$) is shown in Fig.2.6. For $I = 7/2$ and $\eta = 0.45$, it is given by[14,15]

$$\frac{M(\infty) - M(t)}{M(\infty)} = 0.075\exp(-3.025t/T_1) + 0.015\exp(-8.55t/T_1) + 0.91\exp(-17.305t/T_1) \tag{2.1}$$

$\frac{M(\infty)-M(t)}{M(\infty)}$ is well fitted by the above theoretical equation of the eq.(2.1) as presented by the solid line in Fig.2.6.

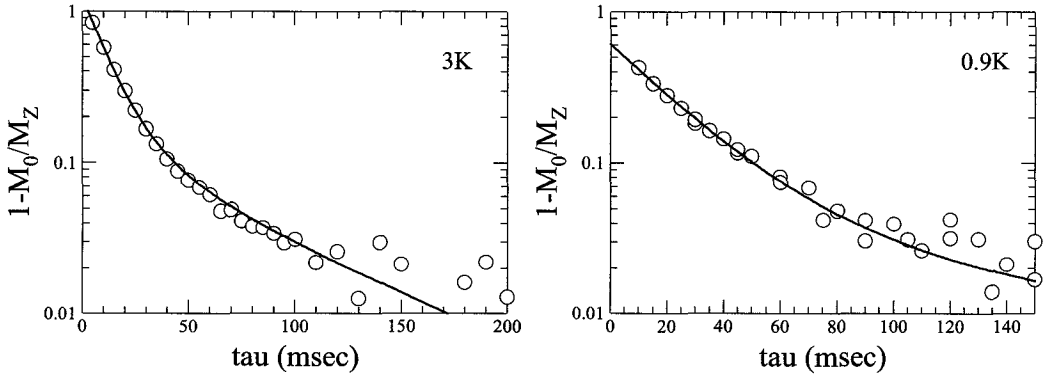

Figure 2.6: Typical recovery curve of nuclear magnetization for ^{123}Sb NQR at $\pm 3/2 \leftrightarrow \pm 5/2$ transition at $H = 0$ in $PrRu_4Sb_{12}$. The solid lines are the least square fitting using eq.(2.1)

Fig.2.7 presents the T dependencies of $(1/T_1T)$ for $PrRu_4Sb_{12}$ and $LaRu_4Sb_{12}$. In the normal state, T_1 reveals a Korringa relation $(1/T_1T)_{Pr} = 1.73(\text{sec}\cdot\text{K})^{-1}$ for $PrRu_4Sb_{12}$, being comparable to $(1/T_1T)_{La} = 1.2(\text{sec}\cdot\text{K})^{-1}$ for $LaRu_4Sb_{12}$. The $1/T_1T = \text{const}$ law deviates at temperatures higher than ~ 30 K in $PrRu_4Sb_{12}$. Since such a deviation is seen in $LaRu_4Sb_{12}$ above ~ 25 K as well, these deviations are not derived by the presence of Pr^{3+} ions, but may be ascribed to a conduction-band derived effect inherent to the filled-skutterudite structure.

In the filled-skutterudite structure, a Pr atom forms in a body centered cubic structure, surrounded by a cage of corner-sharing Ru_4Sb_{12} octahedra. The cage might begin to stretch with increasing T. This stretching motion of cage may be relevant to the decrease in a value of $1/T_1T = \text{const}$ for $PrRu_4Sb_{12}$ and $LaRu_4Sb_{12}$ and $LaRu_4P_{12}$.[16] The measurements of the dHvA effect and the electronic specific heat for $PrRu_4Sb_{12}$ and $LaRu_4Sb_{12}$ revealed that the mass-renormalization effect in the Fermi liquid state is not so significant in $PrRu_4Sb_{12}$, suggesting that Pr^{3+}-$4f^2$ electrons are well localized in $PrRu_4Sb_{12}$. Note that the value of $1/T_1T$ is proportional to the square of the density of states $N(E_F)$ at the Fermi level. Also, it is scaled to the T-linear electronic contribution γ of specific heat, giving rise to the relation of $(1/T_1T)^{1/2} \propto \gamma$. Therefore, the change in value of $(1/T_1T)^{1/2}$ is directly related to a change of $N(E_F)$ in systems. Corroborated by the fact that the value of $1/T_1T$ in $PrRu_4Sb_{12}$ is not so enhanced than that in $LaRu_4Sb_{12}$ with a ratio of $[(1/T_1T)_{Pr}/(1/T_1T)_{La}]^{1/2} = 1.44$, we remark that the $Pr^{+3} - 4f^2$

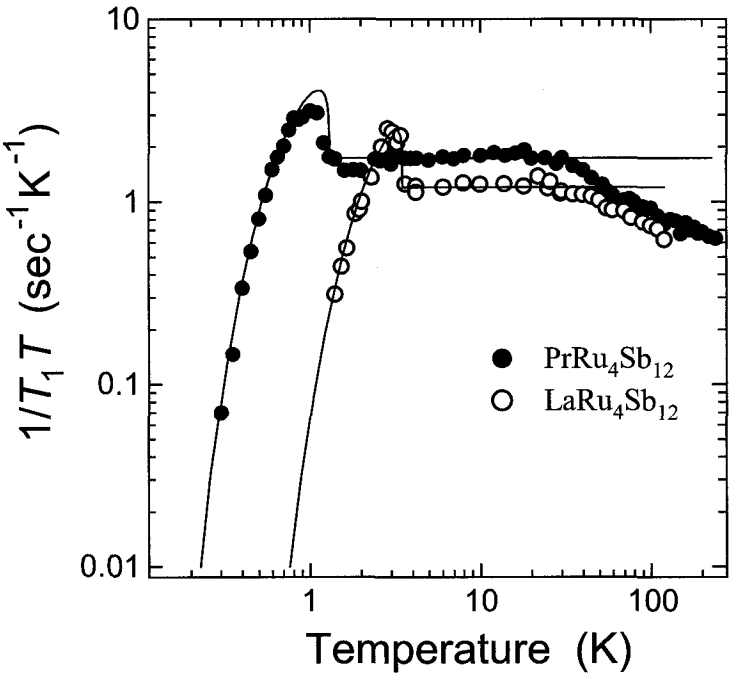

Figure 2.7: The T dependence of $1/T_1T$ for $PrRu_4Sb_{12}$ and $LaRu_4Sb_{12}$. Solid lines are the fits calculated based on the weak-coupling s-wave model assuming a size of isotropic gap $2\Delta/k_BT_C = 3.1$ and 3.6 for $PrRu_4Sb_{12}$ and $LaRu_4Sb_{12}$, respectively.

electrons with the Γ_1 singlet as the ground state does not play a vital role for the electronic and magnetic properties at low temperatures in $PrRu_4Sb_{12}$.

In the SC state for $PrRu_4Sb_{12}$ and $LaRu_4Sb_{12}$, $1/T_1T$ shows a distinct coherence peak, followed by an exponential decrease below T_C with an isotropic gap $2\Delta/k_BT_C = 3.1$ and 3.6, respectively. These results demonstrate that $PrRu_4Sb_{12}$ and $LaRu_4Sb_{12}$ are typical weak-coupling s-wave superconductors.

Fig.2.8 shows the T dependencies of $1/T_1$ for $PrRu_4Sb_{12}$ and $PrOs_4Sb_{12}$. From the comparison in the normal and SC states, it is clear that remarkable differences arise because the quadrupole degree of freedom plays vital role in $PrOs_4Sb_{12}$, associated with either the Pr^{+3}-$4f^2$ derived non-Kramers doublet or the mixing effect between the non-magnetic ground state and the very close first excited state via the hybridization with conduction electrons. In either case, the quadrupole degree of freedom might play vital role in leading to the contrasted SC characteristics in $PrRu_4Sb_{12}$ and $PrOs_4Sb_{12}$. It may indeed argue for Cooper pairing via quadrupolar fluctuations in the latter case.

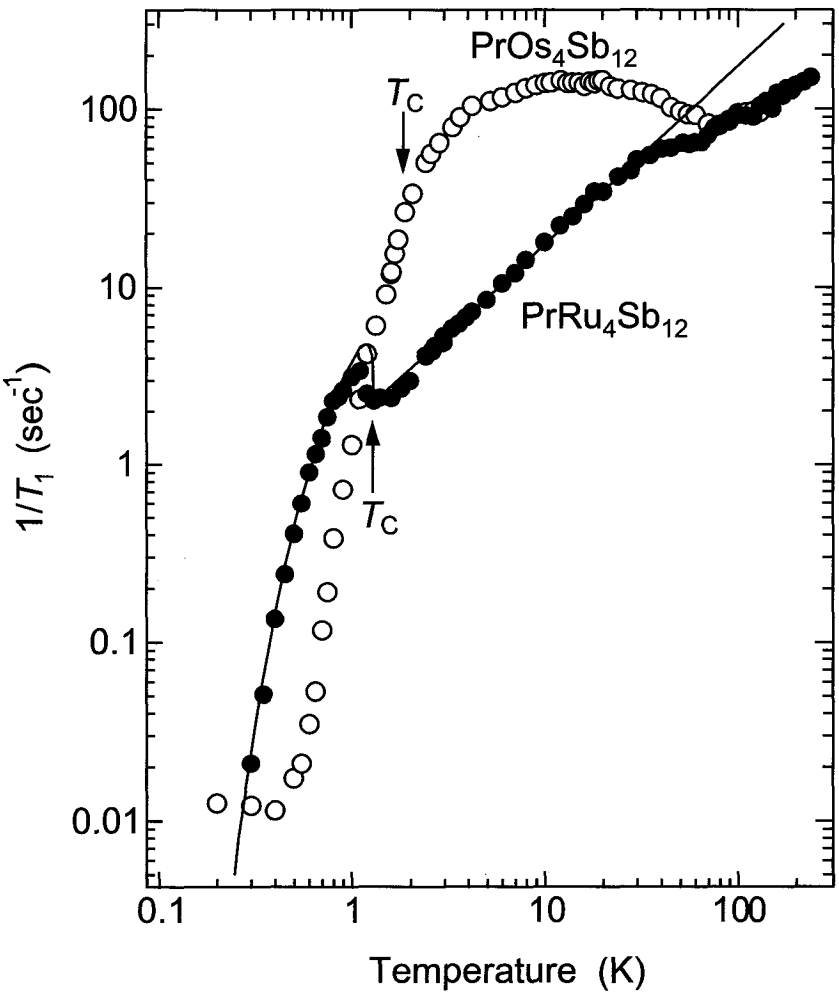

Figure 2.8: The T dependencies of $1/T_1$ for $PrRu_4Sb_{12}$ and $PrOs_4Sb_{12}$.[9] The solid line for $PrRu_4Sb_{12}$ is the fit based on the weak-coupling s-wave model with $2\Delta/k_BT_C = 3.1$.

2.5 Conclusion

To summarize, the electronic and SC properties in the Pr-based filled-skutterudite superconductor $PrRu_4Sb_{12}$ with $T_C = 1.3$ K was investigated through the measurements of NQR frequency ν_Q and T_1 of Sb nuclei. The T dependence of ν_Q has revealed the CEF energy scheme for Pr^{3+} ion that is consistent with an energy separation $\Delta E_1 \sim 70$ K between the ground state and the first-excited level. In the normal state, the Korringa relation of $(1/T_1T)_{Pr}$=const is valid, revealing a comparable value $[(1/T_1T)_{Pr}/(1/T_1T)_{La}]^{1/2} \sim 1.44$ with $(1/T_1T)_{La}$ for $LaRu_4Sb_{12}$. These results are understood in terms of the conventional Fermi-liquid picture in which the Pr-$4f^2$ state derives neither magnetic nor quadrupolar degrees of freedom at low temperatures. In the SC state, $1/T_1$ shows a distinct coherence peak just below T_C, followed by an exponential decrease with the value of $2\Delta/k_BT_C = 3.1$. These results demonstrate that $PrRu_4Sb_{12}$ is a typical weak-coupling s-wave superconductor, in strong contrast with the heavy-fermion superconductor $PrOs_4Sb_{12}$ that is in a unconventional strong coupling regime.[9] The present study on $PrRu_4Sb_{12}$ highlights that the Pr-$4f^2$ derived quadrupole fluctuations play a key role for the unconventional electronic and superconducting properties in $PrOs_4Sb_{12}$, which is caused by either the non-magnetic doublet or the mixing effect between the non-magnetic ground state and the closely lying first excited state via the hybridization with conduction electrons.

Bibliography

[1] I. Shirotani, T. Uchiumi, K. Ohno, C. Sekine, Y. Nakazawa K. Kanoda, S. Todo and T. Yagi, Phys. Rev. B **56**, 7866 (1997).

[2] N. Takeda, and M.Ishikawa, J. Phys. Soc. Jpn. **57** (2000) 868.

[3] E. D. Bauer, N. A. Frederick, P. -C. Ho, V. S. Zapf, and M. B. Maple, Phys. Rev. B **65**, 100506R (2002).

[4] M. B. Maple, P. -C. Ho, V. S. Zapf, N. A. Frederick, E. D. Bauer, W. M. Yuhasz, F. M. Woodward and J. W. Lynn, J. Phys. Soc. Jpn. **71**, 23-28 (2002).

[5] Y. Aoki, T. Namiki, S. Ohsaki, S. R. Saha, H. Sugawara, H. Sato, J. Phys. Soc. Jpn. **71**, 2098-2101 (2002).

[6] M. Kohgi, K. Iwasa, M. Nakajima, N. Metoki, S. Araki, N. Bernhoeft, J. Mignot, A. Gukasov, H. Sato, Y. Aoki, and H. Sugawara, J. Phys. Soc. Jpn. **72**, 1002-1005 (2003).

[7] T. Tayama, T. Sakakibara, H. Sugawara, Y. Aoki and H. Sato, J. Phys. Soc. Jpn. **72**, 1516-1522 (2003).

[8] D. L. Cox, Phys. Rev. Lett. **59**, 1240 (1987).

[9] H. Kotegawa, M. Yogi, Y. Imamura, Y. Kawasaki, G. -q. Zheng, Y. Kitaoka, S. Ohsaki, H. Sugawara, Y. Aoki, and H. Sato, Phys. Rev. Lett. **90**, 027001-1 (2003).

[10] H. Sugawara, S. Osaki, S. R. Saha, Y. Aoki, H. Sato, Y. Inada, H. Shishido, R. Settai, Y. Ōnuki, H. Harima, and K. Oikawa, Phys. Rev. B **66**, 220504R (2002).

[11] T. D. Matsuda, K. Abe, F. Watanuki, H. Sugawara, Y. Aoki, H. Sato, Y. Inada, R. Settai, and Y. Ōnuki, Physica B **312-313**, 832-833 (2002).

[12] K. Abe, H. Sato, T. D. Matsuda, T. Namiki, H. Sugawara, and Y. Aoki, J. Phys.: Condens. Matter **14**, 11757-11768 (2002).

[13] T. Kumagai, Y. Nakanishi, H. Sugawara, H. Sato and M. Yoshizawa, Physica B **329-333**, 471-473 (2003).

[14] D. E. MacLaughlin, J. D. Williamson, and J. Butterworth, Phys. Rev. B **4**, 60 (1971).

[15] J. Chepin, and J. H. Ross, J. Phys.: Condens. Matter **3**, 8103-8112 (1991).

[16] K. Fujiwara, K. Ishihara, K. Miyoshi, J. Takeuchi, C. Sekine and I. Shirotani, Physica B **281-282**, 296-297 (2000).

Chapter 3

The Sb-NQR study of multiple SC phases in heavy-fermion (HF) superconductor $PrOs_4Sb_{12}$

3.1 Introduction

A lot of superconductors, that form in the filled-Skutterudite structure, have been reported to date.[1–7] Among them, only $PrOs_4Sb_{12}$ indicates HF unconventional superconductivity.[8] Measurements of ^{123}Sb-NQR T_1 revealed no coherence peak just below T_C, but the exponential decrease in $1/T_1(T)$, suggesting that $PrOs_4Sb_{12}$ belongs to a new class of unconventional superconductor characterized by rather *isotropic* energy gap (see Fig.3.1 (a)).[9] Beside, Izawa *et al.* have argued that $PrOs_4Sb_{12}$ has gap zero nodes at point from the measurement of angular dependence of thermal conductivity under the rotation of magnetic field H.[10] These results suggest that the superconducting nature in $PrOs_4Sb_{12}$ differs from Ce-based unconventional superconductors with the gap function vanishing along line at the Fermi surface.[11–17]

A remarkable evidence that $PrOs_4Sb_{12}$ has multiple SC phases is put forth from the angular dependence of the thermal conductivity: A change in the structure of SC gap function occurs a deep inside of the SC state and two distinct SC phases with two-fold and four-fold symmetries are present as shown in Fig.3.2 (a).[10] Unexpectedly, a jump of specific heat C/T at T_C indicates a sample dependence as shown in Fig.3.2 (b).[18,19] One sample shows a broad peak at T_C from which it is difficult to determine temperatures where double SC transitions take place, but another one points to the clear double SC transitions. Note that the H dependence of T_{C2} obtained from the specific-heat measurements does not always correspond to the H dependence of the temperature at which the thermal conductivity changes its angular variation with respect to the rotation of H. In any case, however, these results point to the emergence of unconventional SC phase in $PrOs_4Sb_{12}$. In addition, the ZF-μSR measurement has revealed the broken time-reversal-symmetry in the SC state.[20]

In this section, we report the Sb-NQR T_1 measurements under various values of H in order to gain an insight into the possible multiple SC phases under H in this compounds.

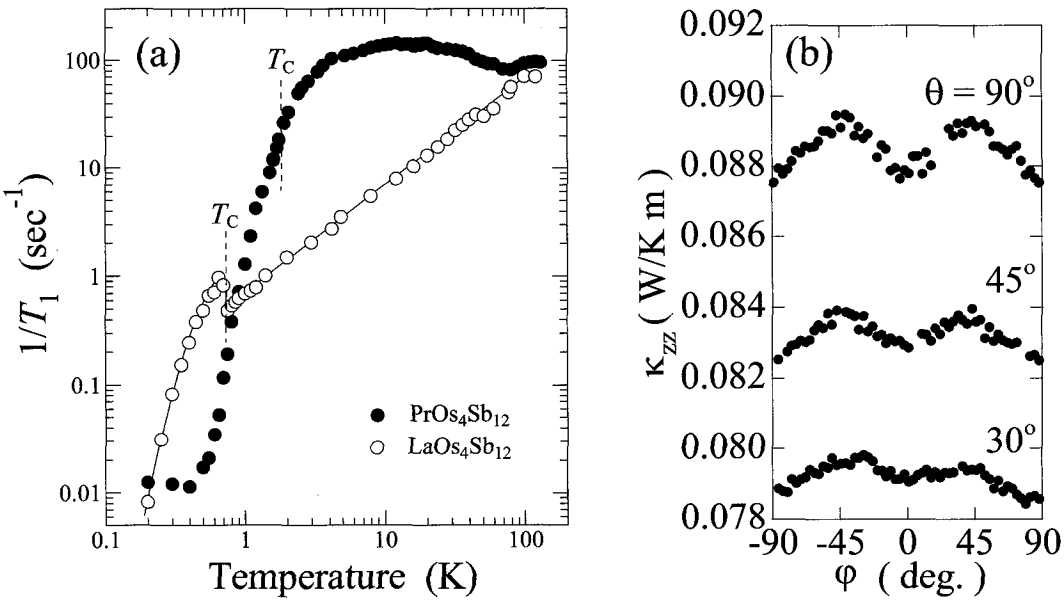

Figure 3.1: (a) The T dependence of ^{123}Sb-NQR $1/T_1$ for $PrOs_4Sb_{12}$ and $LaOs_4Sb_{12}$.[9] (b) The angular variation of thermal conductivity $\kappa_{zz}(H, \phi)$ in $H = 1.2$ T.[10]

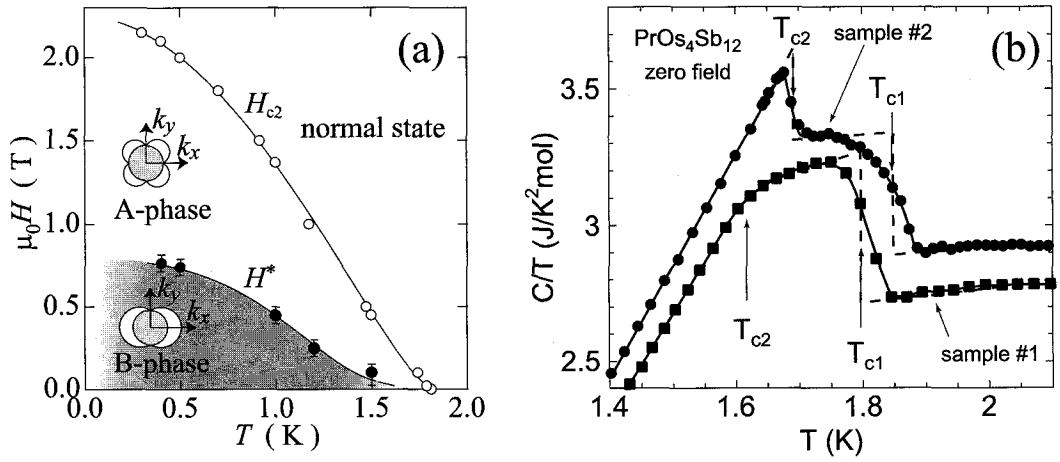

Figure 3.2: (a) The phase diagram determined by the angular dependence of thermal conductivity under the rotation of magnetic field. The A-phase (B-phase) has the symmetry with four-fold (two-fold).[10] (b)The sample dependence of C/T around T_C.[19]

3.2 Sample preparation

Two samples of $PrOs_4Sb_{12}$ were used. Both the samples were grown by Sb-flux method using high-purity elements, 4N (99.99% pure)-Pr, 3N(or 4N)-Os, and 6N-Sb by Sugawara *et al.*.[7] Two samples differ in only a purity of Os element. The observation of dHvA oscillation on the two samples assures their high quality.[7]

Table 3.1: The character of the sample A and B used for the Sb-NQR measurement

	sample figuration	Os purity
sample A	powdered single crystal	99.9%
sample B		99.99%

3.3 Results and Discussions

3.3.1 NQR spectrum

Fig.3.3 displays the Sb-NQR spectra of ^{123}Sb-2ν_Q and ^{121}Sb-1ν_Q transitions at $H = 0$ and 0.2 T. The spectra exhibiting a Lorentzian shape at $H = 0$. With applying H, the spectrum becomes broader due to a typical powder pattern affected by the nuclear quadrupole interaction. $1/T_1$ was measured at the transition equivalent to the NQR transition at which $1/T_1$ was measured at $H = 0$.

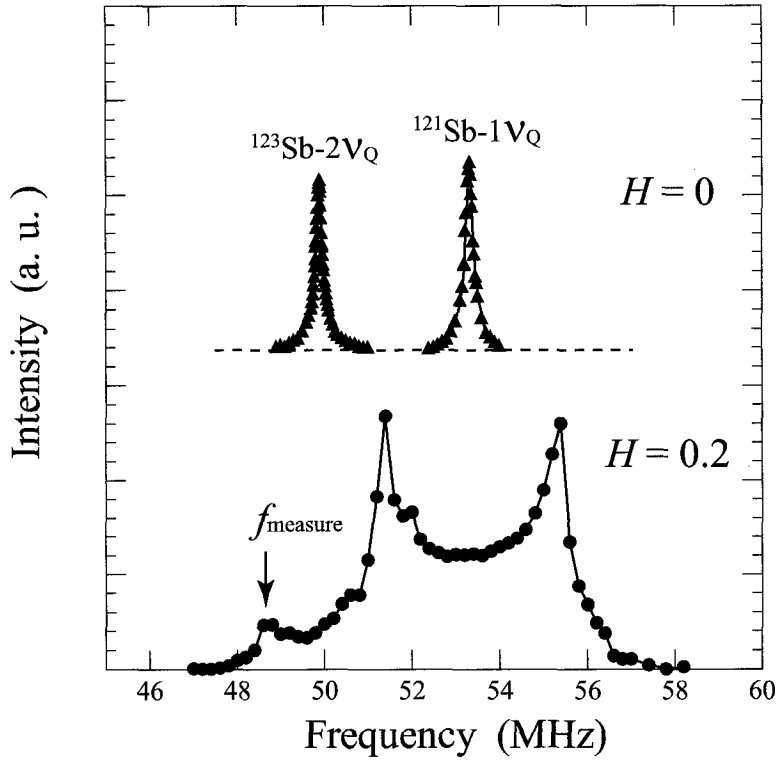

Figure 3.3: The Sb-NQR spectra at ^{123}Sb-2ν_Q and ^{121}Sb-1ν_Q transitions at $H = 0$ and 0.2 T. $f_{measure}$ denotes the frequency where T_1 was measured.

3.3.2 Nuclear spin-lattice relaxation time T_1

Magnetic field effect

The T dependence of $1/T_1$ at various values of H are shown in Fig.3.4. First, we focus on the T dependence of $1/T_1$ below 0.5 K. $1/T_1$ undergoes '$1/T_1$ = const' behavior below 0.4 K at $H = 0$. The value of $1/T_1$ = const at $H = 0.1$ T becomes 10 times larger than the value at $H = 0$. This result indicates that the behavior of $1/T_1$ = const is not caused by some spin-diffusion effect due to the inevitable contamination of magnetic impurities. If this was the case, magnetic fluctuations are suppressed by applying magnetic field. Consequently, $1/T_1$ would continue to decrease than the value at $H = 0$. Therefore, the '$1/T_1$ = const' behavior observed at low temperatures is not due to the impurity effect, but an intrinsic behavior. As a matter of fact, the $1/T_1$ at 0.3 T indicates a behavior of $1/T_1T$ = const below 0.5 K as shown by the solid line of Fig.3.4. This may be associated with the relaxation process due to the vortex cores in the SC mixed state.

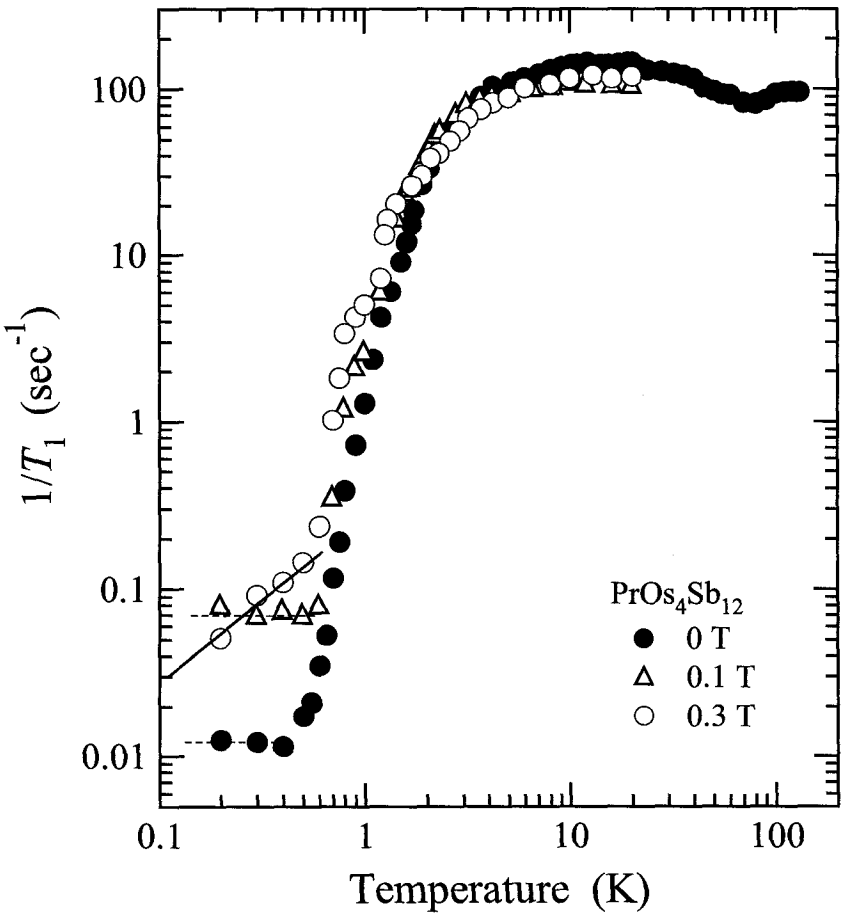

Figure 3.4: The T dependence of $1/T_1$ at $H = 0$ T (closed circles), 0.1 T (open triangles), 0.3 T (open circles). Solid line indicates $1/T_1T$ = const dependence.

Next, in order to uncover an origin of the anomaly in $1/T_1$ near T_C, $1/T_1T$ is plotted as a function of temperature as shown in Fig.3.5. Here, in order to make any anomaly clear, the

values of $1/T_1T$ at $H = 0.1$ and 0.3 T are tentatively scaled up. $1/T_1T$ starts to decrease below T_C at $H = 0$, and the anomaly just below T_C is not so significant if any. With increasing H, $1/T_1T$ indicates no remarkable decrease at $T_C \sim 1.49$ K and 0.3 T, but a rapid decrease at $T \sim 1.25$ K. Moreover, $1/T_1T$ indicates a shoulder like anomaly around 1.1 K, followed by a rapid decrease below ~ 0.8 K. From the T_1 measurement, the anomalies relevant with the multiple SC phases seem to be present in $PrOs_4Sb_{12}$. This results will be compared with the result of the angular dependence of thermal conductivity under the rotation of H later.

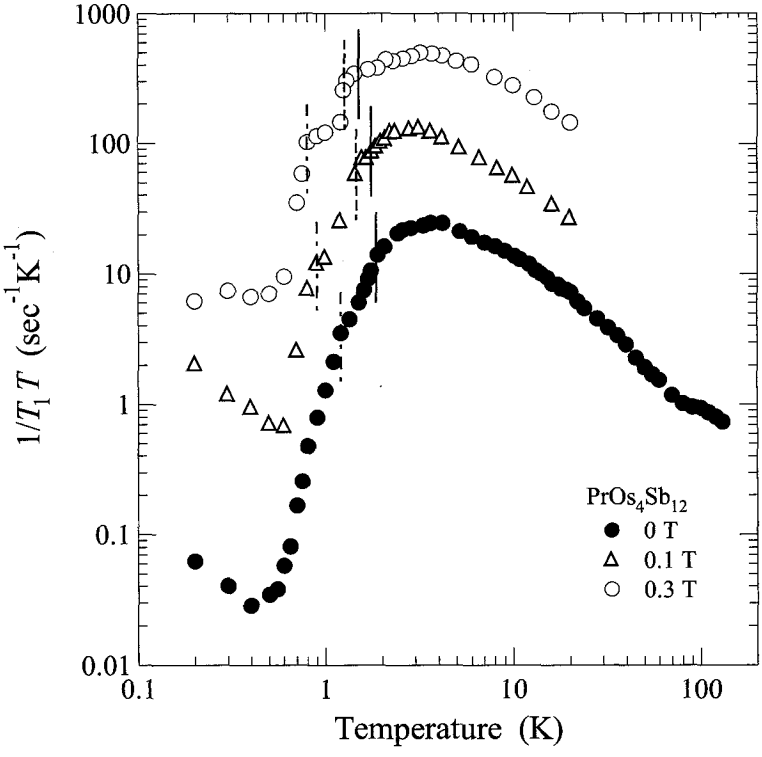

Figure 3.5: The T dependence of $1/T_1T$ at $H = 0$ T (closed circles), 0.1 T (open triangles), and 0.3 T (open circles).

Sample dependence

Fig.3.6 (a) displays the T dependence of $1/T_1T$ at the ^{123}Sb-$2\nu_Q$ transition for the sample A and B which were prepared using a different purity of Os element. The two samples have almost the same $T_C \sim 1.82$ K. Their $1/T_1T$ exhibit nearly the same T dependence over a measured T range, pointing to no significant sample dependence. However, a slight difference of $1/T_1$ is seen just below T_C. The detailed T dependencies of $1/T_1T$ on the sample A and B around T_C are shown in Fig3.6 (b). Although, for the sample A, an anomaly in the T dependence of $1/T_1T$ is not so significant just below T_C, but for the sample B, it reveals a distinct anomaly just below T_C.

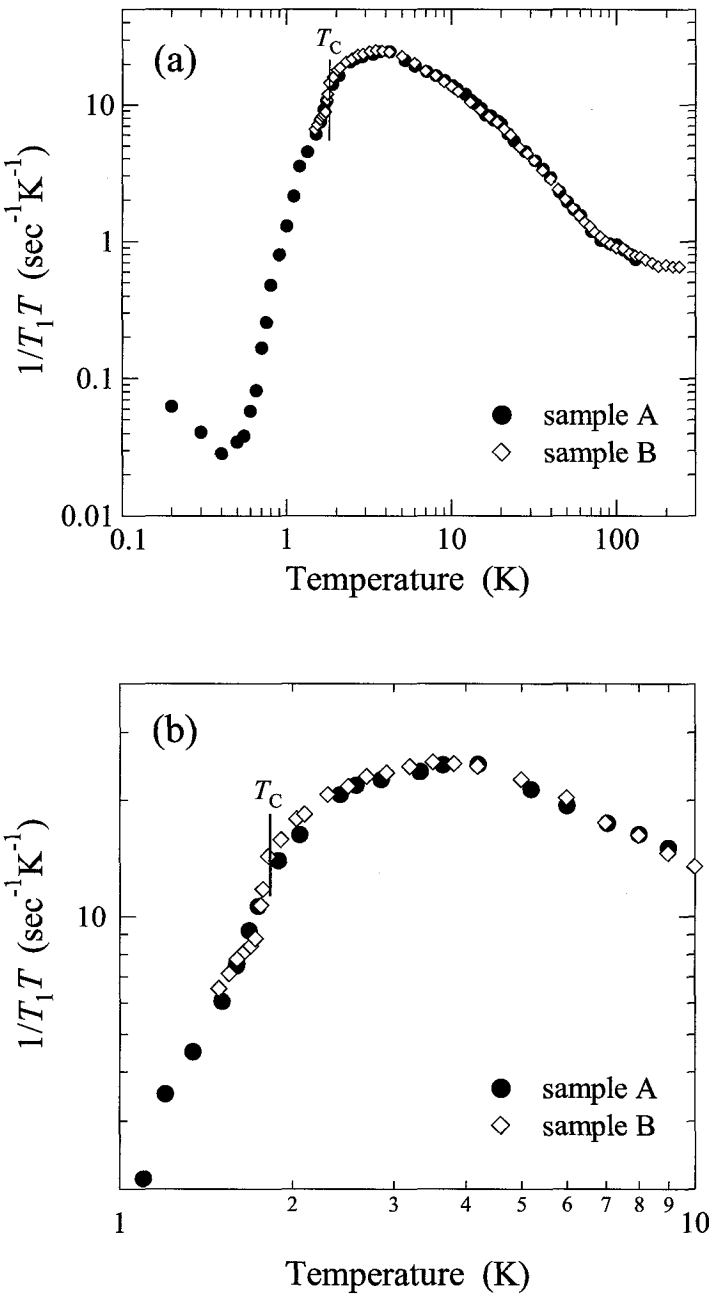

Figure 3.6: (a) The T dependence of $1/T_1T$ for the sample A and B. (b) The T dependence of $1/T_1T$ at low temperatures.

Phase diagram of "multiple SC" states

A temperature at which the anomalies in $1/T_1T$ are seen is plotted on the $T-H$ phase diagram extracted from the thermal-conductivity measurement as shown in Fig.3.7. The respective temperatures where $1/T_1T$ begins to decrease, saturate and again decrease are plotted by marks of open hexagons, open quadrangles, and open-star symbols. Remarkably, the temperature below which $1/T_1T$ starts to decrease corresponds just to the phase boundary between the four-fold point nodal state (A-phase) and two-fold point nodal state (B-phase). The anomaly at the deep inside of B-phase is not understood yet. Further measurements are needed to clarify the underlying SC phases in $PrOs_4Sb_{12}$ including some vortex-lattice state in the SC mixed state.

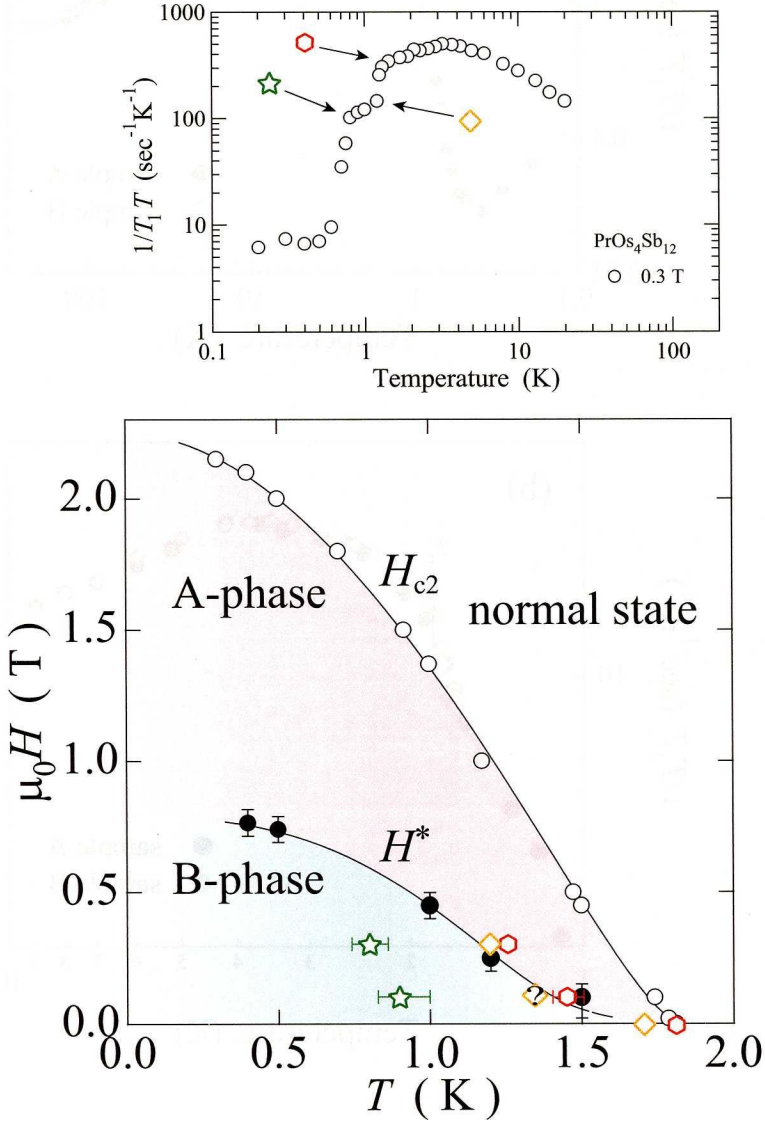

Figure 3.7: Magnetic field vs temperature phase diagram. The symbols of red open hexagons, yellow open quadrangles, and green stars represent the temperatures at which $1/T_1T$ indicates anomalies as shown in the upper figure.

3.4 Conclusion

The detailed measurements of ^{123}Sb-NQR T_1 under zero magnetic field and fields smaller than the upper critical field have revealed the possible multiple SC phases in the first Pr-based HF superconductor $PrOs_4Sb_{12}$. The present results are summarized as follows;

1. The '$1/T_1 = \text{const}$' behavior observed at $H = 0$ well below T_C has been shown to be the intrinsic behavior, suggesting that the ground state is not in a completely non-magnetic regime in origin, but a slight mixing effect with the magnetic first excited CEF states.

2. $1/T_1T$ shows the marked reduction below T_C, consistent with the phase boundary between the A-phase and the B-phase revealed by the thermal conductivity.

3. The second transition temperature has been found to appear at the deep inside of the B-phase, although the origin of this anomaly is not understood yet.

4. The sample dependence of $1/T_1T$ allows us to address how the multiple SC phases are relevant with the character of electronic state.

Thus, $PrOs_4Sb_{12}$ is classified as the novel type of HF superconductor that differs from the unconventional Ce-based HF superconductors mediated by magnetic fluctuations. Rather, $PrOs_4Sb_{12}$ may be mediated by Pr-$4f^2$ derived quadrupole-fluctuations, leading to a novel kind of HF superconductivity.

Bibliography

[1] G. P. Meisner, Physica **108B**, 763 (1981).

[2] L. E. Delong and G. P. Meisner, Solid State Commun. **53**, 119 (1985).

[3] I. Shirotani, T. Uchiumi, K. Ohno, C. Sekine, Y. Nakazawa, K. Kanoda, S. Todo, and T. Yagi, Phys. Rev. B **56**, 7866 (1997).

[4] I. Shirotani, K. Ohno, C. Sekine, T. Yagi, T. Kawakami, T. Nakanishi, H. Takahashi, J. Tang, A. Matsushita, T. Matsumoto, Physica B **281&282**, 1021 (2000).

[5] N. Takeda, and M.Ishikawa, J. Phys. Soc. Jpn. **57**, 868 (2000).

[6] E. D. Bauer, A. Ślebarski, E. J. Freeman, C. Sirvent, and M. B. Maple, J. Phys.: Condens. Matter **13**, 4495 (2001).

[7] H. Sugawara, S. Osaki, S. R. Saha, Y. Aoki, H. Sato, Y. Inada, H. Shishido, R. Settai, Y. Ōnuki, H. Harima, and K. Oikawa, Phys. Rev. B **66**, 220504R (2002).

[8] E. D. Bauer, N. A. Frederick, P. -C. Ho, V. S. Zapf, and M. B. Maple, Phys. Rev. B **65**, 100506R (2002).

[9] H. Kotegawa, M. Yogi, Y. Imamura, Y. Kawasaki, G. -q. Zheng, Y. Kitaoka, S. Ohsaki, H. Sugawara, Y. Aoki, and H. Sato, Phys. Rev. Lett. **90**, 027001 (2003).

[10] K. Izawa, Y. Nakajima, J. Goryo, Y. Matsuda, S. Osaki, H. Sugawara, H. Sato, P. Thalmeier, and K. Maki, Phys. Rev. Lett. **90**, 117001 (2003).

[11] K. Ishida, Y. Kawasaki, K. Tabuchi, K. Kashima, Y. Kitaoka, K. Asayama, C. Geibel, and F. Steglich, Phys. Rev. Lett. **82**, 5353 (1999).

[12] Y. Kawasaki, K. Ishida, T. Mito, C. Thessieu, G.-q. Zheng, Y. Kitaoka, C. Geibel, and F. Steglich, Phys. Rev. B **63**, 140501R (2001).

[13] Y. Kohori, Y. Yamato, Y. Iwamoto, and T. Kohara, Eur. Phys. J. B **18**, 601-604 (2000)

[14] T. Mito, S. Kawasaki, G.-q. Zheng, Y. Kawasaki, K. Ishida, Y. Kitaoka, D. Aoki, Y. Haga, and Y. Ōnuki, Phys. Rev. B **63**, 220507R (2001).

[15] Y. Kohori, Y. Yamato, Y. Iwamoto, T. Kohara, E. D. Bauer, M. B. Maple, and J. L. Sarrao, Phys. Rev. B **64**, 134526 (2001).

[16] G.-q. Zheng, K. Tanabe, T. Mito, S. Kawasaki, Y. Kitaoka, D. Aoki, Y. Haga, and Y. Ōnuki, Phys. Rev. Lett. **86**, 4664 (2001).

[17] Y. Kawasaki, S. Kawasaki, M. Yashima, T. Mito, G. -q. Zheng, Y. Kitaoka, H. Shishido, R. Settai, Y. Haga, and Y. Ōnuki, J. Phys. Soc. Jpn. **72**, 2308 (2003).

[18] R. Vollmer, A. Faißt, C. Pfleiderer, H. v. Löhneysen, E. D. Bauer, P. -C. Ho, V. Zapf, and M. B. Maple, Phys. Rev. Lett. **90**, 057001 (2003).

[19] A. Tsuchiya, Y. Aoki, S. Sanada, T. Namiki, H. Sugawara, and H. Sato, unpublished.

[20] Y. Aoki, A. Tsuchiya, T. Kanayama, S. R. Saha, H. Sugawara, H. Sato, W. Higemoto, A. Koda, K. Ohishi, K. Nishiyama, and R. Kadono, Phys. Rev. Lett. **91**, 067003 (2003).

Chapter 4

The Sb-NQR study of Kondo semiconductor $CeOs_4Sb_{12}$

4.1 Introduction

Filled-skutterudite compounds ReT_4Pn_{12} (Re=rare earth; T=Fe,Ru and Os; Pn=pnictogen) have attracted much attention because of their rich physical phenomena that are not fully understood yet. For instance, $PrFe_4P_{12}$ shows the heavy fermion (HF) like behavior with a large mass of $m^* \sim 70\ m_e$ under magnetic field (H)[1] and undergoes an anomalous transition at a temperature $T = 6.4$ K at zero field $H = 0$, indicative of a quadrupole ordering.[2–4] Note that the large value in the specific heat C divided by temperature (T) C/T for this compound is due not only to such low-energy degrees of freedom as either magnetic or quadrupolar fluctuations, but also to the Schottky anomaly originating from some low-lying CEF splitting. $PrOs_4Sb_{12}$ is the first Pr-based HF superconductor that reveals the large jump in the specific heat at $T_C = 1.85$ K, the slope of the upper critical field near T_C, and the electronic specific-heat coefficient $\gamma \sim 350-500$ mJ/mole K^2 in the normal state.[5] In the Pr-based compounds with the non-Kramers doublet (Γ_3) ground state, quadrupolar interactions play important role. In analogy with the quadrupolar Kondo model,[6] it was suggested that the HF-like behavior exhibited by $PrOs_4Sb_{12}$ may be relevant to a quadrupolar Kondo lattice. An interesting issue to be addressed is what a role of Pr^{3+}-derived quadrupolar fluctuations play in relevance with the onset of the superconductivity in this compound.[5,7]

By contrast, most Ce-based-filled-skutterudite compounds show a semiconducting behavior, that is called *a hybridization-gap semiconductor*.[8] CeT_4P_{12} (T = Fe, Ru and Os) compounds have a hybridization gap of $400 \sim 1500$ K, and the value of energy gap becomes smaller, as a lattice constant increases.[8,9] CeT_4Sb_{12} compounds show a semi-metallic behavior. $CeOs_4Sb_{12}$ is, on the one hand, suggested to exhibit a Kondo insulating behavior with a large value of $\gamma \sim 92$ mJ $mol^{-1}K^{-2}$ and a very small gap of about $\Delta/k_B \sim 10$ K at the Fermi level.[10] Rare earth ion is surrounded by twelve Sb atoms that are strongly hybridized with nearly localized $4f$ electrons. The band calculations on $CeOs_4Sb_{12}$ unraveled a unique band structure where no band gap is formed at the Fermi level.[11] Electrical resistivity measurement under pressure suggests that a hopping conductivity mechanism is realized at low temperatures.[12] Furthermore,

$CeOs_4Sb_{12}$ was reported to exhibit an anomaly around $T \sim 1$ K. An entropy release below this temperature is not large enough to arise from some intrinsic phase transition, but indicative of some impurity effect.[10] On the other hand, the measurement of specific heat under H suggests an onset of the phase transition below $T \sim 1$ K.[13]

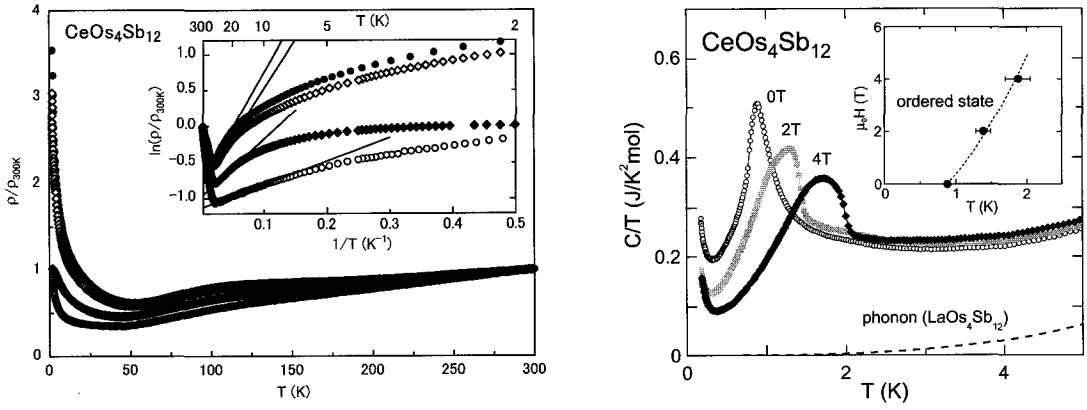

Figure 4.1: Left Figure : The T dependence of electrical resistivity.[10] Right Figure : The T dependence of C/T under various values of magnetic field.[13]

Here we report the novel magnetic phase transition in $CeOs_4Sb_{12}$ that emerges at $T = 0.9$ K on the verge of antiferromagnetic (AFM) quantum critical point (QCP) via the measurements of $1/T_1$ and NQR spectrum of Sb nuclei.

4.2 Crystal Electric Field

Bauer *et al.* proposed a CEF energy scheme via the measurement of magnetic susceptibility as shown in Fig.4.2.[10] The ground state is the magnetic doublet Γ_7, and the first excited state is the quartet Γ_8. The separation between the ground state and the excited state is estimated as $\Delta E_1 \sim 327$ K.[10]

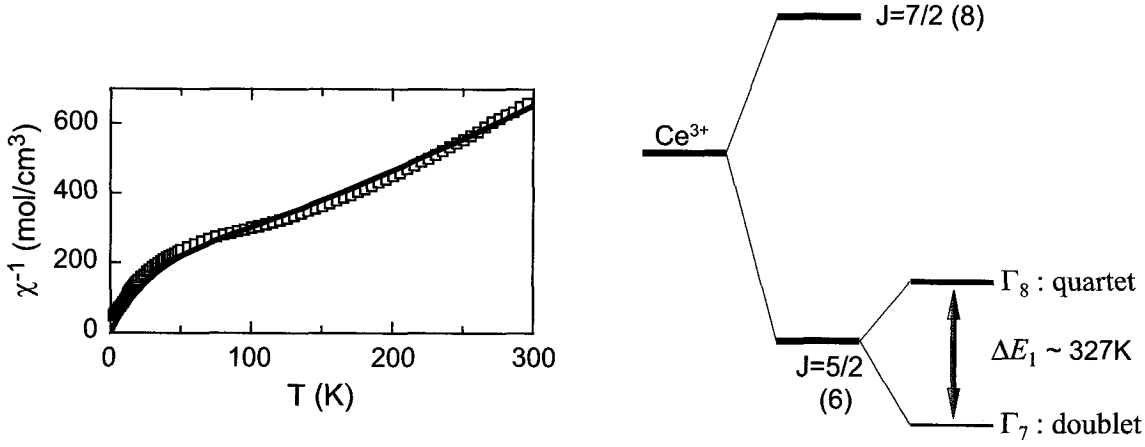

Figure 4.2: Left Figure : The T dependence of χ^{-1}. The solid line shows a theoretical fit assuming a cubic CEF model for Ce^{3+}. Right Figure : The CEF energy scheme for $CeOs_4Sb_{12}$. $\Delta E_1 \sim 327$ K is evaluated to be consistent with the data of magnetic susceptibility as shown in left figure.[10]

4.3 Sample preparation

Single crystal of $CeOs_4Sb_{12}$ was grown by the Sb-flux method described elsewhere.[13] The Sb-NQR measurement on the single crystal, that was crushed into powder, was made using a conventional spin-echo method at $H = 0$ and in the range of $T = 0.2 - 300$ K using a ^{3}He-^{4}He-dilution refrigerator.

4.4 Results and Discussion

4.4.1 NQR spectrum

Fig.4.3 shows ^{121}Sb and ^{123}Sb NQR spectra for $CeOs_4Sb_{12}$ at $T = 4.2$ K. Since ^{121}Sb (^{123}Sb) has the nuclear spin $I = 5/2$ (7/2), two (three) NQR transitions are observed as indicated in Fig.4.3. From the values of respective ^{121}Sb and ^{123}Sb NQR frequencies, $^{121}\nu_Q \sim 43.861$ MHz and $^{123}\nu_Q \sim 26.630$ MHz are estimated together with $\eta \sim 0.463$. These values are almost equivalent with those in $PrOs_4Sb_{12}$ as shown in Table 4.1. The full-width-half-maximum (FWHM) in the NQR spectrum is as small as ~ 65 kHz at 4.2 K, proving a high quality of the sample.

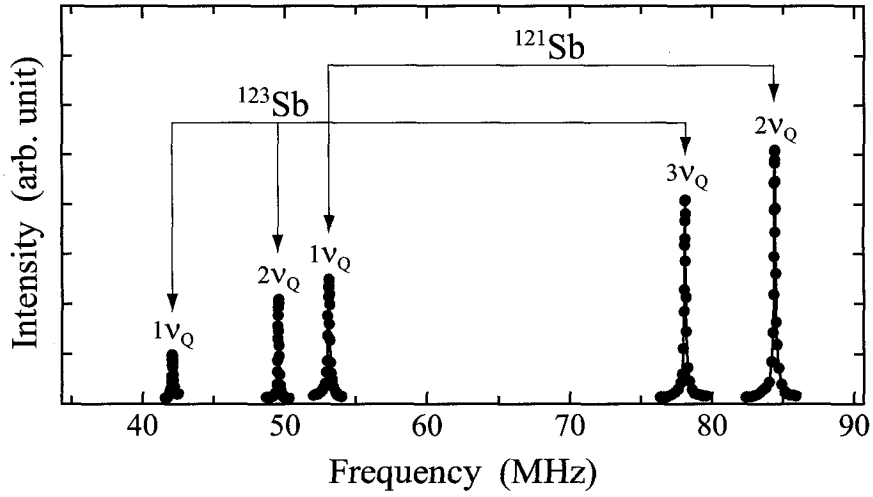

Figure 4.3: ^{121}Sb- and ^{123}Sb-NQR spectra for $CeOs_4Sb_{12}$ at $T = 4.2$ K.

Table 4.1: NQR frequency ν_Q and asymmetric parameter η for $LaOs_4Sb_{12}$, $CeOs_4Sb_{12}$ and $PrOs_4Sb_{12}$.[14]

	$LaOs_4Sb_{12}$	$CeOs_4Sb_{12}$	$PrOs_4Sb_{12}$
$^{121}\nu_Q$ (MHz)	43.776	43.847	44.167
$^{123}\nu_Q$ (MHz)	26.577	26.628	26.81
Asymmetric parameter η	0.450	0.463	0.459

4.4.2 Nuclear spin-lattice relaxation time T_1

$1/T_1$ was measured at the ^{121}Sb-$2\nu_Q(\pm 3/2 \leftrightarrow \pm 5/2$ transition) and ^{123}Sb-$2\nu_Q$. Fig.4.4 displays the recovery curve of magnetization ^{121}Sb ($I = 5/2$) and ^{123}Sb ($I = 7/2$) NQR magnetization , that is given in the case of $\eta = 0.45$ by[15,16]
for $I = 5/2$:

$$\frac{M(\infty) - M(t)}{M(\infty)} = 0.375\exp(-3t/T_1) + 0.625\exp(-8.8t/T_1)) \tag{4.1}$$

for $I = 7/2$:

$$\frac{M(\infty) - M(t)}{M(\infty)} = 0.075\exp(-3.025t/T_1) + 0.015\exp(-8.55t/T_1) + 0.91\exp(-17.305t/T_1) \tag{4.2}$$

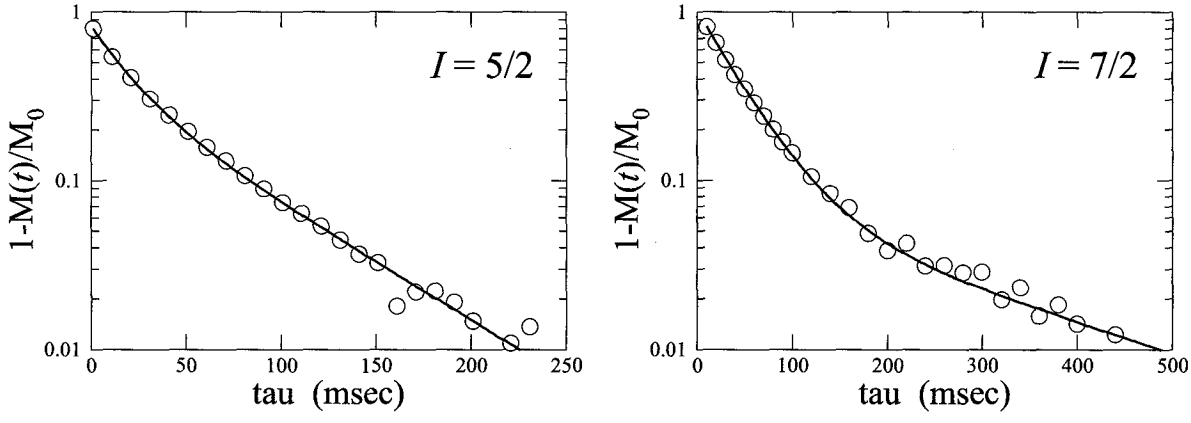

Figure 4.4: Typical recovery curve of NQR magnetization at ^{121}Sb-$2\nu_Q$ and ^{123}Sb-$2\nu_Q$ NQR transitions at $H = 0$ in $CeOs_4Sb_{12}$. The solid lines are the least square fits calculated from eq.(4.1) and eq.(4.2).

The $1/T_1$ of ^{123}Sb-$2\nu_Q$ at $\pm 3/2 \leftrightarrow \pm 5/2$ transition is displayed in Fig.4.5. The $1/T_1$ in the range of $T = 200 - 300$ K markedly decreases, following $1/T_1 \propto \exp(-\Delta/k_BT)$ with $\Delta/k_B \sim 330$ K. This exponential decrease in $1/T_1$ coincides with the energy splitting $\Delta/k_B \sim 327$ between the CEF ground state Γ_7 and the first excited state Γ_8. Here $\Delta/k_B \sim 327$ K is estimated from the result of magnetic susceptibility measurement.[10] With further decreasing T, $1/T_1$ starts to deviate from the exponential behavior below $T = 150$ K, followed by a behavior of $1/T_1T = $ const in the range of $T = 25 - 50$ K as shown in the inset of Fig.4.5. This shows that Fermi liquid state is realized in a low T regime below 50K. Note that the relaxation mechanism at low T is confirmed to be magnetic in origin from the relation of $^{123}(1/T_1)/^{121}(1/T_1) = (^{123}\gamma_N/^{121}\gamma_N)^2$ where γ_N is the gyromagnetic ratio as shown in Fig.4.6 (a).

Most remarkably, the T dependence of $1/T_1$ obeys a relation of $(1/T_1 \propto \sqrt{T})$ below $T = 25$ K. The self-consistent renormalization (SCR) theory for spin fluctuations in itinerant AFM metals was successfully applied to the case for HF systems which are closely located to an AFM

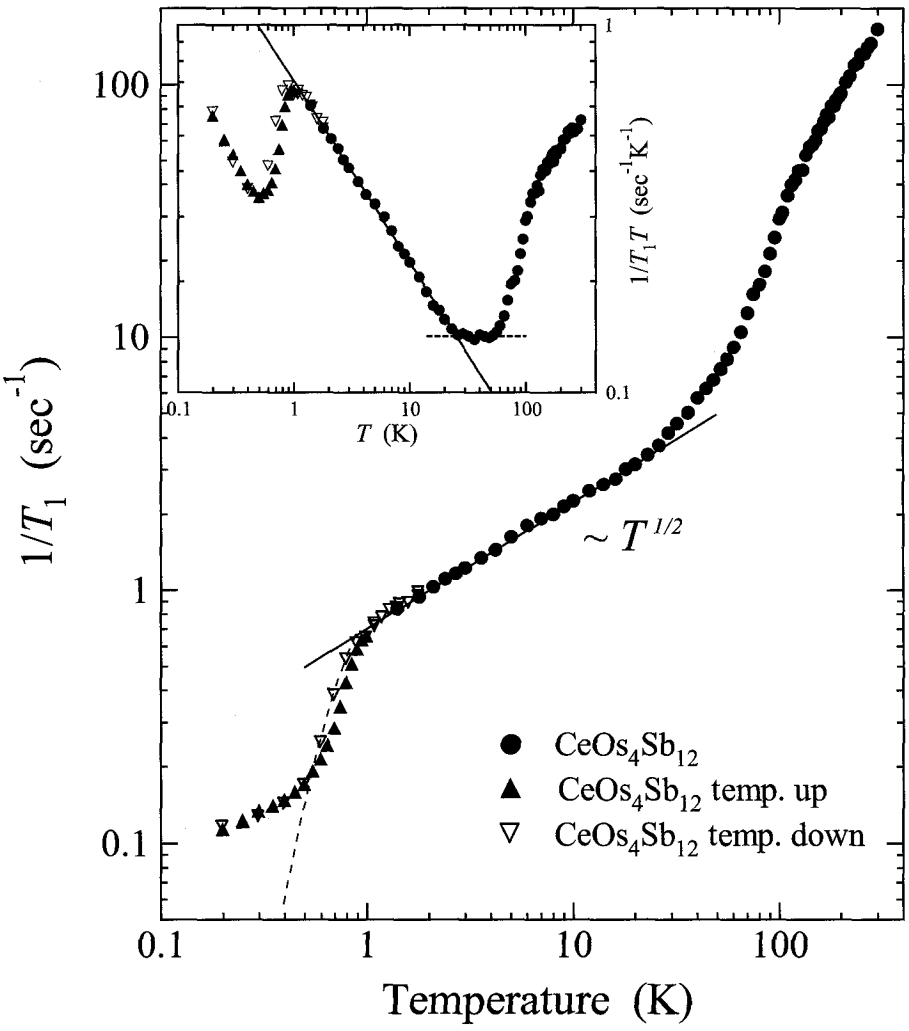

Figure 4.5: The T dependence of $^{123}1/T_1$ at ^{123}Sb-$2\nu_Q$ transition for $CeOs_4Sb_{12}$ at $H = 0$. The solid line is a fit to the relation of $1/T_1 \propto T/(T - T_N)^{1/2}$ with $T_N \sim 0.06$ K that is consistent with the SCR theory for three dimensional itinerant weekly antiferromagnetic metals.[17–19] The dashed line below $T_{SDW} \sim 0.9$ K is a fit to an activated relation of $1/T_1 \propto \exp(-\Delta/k_BT)$ with $\Delta/k_B \sim 1.83$ K.

instability.[17–19] In this case, it is predicted that $1/T_1$ obeys the relation of

$$\frac{1}{T_1} \propto T\sqrt{\chi_Q(T)} \propto \frac{T}{\sqrt{T-T_N}} \tag{4.3}$$

because of the Currie-Weiss law of the staggered susceptibility $\chi_Q(T) \propto 1/(T-T_N)$ with an AFM ordering temperature T_N. Therefore, note that $1/T_1 \propto \sqrt{T}$ is valid in the case of $T_N \sim 0$ at the vicinity of an AFM QCP. In order to see clearly this T dependence of $1/T_1 \propto \sqrt{T}$ in $T = 1.3-25$ K, $(T_1T)^2$ is plotted in Fig.4.6 (b) as a function of T. From this plot, the relation $(T_1T)^2 \propto (T-T_N)$ is valid with $T_N \sim 0.06$ K in the range of $T = 1.3-25$ K. Interestingly, $CeOs_4Sb_{12}$ is demonstrated to be on the verge of antiferromagnetism.

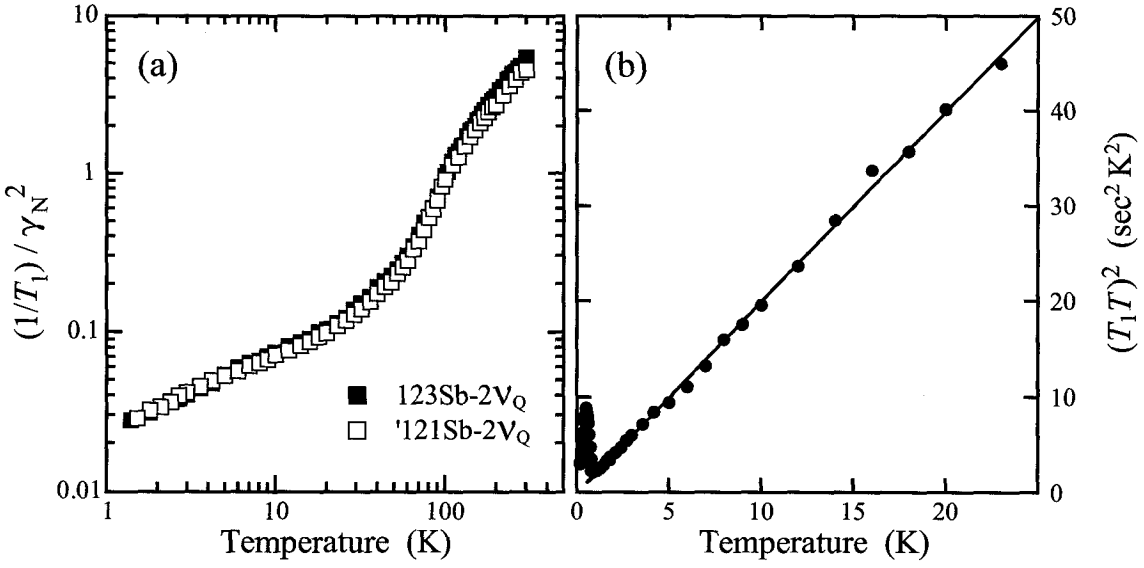

Figure 4.6: (a) The T dependence of $(1/T_1)/\gamma_N^2$. (b) $^{123}(T_1T)^2$ vs T plot. Solid line is a fit to the relation of $(T_1T)^2 \propto (T-T_N)$ with $T_N \sim 0.06$ K in terms of the SCR theory (see the text).

With further decreasing T, a dramatic decrease in $1/T_1$ is observed at $T \sim 0.9$ K, unexpectedly from an estimation of "$T_N \sim 0.06$ K" expected from the T dependence in the staggered susceptibility $\chi_Q(T)$ as argued above. Fig.4.7 shows the detailed T dependence of $1/T_1T$ around $T \sim 0.9$ K. It should be noted that $1/T_1T$ indicates a clear hysteresis upon cooling and heating. This result is indicative of a first-order phase transition emerging at $T \sim 0.9$ K, that is also corroborated by the measurement of the T dependence in NQR spectral shape as shown later.

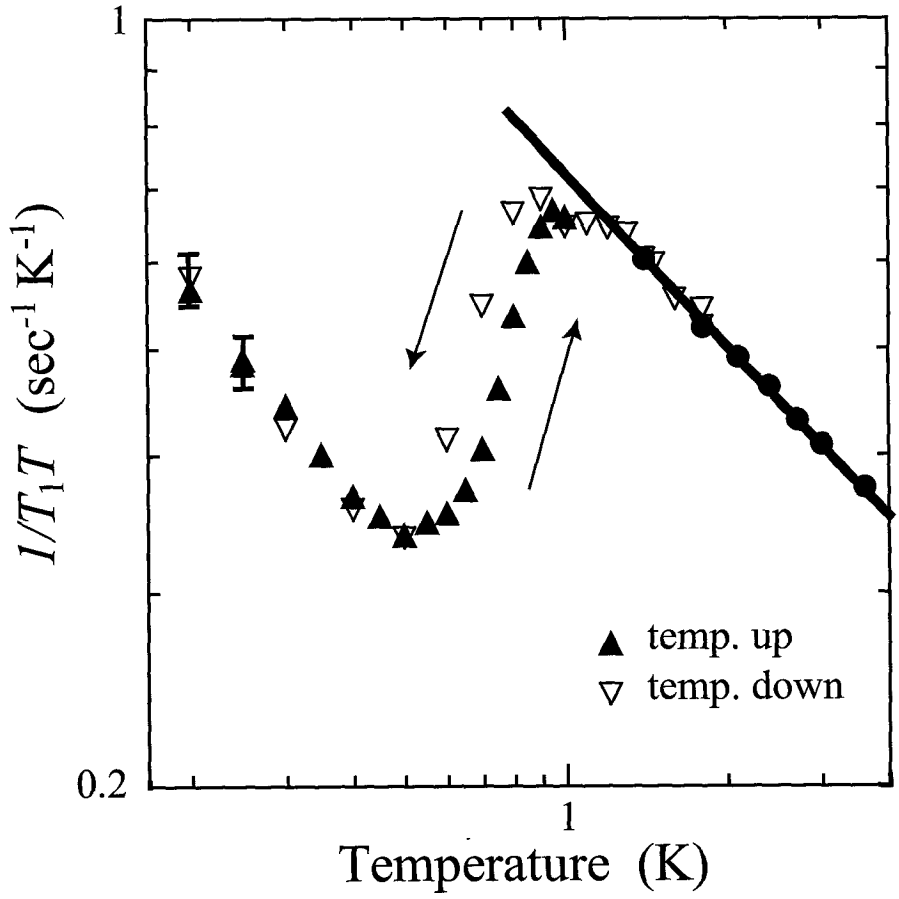

Figure 4.7: The T dependence of $1/T_1T$ at low temperatures reveals a hysteresis upon cooling and heating.

4.4.3 Analysis of spectrum shape

Fig.4.8 (a) indicates the T dependence of NQR spectrum at ^{123}Sb-$2\nu_Q$ transition below 4.2 K. Above 0.9 K, it exhibits a distinct Lorentzian shape with a small value of FWHM about 65 kHz. With decreasing T below 0.9 K, it starts to broaden as clearly seen in the figure, and at the same time, $1/T_1$ is markedly decreased. The data are consistent with such the activation type of behavior as $1/T_1 \propto \exp(-\Delta/k_B T)$ with a gap size of $\Delta/k_B \sim 1.83$ K. These results give evidence for a magnetic phase transition below 0.9 K, accompanying the small gap at the Fermi level. Note that the tail in the NQR spectrum is significantly increased and makes the NQR spectral shape deviate from the Lorentzian type. Such the shape of the NQR spectrum at low T reveals a wide distribution of the internal fields at the Sb nuclei associated with the onset of magnetic order, indicative of a spin-density-wave (SDW) type of ordering triggered by a nesting of the Fermi surface. Furthermore, the T dependence of FWHM in NQR spectrum shows a hysteresis upon cooling and heating as indicated in Fig.4.8 (b). This result suggests that the first-order transition sets in below $T_{SDW} = 0.9$ K, consistent with the hysteresis observed in the T dependence in $1/T_1$. The present results on $CeOs_4Sb_{12}$ have unraveled that the magnetic phase transition near the AFM QCP is of the first order type. It seems to deserve theoretical study on what physics is behind the AFM QCP in f-electrons derived correlated band realized in HF systems in general.

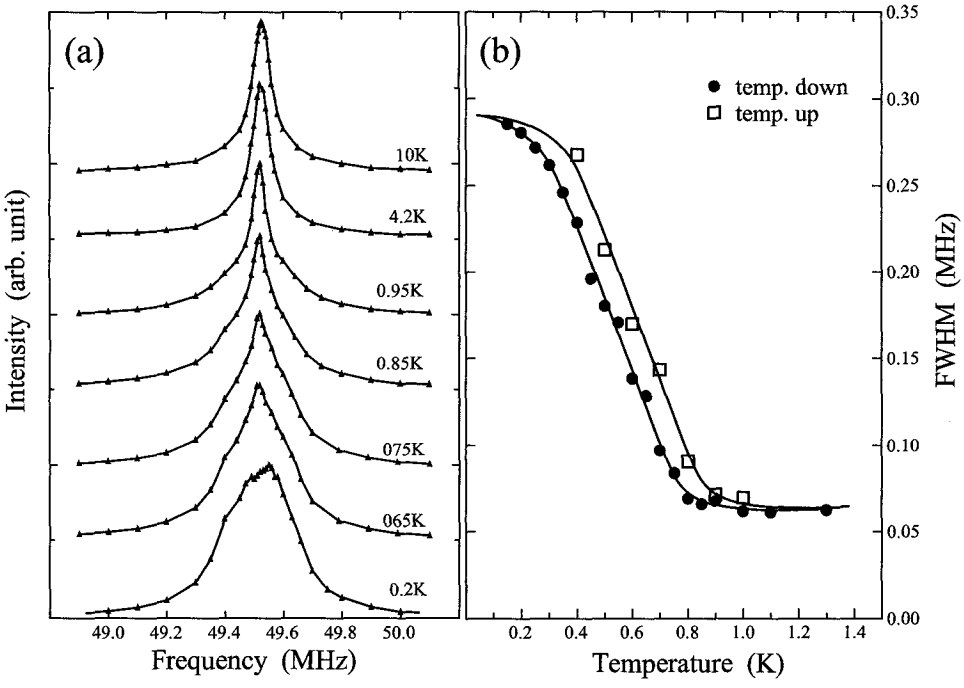

Figure 4.8: (a) The T dependence of the NQR spectrum of ^{123}Sb-$2\nu_Q$ transition. (b) The T dependence of FWHM upon cooling (closed circle) and heating (open circle).

4.5 Conclusion

In summary, by means of the measurements of $1/T_1$ and NQR spectrum of Sb nuclei, we have demonstrated that $CeOs_4Sb_{12}$ is closely located to the AFM QCP. Even in such a situation, a remarkable finding is that the SDW type of magnetic phase transition, that is of the first order type, occurs at $T = 0.9$ K, possibly triggered by the nesting effect of the Fermi surface. The present result, we believe, deserves theoretical study on the physics behind the AFM QCP realized in HF systems in general.

Bibliography

[1] H. Sugawara, T. D. Matsuda, K. Abe, Y. Aoki, H. Sato, S. Nojiri, Y. Inada, R. Settai, and Y. Ōnuki, Phys. Rev. B **66**, 134411 (2002).

[2] T. D. Matsuda, H. Okada, H. Sugawara, Y. Aoki, H. Sato, A. V. Andreev, Y. Shiokawa, V. Sechovsky, T. Honma, E. Yamamoto, and Y. Onuki, Physica B **281&282**, 220-222 (2000).

[3] Y. Aoki, T. Namiki, T. D. Matsuda, K. Abe, H. Sugawara, and H. Sato, Phys. Rev. B **65**, 064446 (2002).

[4] Y. Nakanishi, T. Shimizu, M. Yoshizawa, T. D. Matsuda, H. Sugawara, and H. Sato, Phys. Rev. B **63**, 184429 (2002).

[5] E. D. Bauer, N. A. Frederick, P. -C. Ho, V. S. Zapf, and M. B. Maple, Phys. Rev. B **65**, 100506R (2002).

[6] D. L. Cox, Phys. Rev. Lett. **59**, 1240 (1987).

[7] M. B. Maple, P. -C. Ho, V. S. Zapf, N. A. Frederick, E. D. Bauer, W. M. Yuhasz, F. M. Woodward, and J. W. Lynn, J. Phys. Soc. Jpn. **71**, 23-28 (2002).

[8] G. P. Meisner, M. S. Torikachvili, K. N. Yang, M. B. Maple, and R. P. Guertin, J. Appl. Phys. **57**, 3073 (1985).

[9] I. Shirotani, T. Uchiumi, C.Sekine, M. Hori, S. Kimura, and N. Hamaya, J. Solid State Chem. **142**, 146-151 (1999).

[10] E. D. Bauer, A. Ślebarski, E. J. Freeman, C. Sirvent, and M. B. Maple, J. Phys.: Condens. Matter **13**, 4495 (2001).

[11] H. Harima, and K. Takegahara, J. Phys.: Condens. Matter **15**, S2081-S2086 (2003).

[12] M. Hedo, Y. Uwatoko, H. Sugawara and H. Sato, Physica B, **329-333**, 456-457 (2003).

[13] T. Namiki, Y. Aoki, H. Sugawara, and H. Sato, Acta Phys. Pol. B, **34**, 1161 (2003).

[14] H. Kotegawa, M. Yogi, Y. Imamura, Y. Kawasaki, G.-q. Zheng, Y. Kitaoka, S. Ohsaki, H. Sugawara Y. Aoki, and H. Sato, Phys. Rev. Lett. **90**, 027001 (2003).

[15] D. E. MacLaughlin, J. D. Williamson, and J. Butterworth, Phys. Rev. B **4**, 60 (1971).

[16] J. Chepin, and J. H. Ross, J. Phys.: Condens. Matter **3**, 8103-8112 (1991).

[17] T. Moriya, and T. Takimoto, J. Phys. Soc. Jpn. **64**, 960 (1995).

[18] A. Ishigaki, and T. Moriya, J. Phys. Soc. Jpn. **65**, 3402 (1996).

[19] S. Nakamura, T. Moriya, and K. Ueda, J. Phys. Soc. Jpn. **65**, 4026 (1996).

Published works

1. H. Kotegawa, M. Yogi, Y. Imamura, Y. Kawasaki, G. -q. Zheng, Y. Kitaoka, S. Ohsaki, H. Sugawara, Y. Aoki, and H. Sato: "Evidence for Unconventional Strong-Coupling Superconductivity in $PrOs_4Sb_{12}$", Physical Review Letters **90**, 027001 (2003).

2. M. Yogi, H. Kotegawa, Y. Imamura, G. -q. Zheng, Y. Kitaoka, H. Sugawara, and H. Sato: "Sb-NQR probe for superconducting properties in the Pr-based filled-skutterudite compound $PrRu_4Sb_{12}$", Physical Review B **67**, 180501(R) (2003).

3. H. Kotegawa, M. Yogi, Y. Imamura, Y. Kawasaki, G. -q. Zheng, Y. Kitaoka, S. Ohsaki, H. Sugawara, Y. Aoki, and H. Sato: "Unusual Superconductivity in Skutterudite Compound $PrOs_4Sb_{12}$", Acta Physica Polonica B **34**, 1003 (2003).

4. M. Yogi, H. Kotegawa, G. -q. Zheng, Y. Kitaoka, S. Osaki, H. Sugawara, and H. Sato: "Sb-NQR study of the "Kondo semiconductor" $CeOs_4Sb_{12}$", to be published in *the Proceedings of the International Conference on Magnetism 2003.*

5. M. Yogi, H. Kotegawa, G. -q. Zheng, Y. Kitaoka, H. Sugawara, and H. Sato: "Novel magnetic phase transition near the quantum critical point in the filled-skutterudite compound $CeOs_4Sb_{12}$: An Sb-NQR study", submitted in Physical Review Letters.

Acknowledgment

I would like to express to Professor Yoshio Kitaoka my sincere thanks for giving me the opportunity to study heavy fermion physics. Furthermore, I awfully thanks to Professor Yoshio Kitaoka for your invaluable guidance, argument, and encouragement through this work.

I would like to thank Professor H. Sato, and Dr. H. Sugawara and co-workers (Tokyo Metropolitan Univ.) and Professor Y. Ōnuki and co-workers (Osaka Univ.) and Professor E. Bauer and co-workers (Vienna Univ. of Technology) for providing high quality samples. I would like to thank to Professor G. -q. Zheng for significant discussions, and advices through this work. I would like to thank to Professors K. Ishida, H. Tou, and Dr. Y. Aoki for valuable comments and suggestions. I am very grateful to Professors K. Miyake, H. Harima, and H. Kohno for theoretical advices and suggestions. I would like to thank Dr. H. Kotegawa, Dr. Y. Kawasaki, and Mr. S. Kawasaki for experimental help and valuable comments. I am very grateful to Dr. Y. Tokunaga, and Dr. T. Mito for valuable comments and suggestions. I am very grateful to Professors H. Niki, K. Yagasaki, T. Nakama, and Dr. M. Hedo for their useful comments on experimental technique and suggestions. I would like to thank co-workers of Kitaoka laboratory for their cooperations through this work.

Finally, I am most thankful to my family to understanding and support over the years.